Improving High Angle of Attack Performance of an Aircraft With Leading Edge Mounted Propellers Through Nacelle and Leading Edge Modification

MSc Thesis

N. T. Suard

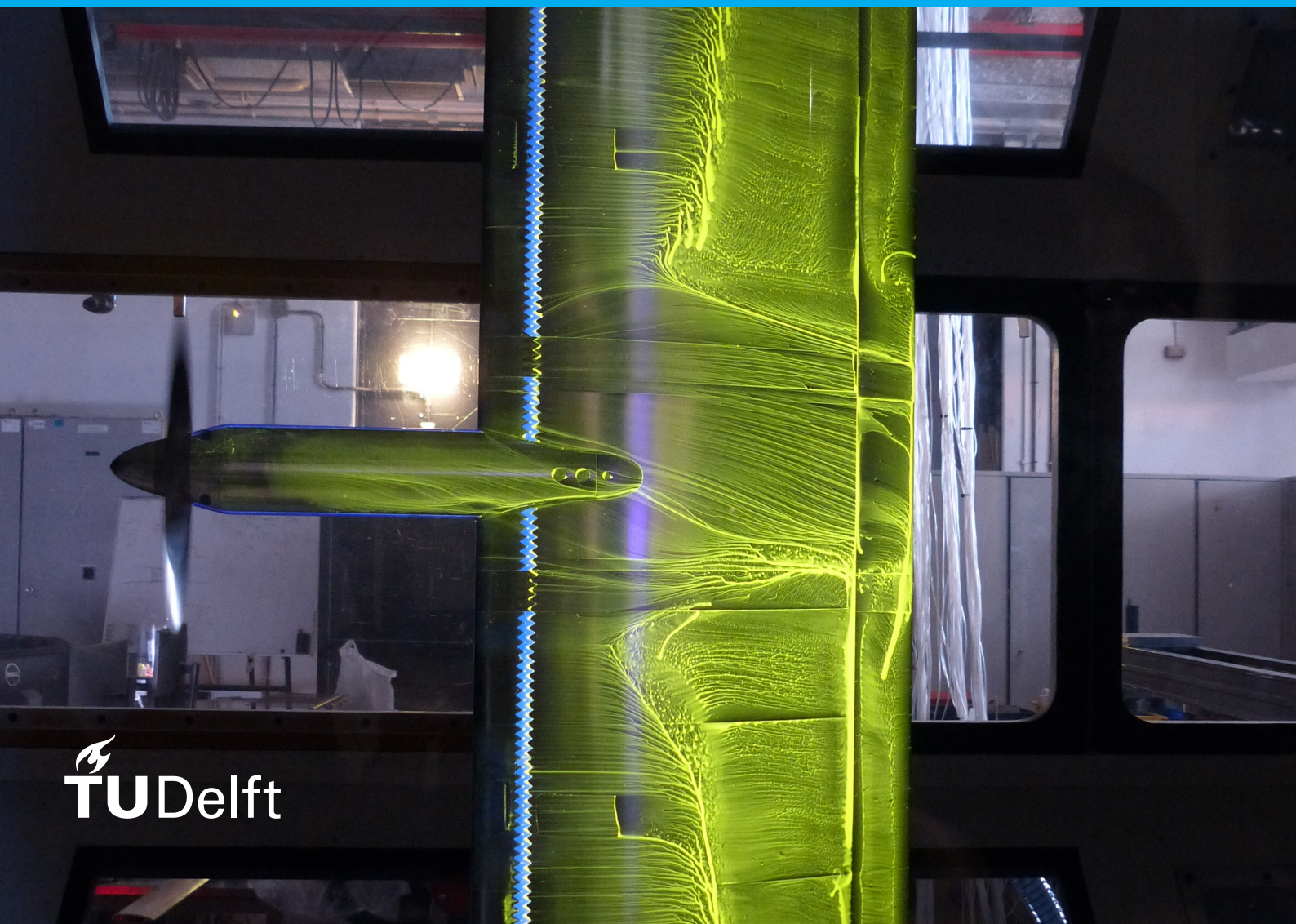

TU Delft

This page is intentionally left blank

Improving High Angle of Attack Performance of an Aircraft With Leading Edge Mounted Propellers Through Nacelle and Leading Edge Modification

MSc Thesis

by

N. T. Suard

to obtain the degree of Master of Science
at the Delft University of Technology,

Student number: 4490932
Supervisors: Prof. dr. ir. L.L.M. Veldhuis, Professor, TU Delft
ir. R. R. Duivenvoorden PhD Candidate, TU Delft

TU Delft

This page is intentionally left blank

Preface

I would like to thank Delft University of Technology for giving me the opportunity and resources to complete this research and complete my MSc in Aerospace engineering. I would particularly like to thank Professor Leo Veldhuis and Ramon Duivenvoorden for their expert advice and guidance over the course of the process. I have greatly appreciated being able to discuss interesting results together and feel that I have learnt a lot about aerodynamics and in particular propellers. In addition to this, I would like to thank all the staff and students that have supported me during the experimental campaign and helped me to set up my simulations. Without this help, I would not have been able to complete this project. I would also like to thank my friends and colleagues from study room NB1.01 for their help and advice in the final phases of this project as well as for the enjoyable lunch and coffee break conversations. Finally, I would like to thank my friends and family for their support throughout the process of completing this thesis. Completing this thesis during a pandemic has been very difficult at times and the support has been essential.

Noah Suard
Delft, May 21, 2022

This page is intentionally left blank

Contents

List of Figures

This page is intentionally left blank

List of Tables

This page is intentionally left blank

Summary

With growing attention on climate change, the aviation industry is required to reduce emissions in order to remain viable. To this end interest in propeller in combination with electric motors are becoming increasingly interesting as a result of their superior efficiency. Placing propellers on the wing leading edge also presents a substantial potential advantage in terms of high lift performance. The high dynamic pressure propeller wake passes over the wing and increases lift. The interactions between the propeller-nacelle-wing system result in the formation of a complex and closely coupled that also introduces some negative interaction effects. Understanding these effects and possible mitigation techniques allows the high lift performance of these propeller wing concepts to be further maximised allowing these concepts to be more competitive.

A survey of available literature on the subject of propeller-nacelle-wing interactions is performed in order to identify the theoretical background of the project. The installation of a nacelle leads to a number of undesirable interaction effects. The positioning of the nacelle on the leading edge leads to the formation of a higher pressure region that leads to spanwise flow expansion behind the nacelle causing boundary layer accumulation. In addition to this, the induces a higher local angle of attack as a result of flow accelerating as it passes the nacelle. Finally, the nacelle sheds vorticity that can burst as it passes through a strong adverse pressure gradient leading to boundary layer growth. Together these effects can lead to the early onset of stall in the vicinity of the nacelle.
The inclusion of a propeller causes the wing to be influenced by the combination of the high dynamic pressure propeller wake and propeller swirl. The propeller wake leads to an increase in lift by accelerating the flow that passes over the wing. Swirl induces changes in the local angle of attack. The down-going blade side downwashes the wing reducing the effective angle of attack and the up-going blade side upwashes the wing increasing the local angle of attack. The propeller also injects high-energy, turbulent flow into the boundary layer that can delay the onset of stall. In addition to this, the wing also influences the propeller performance. The upwash introduced by the wing leads to a non-uniform inflow condition that leads to non-uniform disc loading. Additionally, the wing provides some swirl recovery acting as a stator reducing the swirl in the wake effectively increasing the propeller thrust. The propeller wake also interacts with the wing causing it to deform and shear. The impact of the propeller on the nacelle interaction effects is unclear. While the high dynamic pressure wake seems to mitigate some of the nacelle-wing interaction effects there is limited research on this.
The use of multiple propellers and nacelles results in much of the wing being blown which can significantly increase the high lift performance. The resultant lift distribution is influenced heavily by the choice of propeller rotation directions however the wing lift distribution is largely a superposition of the effects of a single propeller and therefore it seems likely that the conclusions from an isolated propeller are still applicable to a multiple propeller configuration.
Finally, the methods to mitigate the negative impacts of propeller-nacelle-wing interactions at high angle of attack are considered. The use of a strake to shed a vortex structure that can help to suppress stall is widely applied to turbofan engines and has some limited application to propeller nacelles. they do not result in any significant impact with the propeller active and require a lot of optimisation in order to be effective. Lowering the nacelle helps to improve the performance in the case without the nacelle by reducing the high-pressure region that forms behind the nacelle however it also impacts the propeller performance and therefore requires a complex trade-off to determine the ideal position. The use of droop offers the potential to increase the maximum lift coefficient and delay stall although it has not been extensively applied to propeller wing interaction problems> overall research into the use of wing and nacelle modifications to enhance high angle of attack performance is limited.

Based on the background research a gap in the current state of the art is identified. There is relatively limited research regarding the influence of the nacelle on the high angle of attack performance at high angles of attack of propeller aircraft. In addition to this understanding of how to mitigate these effects is limited. Based on this knowledge gap the following research question arises: ”How can wing leading

edge and nacelle geometry be modified to reduce the negative effects of propeller-nacelle-wing interactions to improve high angle of attack performance for an aircraft with leading edge mounted propellers?" Answering this question is split into two parts. The first aspect of the research is to understand how the nacelle influences the high angle of attack performance and how these interactions are impacted by the introduction of a propeller. The second part of the research concerns how the nacelle and wing leading edge can be modified in order to mitigate the interaction effects and the effect of these modifications in different conditions.

The first part of the research question is answered through the use of experimental and Reynolds-Averaged Navier-Stokes (RANS) Computational Fluid Dynamics (CFD) numerical results. A wing with a single leading edge mounted TUD-XPROP-S propeller is used. This model is tested at the Delft University of Technology Low Turbulence Wind Tunnel to gain an initial understanding of the propeller-nacelle-wing interaction effects and to validate the numerical model. The numerical model is matched to the wind tunnel model both in physical geometry and the conditions it is run in. Both models will be evaluated at an angle of attack of 10°. The propeller is modelled numerically using an actuator disc.

The wind tunnel testing showed that the addition of a nacelle to the leading edge of a wing results in the development of a spanwise expansion of the flow behind the nacelle and the development of to regions of separated flow on either side of the nacelle towards the trailing edge. The addition of a propeller alters the flow significantly. The structures shed by the nacelle are still visible and two additional regions of separation form at the edge of the propeller wake. Overall the CFD model is able to model the key effects seen in the wind tunnel and is therefore considered suitable for the purposes of the study.
The addition of a nacelle introduces a high-pressure region as was seen in literature that leads to flow expansion. In addition to this the interaction between the nacelle and wing boundary layer causes some initial boundary layer growth that feeds into the regions of separation. The vorticity does not appear to play a significant role in the early onset of flow separation. The addition of the propeller complicates the interaction effects by introducing two additional structures that form as a result of the interaction between high-velocity wake and the slower flow surrounding it. The nacelle effects are still present although the propeller swirl translates the structures.

The second part of the report consists of a design study. For this, the far-field domain is simplified from the original domain that aimed to model the wind tunnel walls to a slip condition at the walls. Based on the previous results two modifications are proposed in order to address the nacelle-wing interactions. Leading edge droop is used in an attempt to reduce the magnitude of the leading edge pressure peak with the aim of reducing boundary layer growth to prevent separation. The leading edge is drooped 10°. The second modification is to apply a 20mm fillet between the nacelle and the wing that aims to smooth the junction between the nacelle to help to ameliorate the boundary layer interactions.

The simplified development model geometry changes had little impact on the propeller-nacelle-wing interactions. Attempts to mitigate the interactions through the use of leading edge droop achieved limited success. The reduction in the magnitude of the leading edge pressure peak as a result of better leading edge alignment results in a weaker adverse pressure gradient and therefore the wing boundary layer grows more slowly. This delays the onset of separated flow and reduces the size of the separated region however this modification was not able to eliminate the flow separation entirely and only results in a small improvement in wing lift and little change in drag performance. The addition of the actuator disc causes the drooped wing to perform particularly poorly on the down-going blade side as a result of the poor leading edge alignment. The propeller swirl reduces the local angle of attack and therefore the droop effect is detrimental. The droop also resulted in a growth of the regions of separated flow that form at the boundary of the propeller wake.
The nacelle wing fillet similarly achieves its primary goal of reducing the interaction between the nacelle and wing boundary layer. It is able to spread the junction losses over a larger area resulting in a thinner initial boundary layer in the vicinity of the nacelle and thus more suction on the forward portion of the wing. These improvements do not prevent the flow from separating, the spread boundary layer is still thicker than the boundary layer in the undisturbed portion of the wing and is, therefore, less able to resist the adverse pressure gradient at the trailing edge of the wing and so still separates before the flow on the surrounding airfoil. The modification increases the lift coefficient for similar drag but

does eliminate the separated flow structures. With the addition of the actuator disc, the fillet continues to offer some advantage in terms of reducing the interaction between the nacelle and wing boundary layers. The junction between the nacelle and propeller shows a reduction in the loss that originates from the junction. This effect seems to result in some increases in suction close to the leading edge and reduces the magnitude of the separated flow. The modification however once again increases the size of the flow separation that forms at the edges of the propeller wake and therefore it is also likely that this also impacts the nacelle structures and so it is difficult to determine if this local improvement is a direct result of the fillet.

Overall, the fillet, in particular, seems to offer some benefit in terms of performance but it is unable to eliminate the flow separation that is introduced by the nacelle. The flow expansion resulting from the high-pressure region behind the nacelle seems to be the dominant effect in terms of dictating the flow separation and therefore lowering the nacelle appears to be more effective. Further analysis including different configurations it likely required in order to further understand the problem.

This page is intentionally left blank

1

Introduction

Climate change is one of the key challenges facing humanity and in order to address it every industry is required to reduce emissions. The aviation industry must also rise to this challenge so that air transport can remain viable for the future. A key feature of many concepts that aim to reduce aircraft emissions is the use propellers. Propellers can achieve higher fuel efficiency than turbofan engines as a result of being able to achieve bypass ratios that far exceed what is possible with current turbofan technology [39]. In addition to this propellers offer the possibility of being electrically driven whether this be as part hybrid electric system, battery-driven aircraft or a hydrogen fuel cell configuration. These electrically driven propeller concepts have the potential to deliver even larger increases in efficiency and also allow for novel propulsion concepts such as distributed propulsion where multiple propellers can be used to blow the wing. This renewed interest in the use of propellers has made research into how the performance of propeller-wing systems can be maximised more pertinent than ever.

Exploring the possibilities of this technology for large passenger aircraft is one of the key goals of the Novel Aircraft Configurations and Scaled Flight Testing Instrumentation (NOVAIR) project, that this research forms a part of. As part of Delft University of Technology's contribution to the project one concept being investigated is leading edge mounted, electrically driven distributed propellers [44].

In addition to the potential efficiency advantages, the use of propellers also offer significant potential opportunities to increase aircraft performance in other ways. Positioning propellers on the wing leading edge results in them blowing the wing. The propeller wake increases the local dynamic pressure increasing the local wing lift coefficient and can help prevent stall [25][30]. This effect is particularly relevant when considering distributed propulsion concepts where a large number of propellers means that much of the wing is influenced by the wake of the propellers and therefore any lift augmentation effect is maximised [14]. If the increase in lift coefficient resulting from propeller wing interactions can be realised it can lead to an increase in the aircraft maximum payload mass or to reduced take-off distances. Alternatively, this can be used to reduce the complexity of the required high lift devices, reducing weight and therefore further improving aircraft performance.

Improving the performance of the high angle of attack propeller wing system can help to make propeller concepts more attractive. Propeller-wing interaction however result in a complex, closely coupled system that experiences strong mutual interference [40]. Investigating and understanding these interference effects will be key to maximising the performance of leading edge mounting propeller concepts. While the high dynamic pressure region undoubtedly offers the potential to increase the local lift coefficient, the complex 3D flow interaction effects can induce local stall regions. This study aims to understand and address these interactions such that the high angle of attack performance of a propeller-wing system can be maximised. Research is therefore conducted into the propeller, nacelle and wing interactions at high angles of attack for a leading edge mounted propeller configuration. The interaction effects that limit the performance in this flight condition are identified and a design study is conducted with the aim of maximising the performance of the combined system.

This report will present the methodology, results and conclusions from the investigation into propeller-nacelle-wing interaction effects at high angles of attack. Chapter 2 covers the theoretical background to the propeller-nacelle-wing interaction problem, exploring the current state of the art regarding the understanding and mitigation of the negative impacts of propeller nacelle wing interaction effects. Based on this literature survey a gap in current knowledge will be identified. Chapter 3 contains the research questions that are derived from the knowledge gap as well as defining the scope of the research project. Chapter 4 presents the methodology that is used to generate initial understanding of the propeller-nacelle-wing interaction problem through the use of experimental and numerical results. In addition to this, the chapter outlines the validation methodology that is used for the numerical model. Chapter 5 presents the wind tunnel testing results and provides details of the validation of the numerical model. Finally, this chapter presents the preliminary numerical results for the baseline configuration. Chapter 6 outlines the methodology that will be used to complete the development study into ways in which the interaction effects can be mitigated. Chapter 7 will present the results of the development study. Finally, Chapter 8 presents the conclusions of the research as well as suggesting recommendations for future studies.

2

Theoretical background

This chapter will outline the current state of the art regarding propeller-nacelle-wing interactions. It gives the theoretical background to the problem that is to be investigated and will identify the key gaps in current knowledge that will be used to form the basis of this study.

2.1. Nacelle-Wing Interaction Effects

The presence of a propeller nacelle modifies the flow over the wing and can influence the high angle of attack performance of a wing. This section will discuss the key interaction effects resulting from the integration of a nacelle.

2.1.1. Nacelle High-Pressure Region

Perhaps the most intuitive and obvious effect of installing a nacelle is that the pressure in the region of the wing directly behind increases. The nacelle effectively locally removes the leading edge. This eliminates the leading edge pressure peak and therefore results in a region of higher pressure on the upper surface [28]. This is shown in Figure 2.1. The high-pressure region behind the propeller creates a pressure gradient which becomes more significant at higher angles of attack, where the upper surface suction increases. Qiu et al. [28] show that this pressure gradient leads to streamline expansion behind the nacelle introducing a spanwise flow component. This can lead to boundary layer accumulation and growth as is shown in Figure 2.2. The boundary layer growth can make the wing more susceptible to local separation in the regions with a thicker boundary layer.

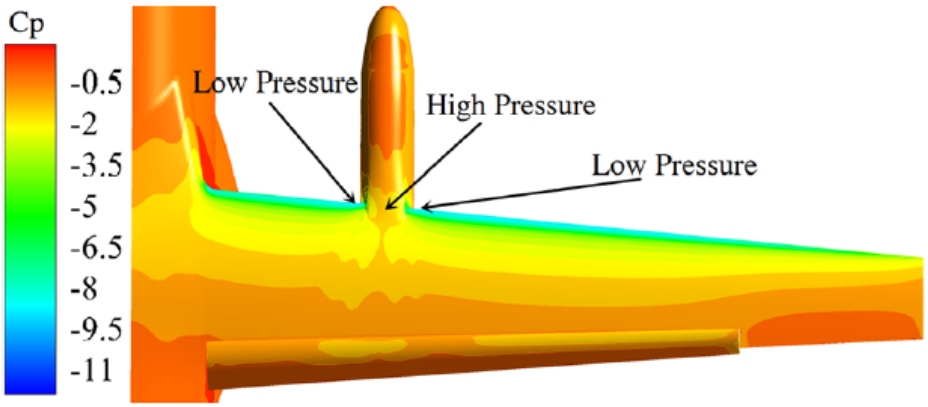

Figure 2.1: Surface static pressure coefficient distribution showing the high-pressure region found behind the nacelle [28]

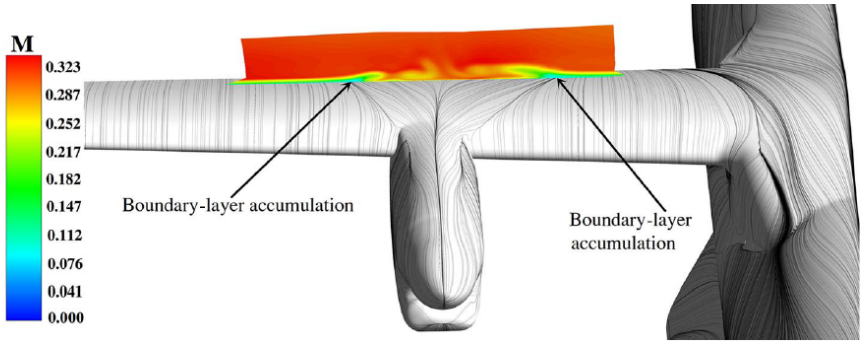

Figure 2.2: Surface streamlines and off surface mach number distribution indicating the influence of the nacelle on boundary layer growth [28]

2.1.2. Increase in Local Angle of Attack

In addition to the higher pressure region behind the nacelle, the nacelle also alters the wing inflow conditions in the regions directly adjacent to it. A propeller nacelle is typically either roughly cylindrical or rectangular in shape and at high angles of attack, there is a significant flow component perpendicular to the nacelle centre line. As this vertical flow component passes the nacelle it accelerates. Flow perpendicular to a cylinder, is well understood. In the case of 2D flow perpendicular to a cylinder the velocity at the point 90 degrees from the free stream is double the free stream velocity [2] and while the flow over a rectangle with rounded corners is a little more complex than a cylinder, the flow similarly accelerates [8]. This leads to the effective increase of the vertical velocity component in the region close to the maximum width point of the nacelle causing a local increase the angle of attack seen by the wing [28]. An example of the resulting angle of attack distribution due to the nacelle is presented in Figure 2.3. The increase in local angle of attack increases the magnitude of the leading edge pressure peak. The increase in the magnitude of the leading edge pressure peak requires a more aggressive pressure recovery close to the leading edge that can lead to boundary layer growth. At high angles of attack the induced angle of attack increase can lead to the early onset of separation in the region directly adjacent to the nacelle.

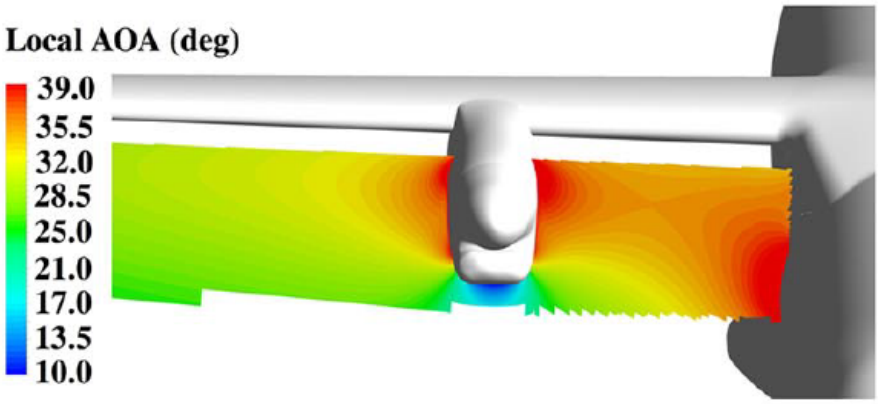

Figure 2.3: The local flow angle distribution at a plane in front of the wing leading edge showing the angle of attack increase close to the nacelle [28]

2.1.3. Nacelle Vorticity

Finally, the nacelle also introduces off-surface flow structures that can influence wing performance. At higher angles of attack, a nacelle introduces two discreet vortices due to flow separation on the top of the nacelle [15]. A schematic representation of the vortices is indicated in Figure 2.4. The presence of the vortex structures can have a significant effect on the high angle of attack and stall behaviour of a wing. At high angles of attack and landing condition Reynolds numbers (around 12 million in the case described by Hasan [15]) the flow separates on the upper surface of the nacelle leading to the formation of two nacelle vortices that then pass over the wing. These vortices carry significant

momentum and can help with boundary layer mixing which can help to delay stall but can also cause local boundary layer growth if the structures break down. The vortices shed by the bluff body of the nacelle are often shed particularly cleanly and therefore are more prone to bursting when subjected to an adverse pressure gradient (for instance when interacting with a flap) which can lead to vortex bursting [17]. The burst vortex can interact with the flap resulting in a reduction in flap suction or even separation [26]. In this way, the vortex bursting can cause the flap to separate or at least reduce the flap loading [18]. This bursting effect shown in Figure 2.5 is unlikely to be critical in the case without the presence of a flap or other similar features.

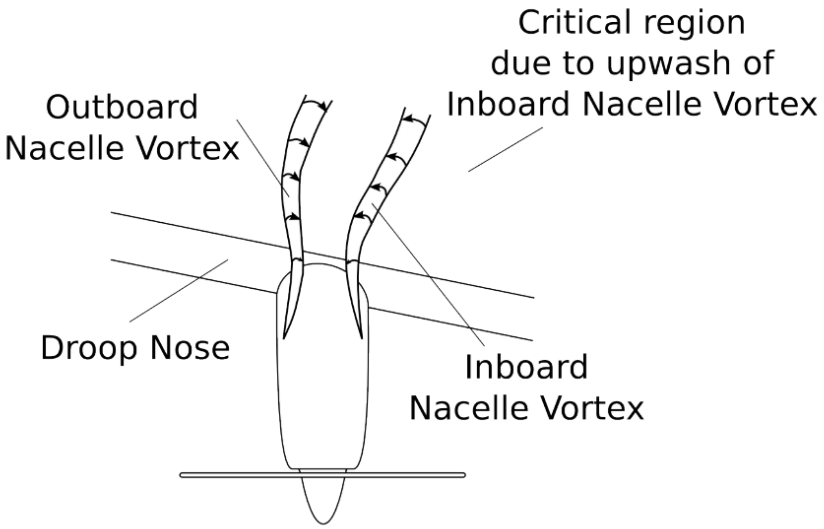

Figure 2.4: Sketch showing the key nacelle vortex structures shed from a propeller nacelle at high angles of attack [15]

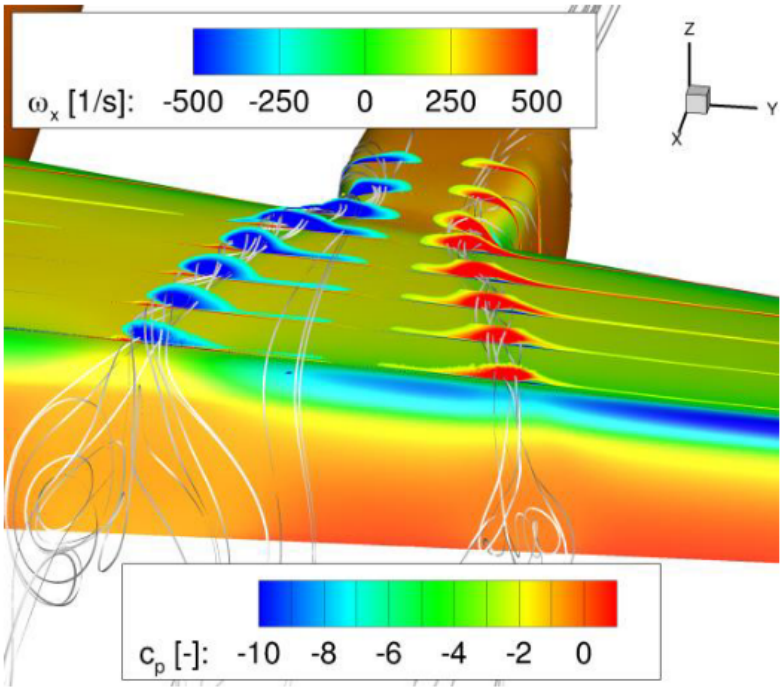

Figure 2.5: Surface static pressure distribution and vorticity slices showing the nacelle vortex bursting as it passes over the flap leading to a loss of suction on the flap [29]

The interaction between the nacelle and wing has a significant impact on the wing behaviour at high angles of attack. The combination of the interaction effects listed above can lead to early onset of stall and therefore a reduction in wing maximum lift coefficient as is shown in Figure 2.6 [28].

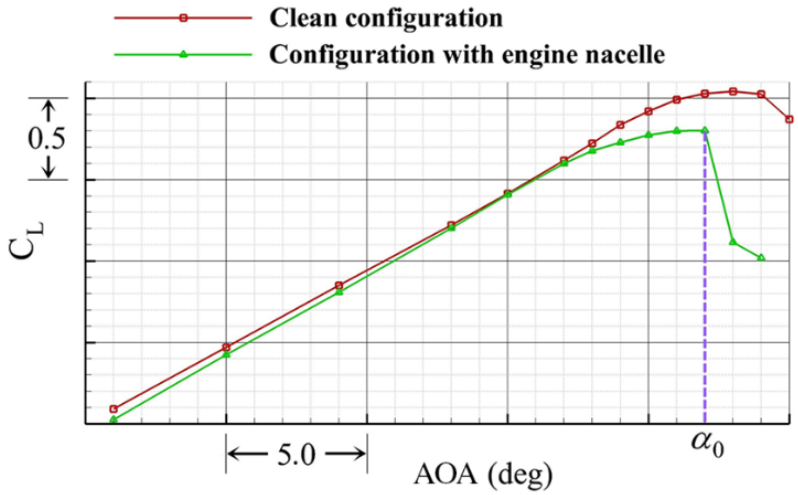

Figure 2.6: Lift polar for a wing with and without nacelle attached for the configuration shown in Figures 2.1 to 2.3 [28]

2.2. Propeller-Wing Interaction Effects

In addition to the interaction effects that result from the nacelle, the interactions between the propeller wake and the wing will have a significant effect of the wing lift performance.

2.2.1. Distortion of Lift Distribution

The importance of propeller wing interactions was first noted in 1921 by Prandtl [27] who described how the combination of the variations in velocity and directions of air currents produced by the propeller influenced wing behaviour. In addition to this, he emphasised the importance of not treating the propeller and wing in isolation when considering the wing lift and drag.

The propeller wake substantially alters the inflow conditions of the wing resulting in significant distortion of the wing lift distribution. Veldhuis described in 2004 [40] how the propeller slipstream results in a ”strong deformation of the wing loading distribution”. Perhaps the most significant effect is that the high dynamic pressure behind the propeller blows the wing increasing the upper surface suction resulting in a local increase in local lift in the region of the propeller[24]. In addition to this, the propeller rotation causes the propeller wake to swirl inducing asymmetric changes in the local angle of attack. The up-going blade side increases the local angle of attack while the down-going blade side reduces the angle of attack [41]. The effect of the combination of these effects on the lift distribution is presented in Figure 2.7.

The theoretical impact of the lift distribution is nicely summarised by Veldhuis [40] in Figure 2.7 which shows the expected impact of these propeller wake effects on the wing. Veldhuis [40] suggests that the influence of the propeller on the wing can be broken down into four main sections, W-I to W-IV. In the inboard up case (the solid line in Figure 2.7), section W-II experiences an increase in local angle of attack due to the swirl and increased dynamic pressure due to the propeller wake. The combination of these two effects leads to a peak in lift coefficient. In region W-III the two propeller slipstream effects counteract each other with the effective angle of attack being reduced due to swirl but the wing still experiencing an increase in lift due to the increase in dynamic pressure behind the propeller. This results in a decrease in local lift coefficient however as the swirl and dynamic pressure effects counteract each other the magnitude of the lift coefficient reduction is smaller than the lift augmentation in section W-II and in some cases the depending on the balance of swirl and the increase in dynamic pressure the net result may still be an increase in lift compared to the un-blown case. The regions W-I and W-IV also experience a distortion in lifting distribution as a result of the distorted vorticity sheet leaving the wing

however this effect is comparatively smaller. In the outboard up case the dashed line in Figure 2.7) the effects experienced by W-II and W-III are inverted. The changes in the vortex sheet therefore also change the influence on sections W-I and W-IV.

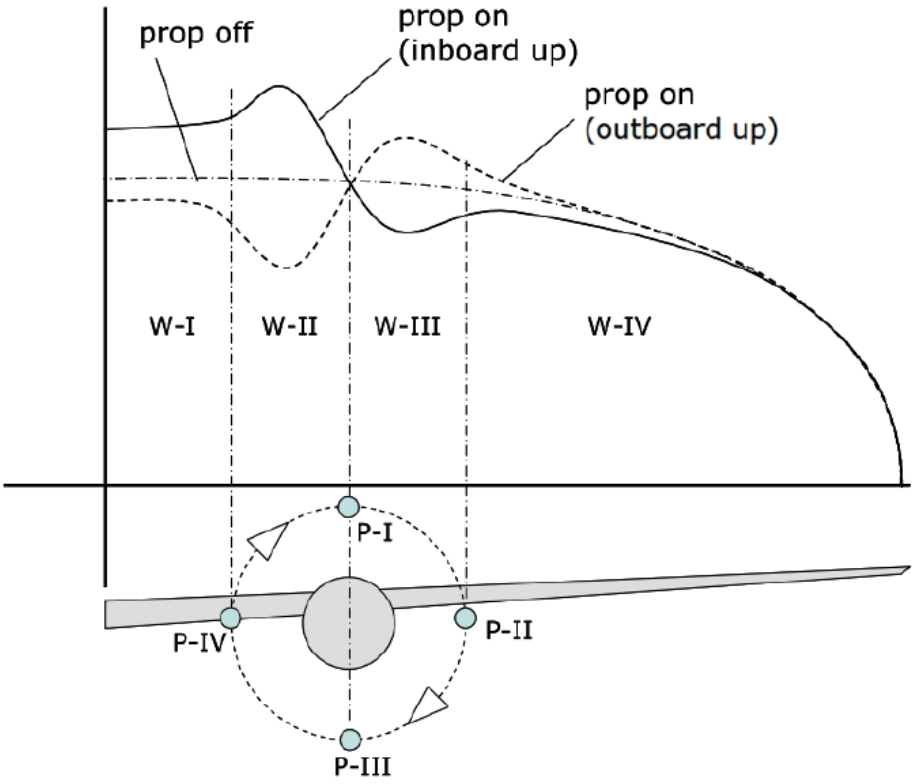

Figure 2.7: Diagram showing the predicted influence of the propeller wake on the wing lifting distribution [40]

2.2.2. Boundary Layer Effects

In addition to the macro effects on the lift distribution, the presence of the propeller wake affects the boundary layer formation on the wing. The propeller injects high velocity, high energy flow into the boundary layer. As this flow interacts with the wing it can modify how the boundary layer grows. Brenckmann [6] observed that at higher angles of attack the centre of pressure moves further aft in the presence of a slipstream compared to a wing in free stream. He suggests that this is the result of delaying trailing edge separation. Brenckmann [6] suggests that the primary cause of this destalling effect is the added velocity within the slipstream injecting energy into the boundary layer making it more resistant to flow separation.

Catalano [9] analysed the effect of the propeller on the boundary layer transition location using the sublimation technique (a flow visualisation technique that uses a chemical that sublimates at different rates depending on if the flow is laminar or turbulent allowing for easy determination of the transition location [20]). He concluded that the region in the propeller wake underwent transition more or less immediately near the leading edge. The propeller wake influences not only the region directly behind the propeller but due to viscous mixing and interference with the wing the wake's influence grows. The early transition prevented the formation of a laminar separation bubble. The transition location in the propeller wake was not greatly impacted by the propeller swirl in Catalano's experiments. In addition to this using hot wire measurements Catalano [9] noted that with each passing blade, turbulence and velocity was injected into the boundary layer. This produces a cyclic change in the boundary velocity. This is shown in Figure 2.8 where clear 'ridges' can be seen in the boundary layer velocity distribution that corresponds with each passing blade.

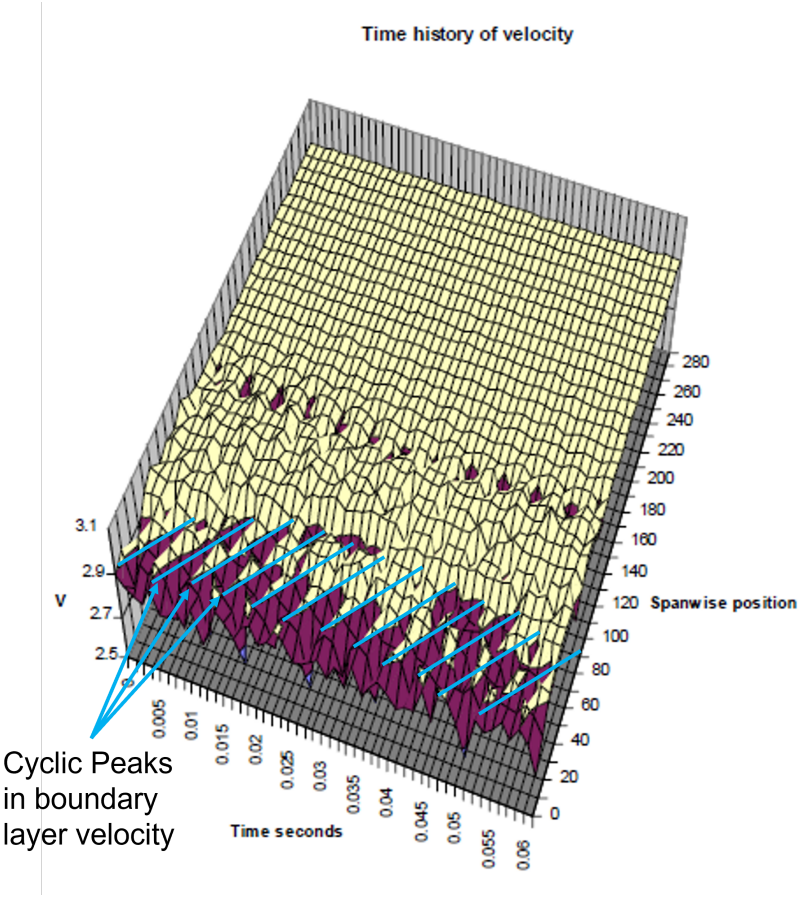

Figure 2.8: The time evolution of the boundary layer velocity based on hot wire measurements for a wing with a tractor propeller (modified based on the work of Catalano [9])

This effect is further discussed by Miley and Howard [22] who performed hot wire measurements behind a propeller in both the wind tunnel and in flight. They suggest that the periodic shedding of viscous wake by each passing blade can result in the wing boundary layer oscillating between laminar and turbulent. A diagram of this effect is illustrated in Figure 2.9. This effect occurs when the pressure gradient is favourable for laminar stability and the blade passage frequency is low enough to allow for the boundary layer to recover. It is therefore unlikely to be observed at high angles of attack where the pressure gradient is not favourable. The periodic injection of velocity and turbulence from the blade wake results in higher resistance to turbulent separation. This result goes some way to understanding Brenckmann's results.

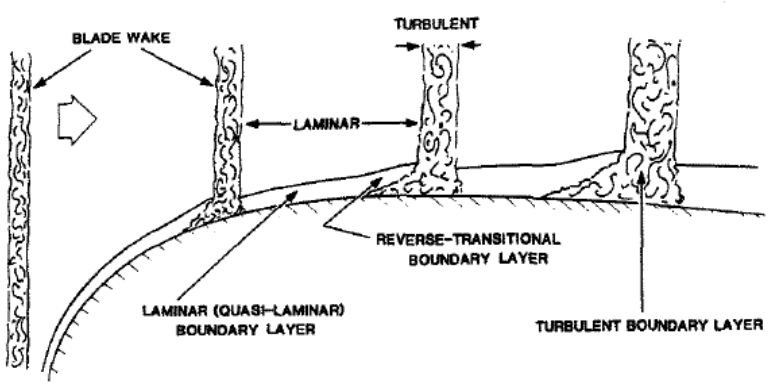

Figure 2.9: Diagram showing the effect of the propeller wake on the boundary layer turbulence indicating the regions of turbulence originating from the propeller wake [22]

2.2.3. Wing Impacts on Propeller Performance

Although the main focus of this study is to investigate the influence of the propeller on the wing performance the propeller-wing system is extremely closely coupled and therefore it is not possible to look at the effect of the propeller wake on a wing without considering how the wing influences the propeller wake and inflow. This in turn effect may have an impact on the wing performance.

The presence of the wing distorts the propeller wake but also directly influences the propeller performance which in turn indirectly influences the wing performance. Veldhuis [40] indicates that the presence of the up-wash due to the wing alters the local angle of attack of the blades differently throughout their rotation resulting in a difference in blade loading during one rotation. The vertical component due to the wing has the effect of increasing the effective angle of attack of the blade on the down-going blade side (azimuthal angle of 90° for a counterclockwise rotating blade). The effect on the up-going blade side (azimuthal angle of 270° for a counterclockwise rotating blade) is an effective reduction in the angle of attack. This is sketched in Figure 2.10.The difference in angle of attack results in a change in the propeller lift across the propeller disc introducing asymmetric propeller loading. This loading asymmetry must be accounted for when considering the propeller wake and how it interacts with the wing.

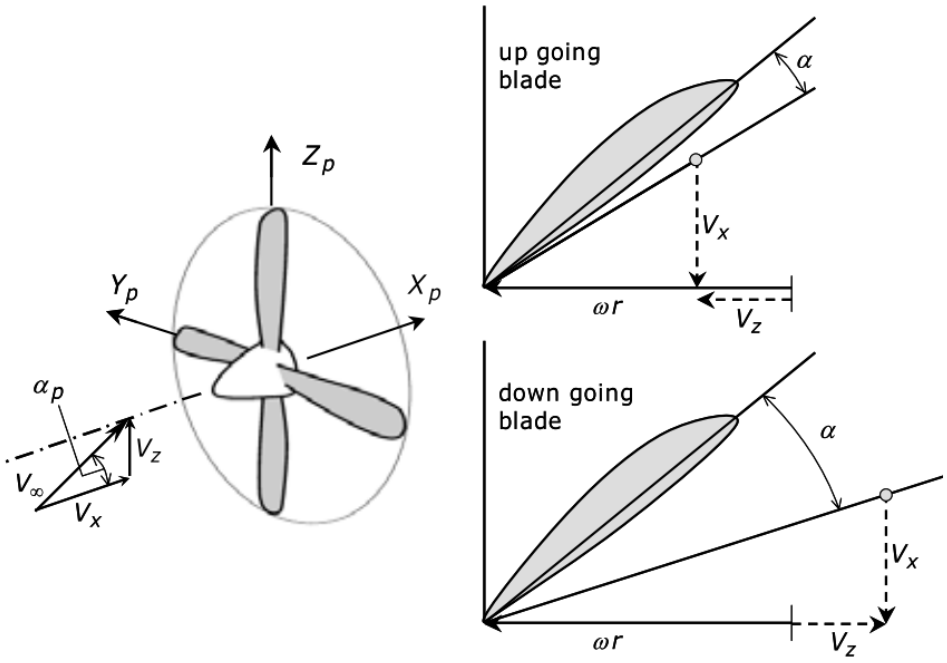

Figure 2.10: Sketch indicating how the wing up-wash introduces asymmetrical angle of attack variations on the propeller blades [40]

The presence of the wing reduces the swirl velocity component in the propeller wake in a similar way to the stator vanes in a turbine. Veldhuis [41] writes that both numerical and experimental studies have found this result. They suggest that this effect and the magnitude of the reduction in swirl velocity is dependent on a variety of factors such as the propeller location and power setting as well as the wing loading. Veldhuis suggests that the most important aspect that causes this effect is the reduction in helix angle due to the wing upwash generated in front of the wing. The flow coming from down going blade side is directly reduced due to the upwash produced by the wing. The helix angle on the up-going blade side is reduced due to the increased downwash behind as a result of the wing lift due to the propeller augmentation. Given the importance of swirl on the wing lift distribution shown in Section 2.2.1 it is clear that this swirl reduction effect will have an effect on the wing performance and therefore must be modelled when considering the impact of a propeller on wing performance. This swirl recovery also has the effect of increasing the propeller efficiency by reducing the swirl losses.

In addition to the swirl recovery effect, the flow rotation can lead the slipstream to deform as is described by Leng et al. [21]. The wing shears the propeller wake due to interaction between the rotating wake and the solid surface of the wing. The differences in angle of attack induced by the wake rotation produce a spanwise pressure gradient [13]. In the case of a symmetric wing at zero angle of attack the upper and lower portions of the wake experience an equal shearing in opposite directions with the wake on the upper surface of the wing being translated towards the down-going blade side and the wake on the lower surface being translated towards the up-going blade side [21]. In the case of an asymmetric wing or a symmetric wing at a non zero angle of attack airfoil, the wake does not simply shear as in the symmetrical case. In addition to the wake shearing the downwash induced by the circulation on the forward portion of the wing results in the lower surface wake being stretched downwards and the upper surface wake being 'crushed' against the wing surface resulting in a T-shaped wake. Leng et al [21] observed this phenomenom by deflecting a flap on their wing. This is shown in Figure 2.11.

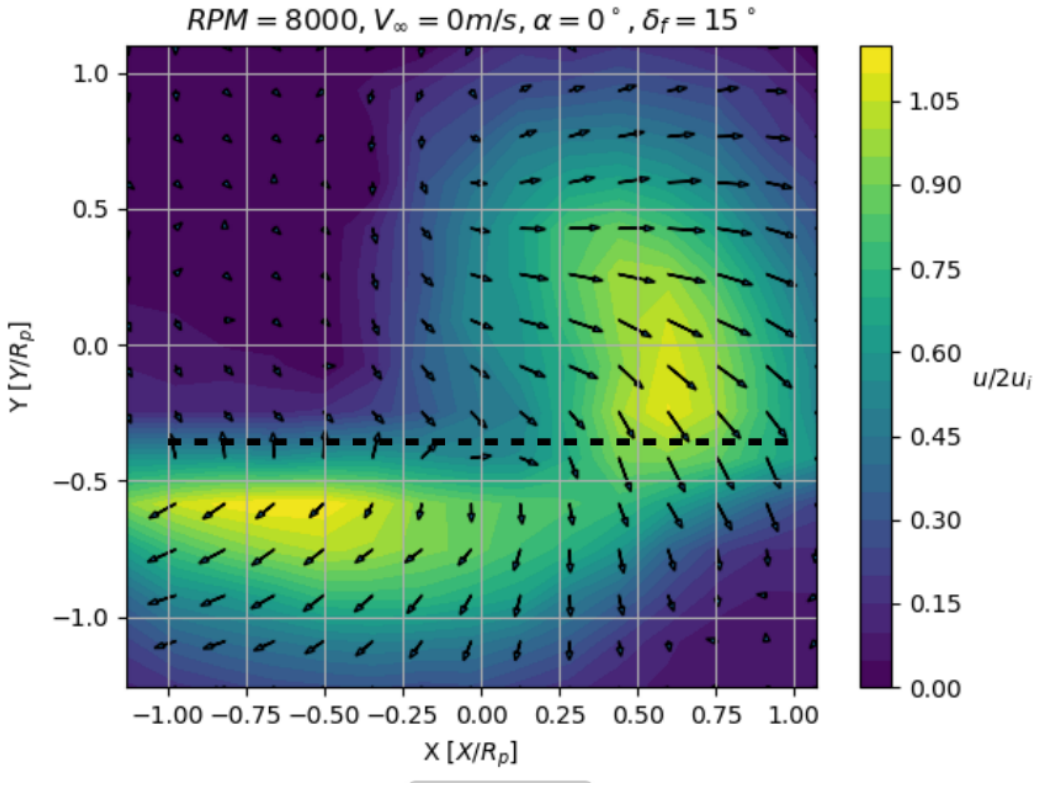

Figure 2.11: Velocity distribution behind the wing based on a wake survey carried out using a five-hole probe for a wing with flap deflected 15° downwards [21]

Not accounting for this deformation effect may lead to an incorrect prediction of the wing lift distribution if a simple cylindrical propeller wake is assumed therefore although this effect primarily concerns the propeller wake is has a direct effect on the wing performance.

2.2.4. The Impact of the Propeller on Wing Nacelle Interactions

The presence of a propeller seems to help mitigate some of the negative stall effects produced by the nacelle. Keller and Rudnik [17] describe how the additional energy delivered to the boundary helps to alleviate total pressure losses within the vortices which reduces boundary layer growth and delays breakdown. Additionally, the higher velocity behind the propeller reduces the local angle of attack induced by the nacelle which further helps to delay stall. The result of this is that in the configuration used by Keller and Rudnik [17] (a wing with a turboprop, leading edge droop and a blown trailing edge flap) the maximum lift angle of attack is increased from 7° to 20° which represents a substantial increase in maximum lift angle of attack however still falls short of the 23° seen in the clean wing configuration.

The stall behaviour found in this experiment is compared in Figure 2.12. The presence of the propeller eliminates the limiting trailing edge stall on the flap inboard of the nacelle. While there is a recirculating region on the outboard of the flap this was compensated by an increased pressure peak at the flap leading edge resulting in no overall loss of lift. The limiting effect in the case with nacelle was leading edge separation at the wing root as a result of the interaction with the fuselage. This effect was aggravated by the increased local angle of attack due to the propeller [17].

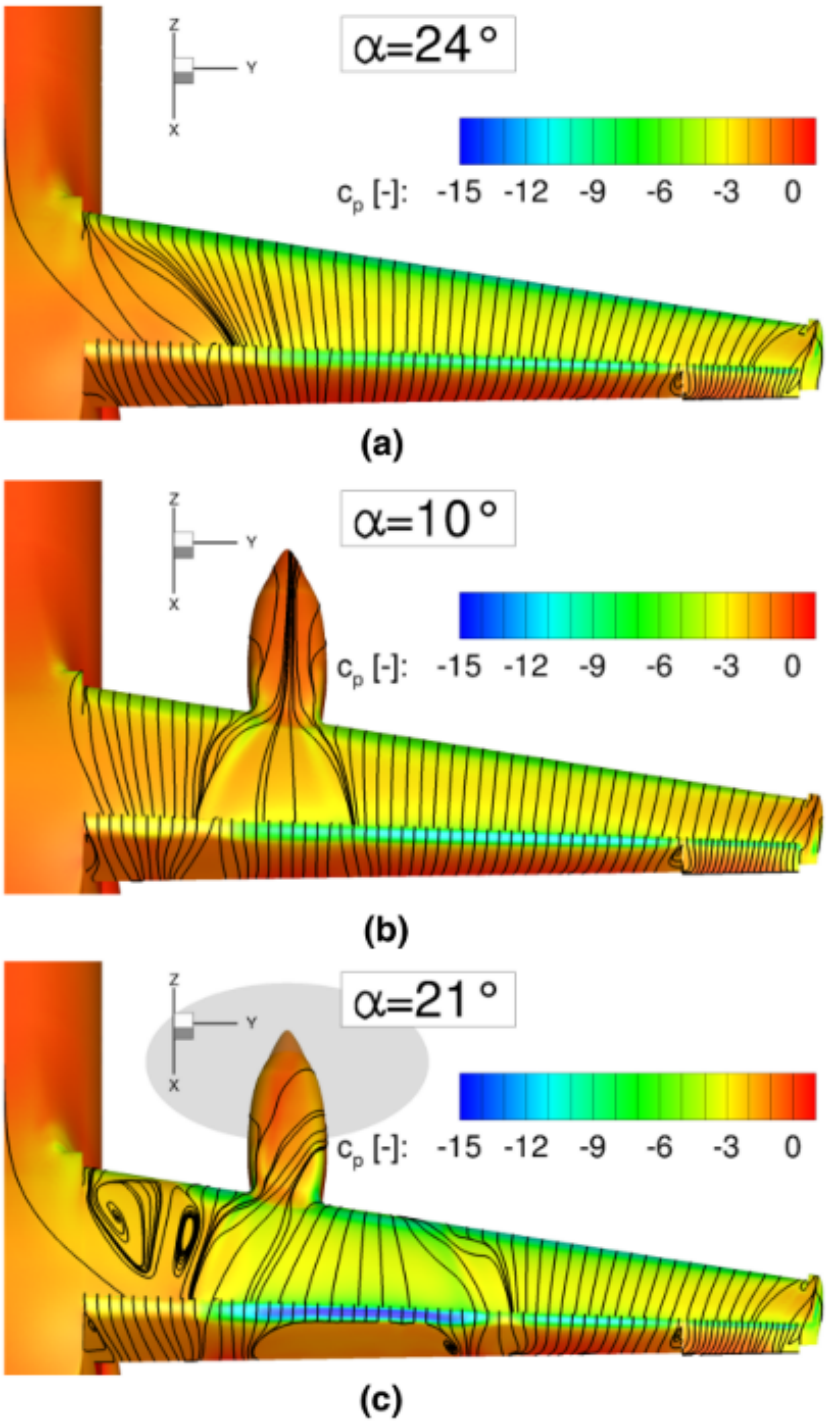

Figure 2.12: Surface streamlines and static pressure coefficient distribution of the clean wing (top), wing with nacelle (middle) and wing with nacelle and propeller rotating inboard up (bottom) at their respective maximum lift angle of attack. From RANS simulations with an actuator disc carried out by Keller and Rudnik [17]

Zhang et al. [43] look at the combination of a nacelle and propeller. The stall behaviour is quite distinct from that shown by Keller and Rudnik [17]. This behaviour is presented in Figure 2.13. Zhang et al. [43] observed that at the relatively low angle of attack of 6° the propeller swirl induces a trailing edge separation that is not present in the propeller off configuration. At higher angles of attack the propeller does appear to reduce some of the trailing edge separation seen in the propeller off configuration but overall the nacelle effects appear to remain dominant in determining the stall mechanism. This is in stark contrast to Keller and Rudnik who observed a complete change in stall behaviour.

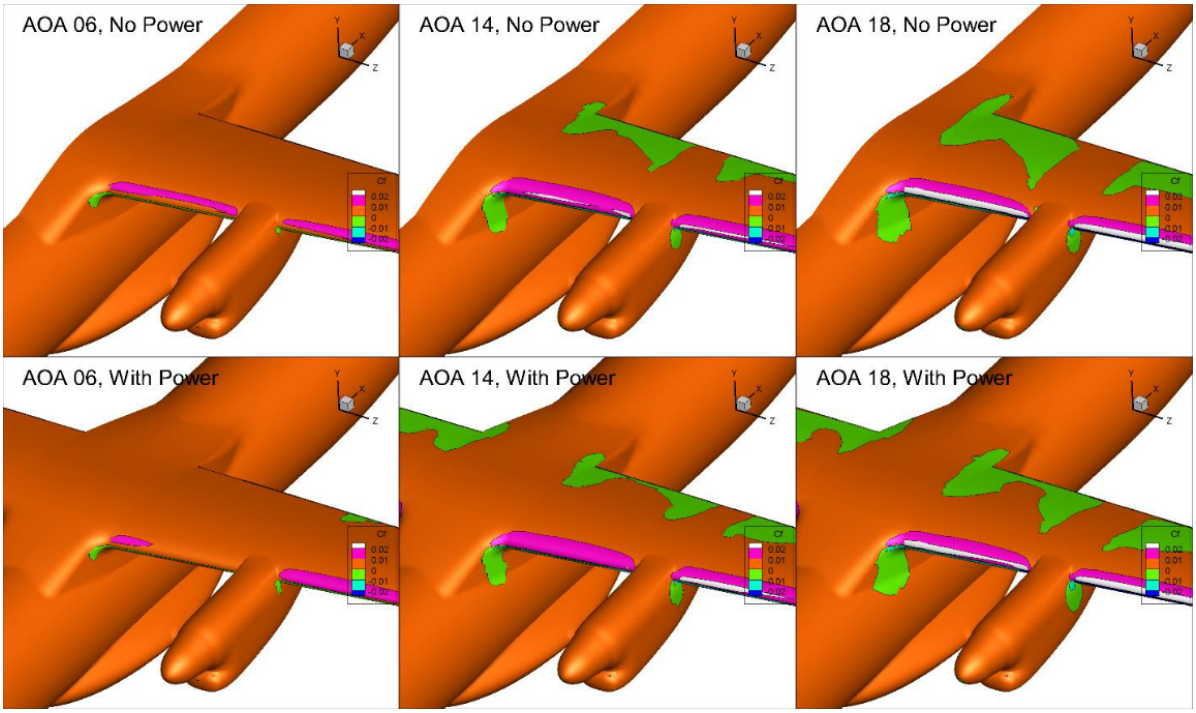

Figure 2.13: Surface friction coefficient distribution for three angles of attack in the case with only a nacelle (top) and with a clockwise rotating propeller and nacelle (bottom) [43]

2.3. Impact of Multiple Propellers

Distributed propulsion concepts use multiple propellers to generate thrust. The interaction effects of these propellers is therefore important when considering such a concept. This section will outline the research into the interaction effects between multiple propellers and the wing. The impact on the high lift and stall behaviour will be studied.

Staggered, overlapping propeller configurations such as those studied by Kuhn and Draper [19] will not be considered in significant detail. As was suggested by Usai [36] these configurations result in a significant loss of performance for the rear propeller as. result of the impinging of the front slipstream on the rear propeller. Given that the goal of this project is to maximise performance and most modern concepts do not use overlapping propellers this is considered to not be of interest at this stage.

2.3.1. Distortion of Lift Distribution

Aref et al. [3] used a series of numerical simulations to investigate propeller-wing interactions effects of the four-engined C130J aircraft. Simulations were completed for a variety of propeller rotation configurations. The resultant lift distribution for a co-rotating case is presented in Figure 2.14. Comparing the lift distribution for the case with both propellers installed with the single propeller cases in Figure 2.14 Aref et al. [3] observed that in the region between the two propellers the lift is higher than in the single propeller cases however elsewhere the lift distribution is largely similar to the single propeller case. The magnitude of the peaks in lift coefficient as a result of the propeller do not increase in the multiple propeller case when compared to the isolated propellers. Something of note is that in the case of a single outboard propeller the influence on the wing lift distribution does extend far inboard and therefore

if a simple superposition was considered some interaction between the inboard and outboard propeller would be expected. However, in the case with both propellers, there is no observable augmentation of the peak behind the inboard propeller suggesting that the wake of the inboard propeller is not significantly altered by the influence of the outboard propeller. The distribution that results from multiple propellers is relatively close to a simple superposition of single propeller lift distributions and therefore does not introduce any strong new interaction effects.

Aref et al. [3] also simulated several perturbations of this configuration by looking at the two cases where the propellers rotate in opposite directions. This result is presented in Figure 2.15. Aref et al. [3] point out that the propeller rotation direction has a significant effect on the overall lift distribution and likely has a significant effect on the aircraft control and stall characteristics. Perhaps, the case with the strongest interaction effect occurs when both propellers generate up-wash in the centre (inboard propeller counterclockwise and outboard propeller counterclockwise). In this case, the lift in the region between propellers is higher than in the single propeller case however it is still not the limiting point in terms of lift coefficient. Interference between multiple propellers do not result in a significant magnification of the lift coefficient distortion compared to the superposition of multiple single propellers.

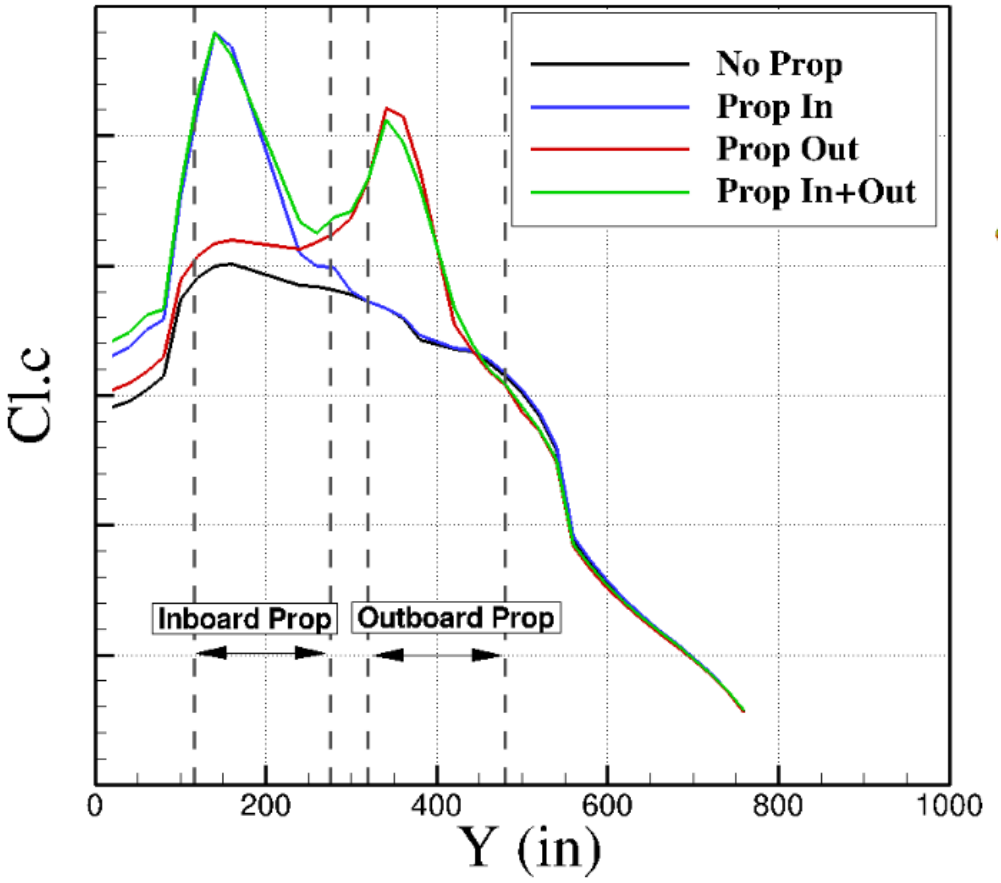

Figure 2.14: Spanwise lift coefficient multiplied by local chord for the inboard and outboard propeller in isolation and together in a co-rotating configuration for the C130J aircraft [3]

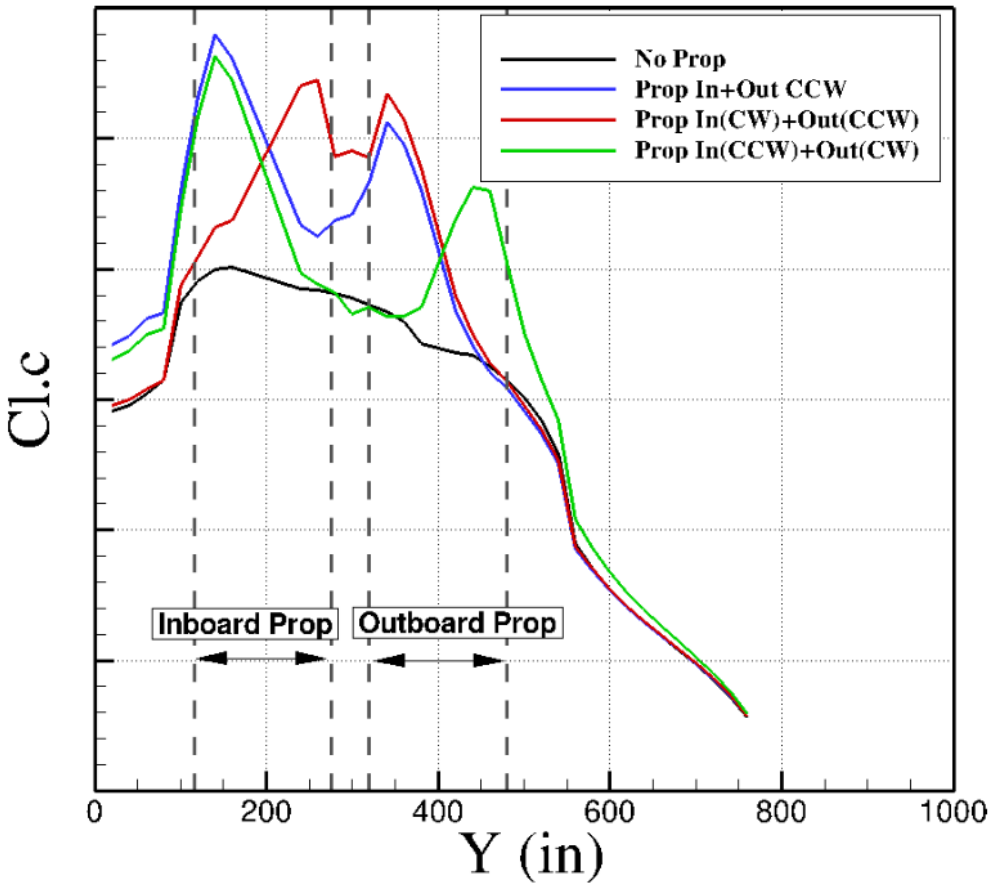

Figure 2.15: Spanwise lift coefficient multiplied by local chord for all the permutations of co-rotating a counter-rotating propeller configurations on the lift for the C130J aircraft [3]

2.3.2. Lift and Stall Behaviour

Aref et al. [3] investigated the stall characteristics of the C130J with no propellers, one propeller and both propellers fitted for a variety of angles of attack. The pressure coefficient and iso-surfaces for this are shown in Figure 2.16. Aref et al. [3] note that without the propellers the flow separated first behind the nacelle at an angle of attack of 11° which is consistent with what was shown in Section 2.1. However, the presence of a single propeller can aggravate the nacelle stall. In the case with both propellers installed the stall is delayed.

Reckzeh [30] suggests that on the A400M, an aircraft with four propellers that blow much of the wing, the impact of propeller blowing can contribute almost as much additional lift as the high lift devices. The A400M was designed with counter-rotating propellers. This was done as this proved to be the best compromise between cruise and high lift performance [30]. The propellers were found to have a strong influence on stall and in a co-rotating configuration introduced asymmetry which would have required significantly limiting the flight ranges at the border of the envelope resulting in reduced performance [30]. This effect is however not a result of mutual interaction but rather a consequence of the extremely asymmetrical lift distortion introduced by the propeller and therefore when mounting multiple propellers the symmetry of this behaviour should be considered.

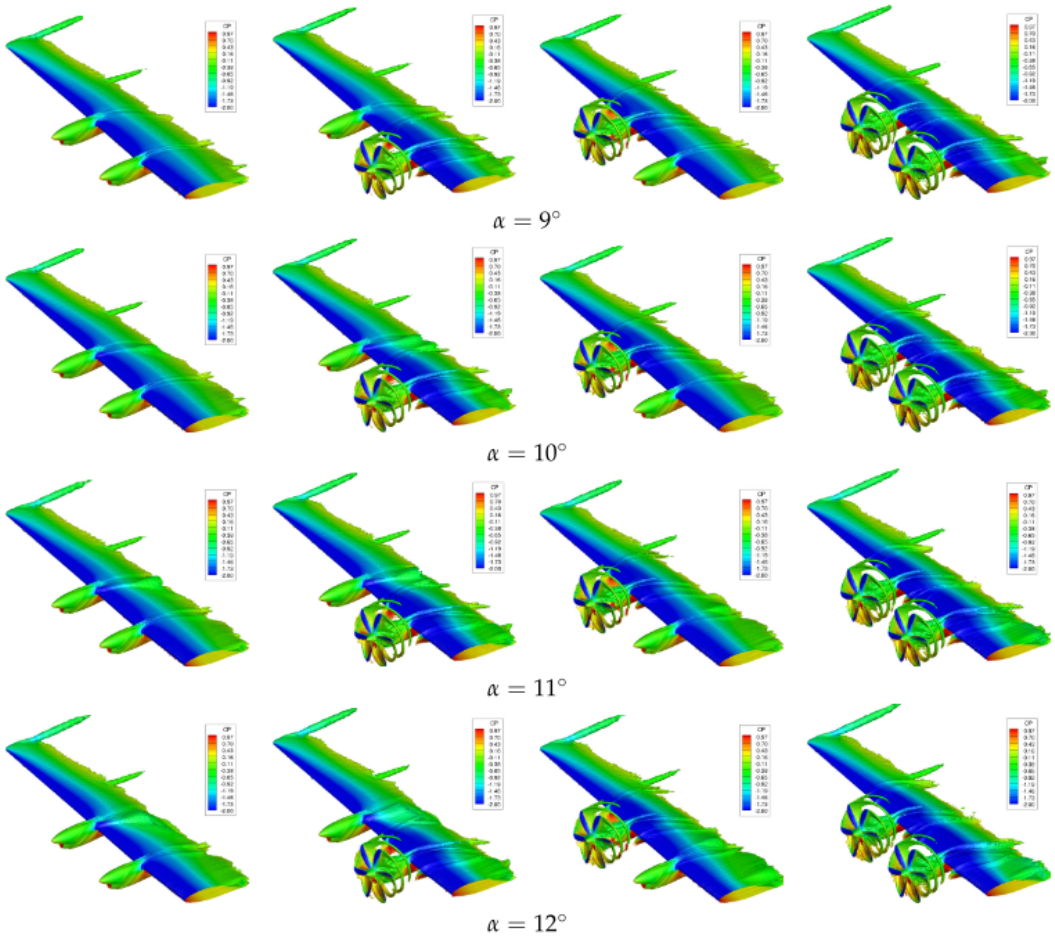

Figure 2.16: Surface static pressure distribution showing the effect of the inboard and outboard propeller in isolation and together on the stall behaviour for the C130J aircraft [3]

2.3.3. Nacelle Blockage

Increasing the number of propellers mounted on the wing also results in an increase in the number of nacelles. The increase in the number of nacelles will increase the blockage and therefore will augment the effects described in Section 2.1.2[10]. In addition to this De Vries et al. [10] describe how in the propeller in the presence of multiple nacelles results in a reduction of thrust. The propeller experiences an increase in inflow velocity due to the blockage of the adjacent nacelles resulting in a reduction in thrust. The blockage limits the contraction of the upstream stream tube resulting in higher flow velocities at the propeller. In their testing, De Vries et al. [10] found that the impact of the nacelles was more significant than the effect of the adjacent propellers themselves. This effect resulted in roughly a constant offset in thrust coefficient in the case with multiple side by side propellers when compared to the case with the isolated propeller. The reduction in thrust coefficient has been shown to result in the reduction of the lift curve slope [41]. The nacelle blockage and propeller wake interaction effect is schematically indicated in Figure 2.17.

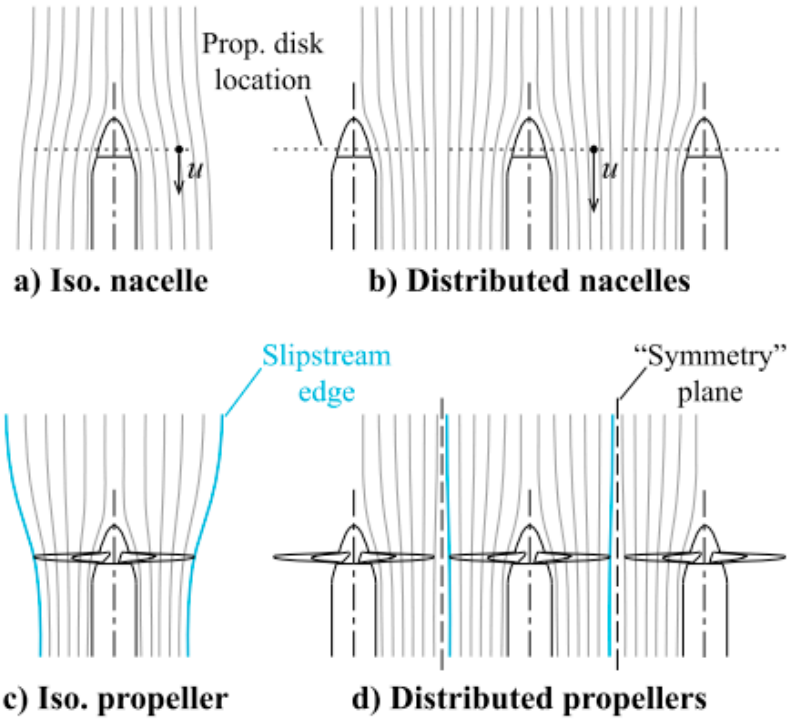

Figure 2.17: Diagram indicating the effect of multiple nacelles and propellers on the propeller streamlines and stream tube [10]

2.4. Nacelle and Wing Modifications

As part of previous research, attempts have been made to increase the high angle of attack performance of propeller wing systems. Details of these modifications are detailed below.

2.4.1. Nacelle Strakes

Nacelle strakes are angled plates attached to the side of the nacelle with the intention to generate a vortex that can suppress the nacelle vorticity and help to energise the boundary layer to delay stall. Drawings showing these devices are presented in Figure 2.18. Higher bypass ratio turbofans have lead to wide application of these strakes to turbofan nacelles to delay stall. High bypass ratios have resulted in nacelles becoming considerably larger. These larger high bypass ratio, larger nacelles produce more powerful vortices and have a larger effect on the flow passing over the wing adversely affecting wing high lift performance leading to early onset of lift breakdown [33][42][11]. More powerful, larger turboprop engines that are currently employed on modern turboprop aircraft require larger nacelles and therefore start to encounter similar problems to those faced by turbofan engines. The concept of nacelle strakes has therefore also been applied to turboprop nacelles for instance on the A400M [30].

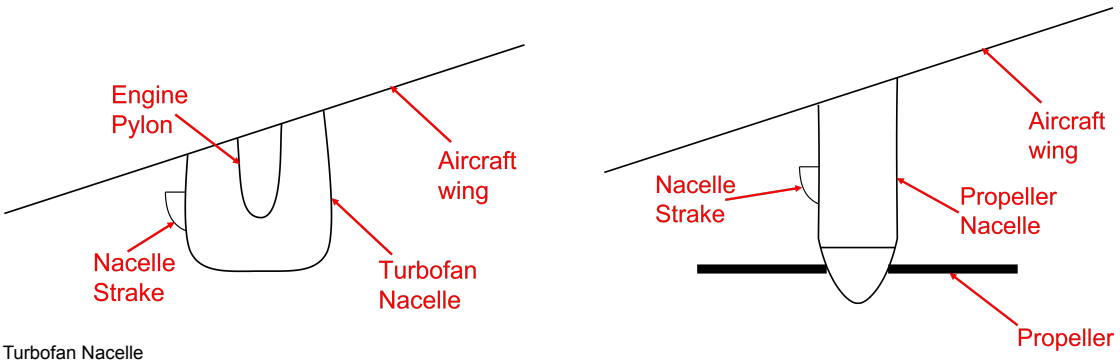

(a) Turbofan Nacelle

(b) Propeller Nacelle

Figure 2.18: Drawings indicating nacelle strakes on a turbofan and propeller nacelle

Hasan [15] examined the installation of nacelle strakes to delay stall for a hypothetical STOL turboprop aircraft proposed by DLR to reduce emissions and travel time as part of the Flightpath 2050 program. They use the nacelle strake to suppress the boundary layer growth associated with the weak nacelle vorticity that is shed from the top surface of the nacelle (as described in Section 2.1.3) in order to improve the stall characteristics. Hasan investigated various strake configurations using numerical simulations. The results of this analysis are shown in Figure 2.19. It shows that the presence of the strake vorticity suppresses the nacelle vortex growth. This in turn delays the trailing edge separation on the flap and therefore increases the maximum achievable lift coefficient and the angle of attack of maximum lift. The lift polar with and without the strake is shown in Figure 2.20. As can be seen, the maximum lift coefficient is increased significantly. Moreover, the stall behaviour is much more progressive.

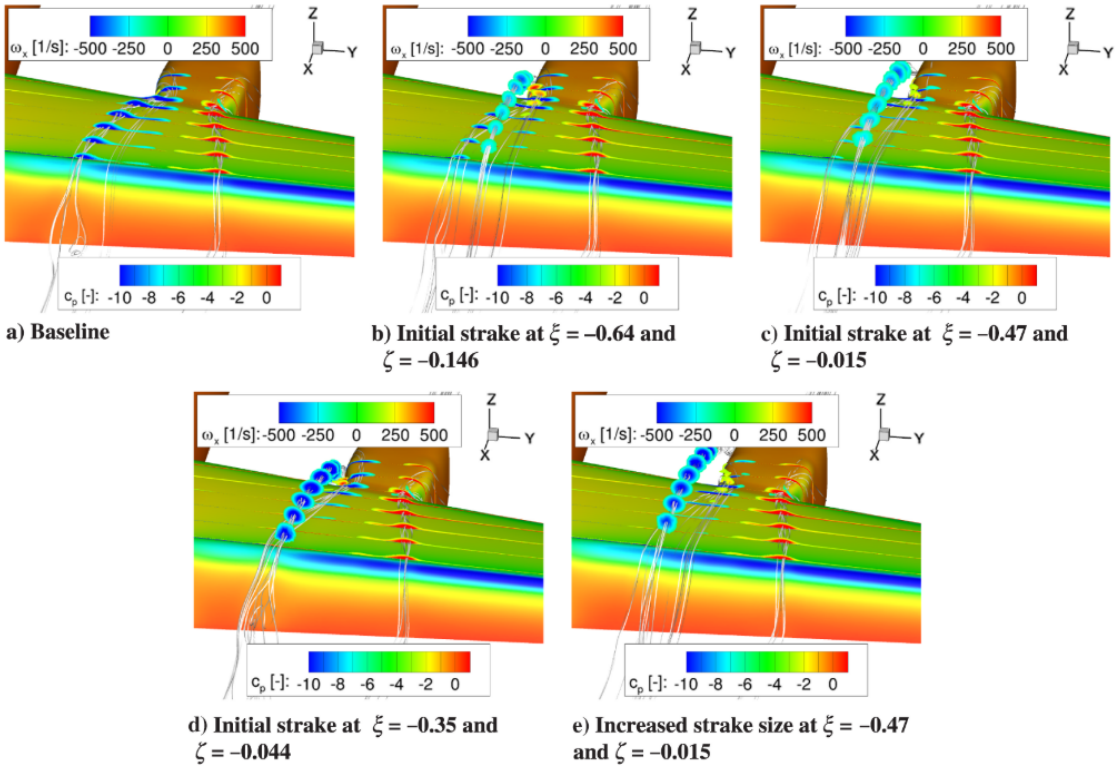

a) Baseline

b) Initial strake at $\xi = -0.64$ and $\zeta = -0.146$

c) Initial strake at $\xi = -0.47$ and $\zeta = -0.015$

d) Initial strake at $\xi = -0.35$ and $\zeta = -0.044$

e) Increased strake size at $\xi = -0.47$ and $\zeta = -0.015$

Figure 2.19: Surface static pressure distribution and vorticity slices showing the effect of various nacelle strake configurations on the nacelle vortices at angle of attack of 6° [18]

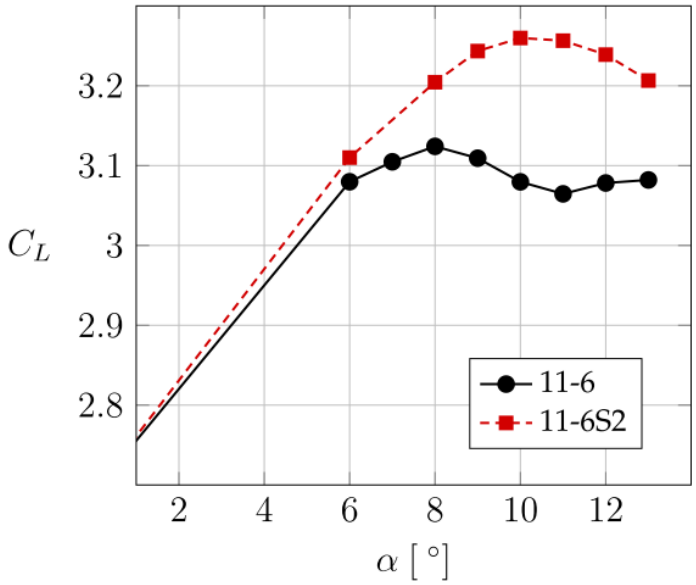

Figure 2.20: Wing lift polar for the wing with (11-6) and without (11-6S2) the nacelle strake [15]

It is clear that the use of a strake is effective at improving the wing stall characteristics induced by the nacelle. As part of the paper written by Keller et al. [18] the impact of the strake on the nominal condition with the propeller running was considered. Figure 2.21 shows that the presence of the strake has a significant impact on the un-blown maximum lift angle of attack and maximum lift coefficient however with the propeller installed the stall behaviour is virtually identical. This suggests that while the use of a strake is effective in improving the propeller off stall behaviour it does little to improve the powered lift performance in this case.

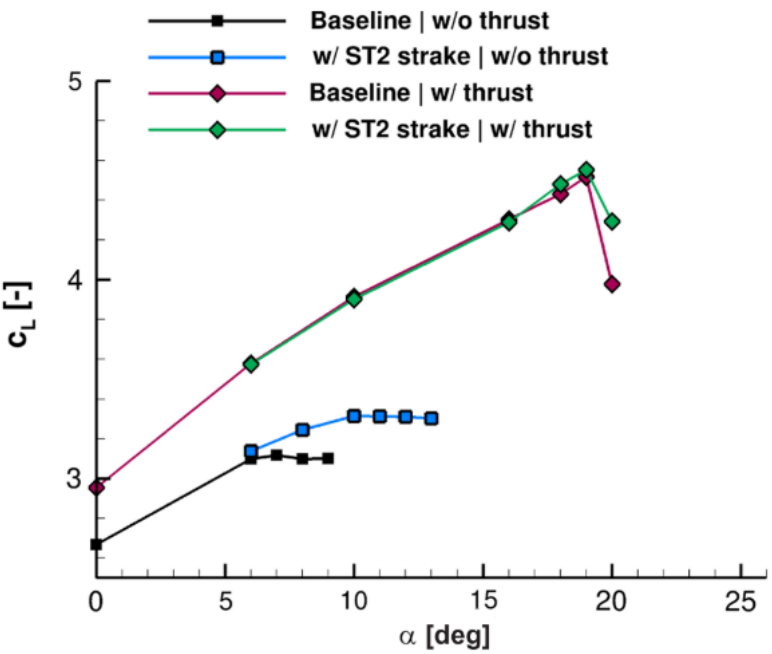

Figure 2.21: Figure showing the lift polar for the wing with and without the nacelle strake both with and without propeller [18]

2.4.2. Nacelle Vertical Position

Perhaps the simplest technique that has been applied both in literature and to some aircraft to improve high lift performance and negate some of the detrimental effects introduced by the nacelle is lowering

the nacelle. Qiu et al. [28] suggest that lowering the nacelle helps to increase the strength of the nacelle vorticity. In a similar way to the strakes described in Section 2.4.1 the more powerful vortices are able to suppress the boundary layer growth on the wing. Additionally, these vortices generate additional suction as they pass over the leading edge of the wing. This lowering of the pressure behind the nacelle helps to mitigate the crossflow effects introduced by the higher pressure region described in Section 2.1.1. This is shown in Figure 2.22. Overall, this results in a higher maximum lift coefficient. The lift polar for this configuration is presented in Figure 2.23. As can be seen, lowering the nacelle is able to recover much of the clean wing lift at higher angles of attack however stall still occurs at the same angle of attack and occurs significantly before it does on the clean wing. This modification has been applied to aircraft such as the A400M to improve the high lift performance [30]. Qiu [28] notes that moving the engine nacelle down while beneficial for maximum lift coefficient results in a significant rise in cruise drag therefore a compromise must be reached to achieve maximum performance across the flight envelope.

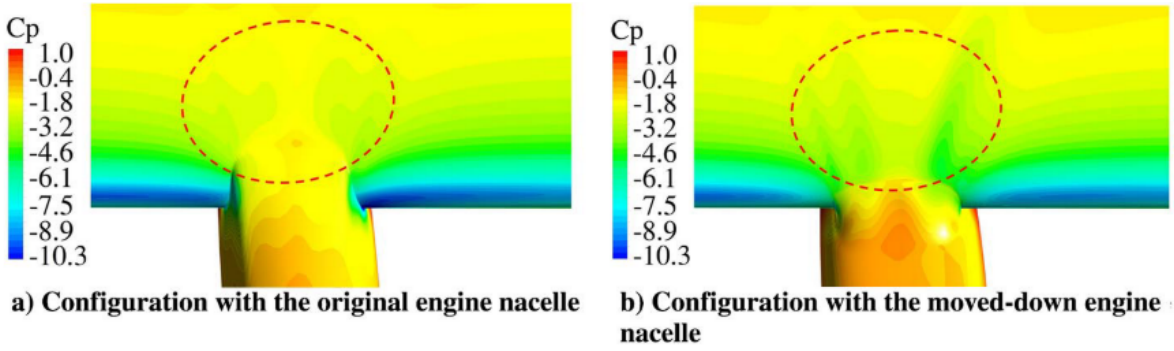

Figure 2.22: Surface static pressure distribution showing the effect of lowering the nacelle and the resultant strengthening of the nacelle vorticity on the wing leading edge pressure distribution without propeller [28]

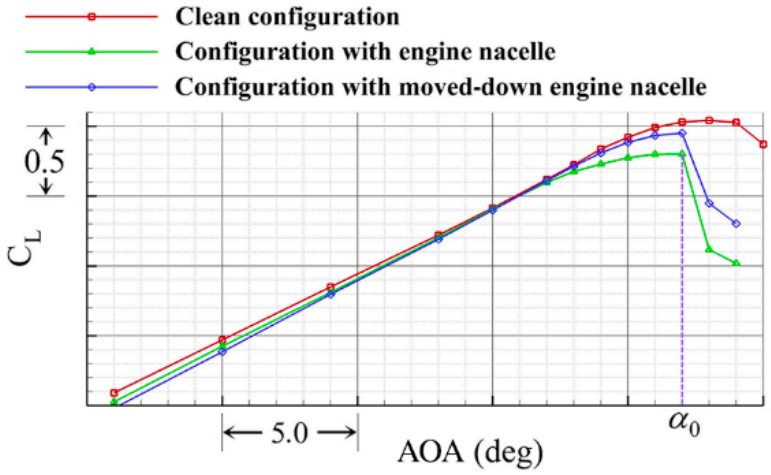

Figure 2.23: Wing lift polar showing the effect of lowering the nacelle without propeller [28]

In addition to the nacelle effects resulting from changing the nacelle height, it also introduces differences in wing performance as a result of shifting the propeller. The wing lift performance is maximised for the case where the propeller is positioned slightly above the wing leading edge and the lowest drag occurs when the propeller is close to the wing centre line [41][12].

Overall the propeller and nacelle position has a significant effect on the high lift performance with the nacelle effects favouring lowering the nacelle but the propeller effects often favouring moving it upwards

in terms of high lift performance. Moving the nacelle away from the centre line position increases drag. Determining the optimal nacelle position is therefore not straightforward as it is likely very configuration dependent as to which effects will be most important.

2.4.3. Droop

Another technique that can be applied to increase the maximum lift coefficient is leading edge droop. Droop involves lowering the leading edge of the wing to increase the wing camber and better align the wing leading edge with the flow at high angles of attack. The better alignment reduces the magnitude of the leading edge pressure peak and therefore reduces the strength of the adverse pressure gradient close to the wing leading edge. This has the effect of increasing the wing maximum lift coefficient and delaying the stall. This technique has been applied in practice on the A400M [30]. The specifics of the wing profile changes are not publicly available however Reckzeh [30] describes how the leading edge was thickened and the leading edge line lowered compared to the classic super-critical airfoil profiles that are optimised for cruise only in order to increase the wing maximum lift coefficient. This modification was applied particularly in regions that were prone to early stall for instance in areas close to the nacelle [30].

In addition, using a fixed droop as a way to increase the maximum lift coefficient of a wing droop has been considered an alternative to other high lift devices such as leading edge slats, however, this is usually in the context of leading edge morphing which aims to produce a high lift device with increased laminar flow resulting in a reduction in noise and drag [23][16]. The presence of a droop nose increases the wing maximum lift coefficient and increases the angle of attack at which this maximum lift coefficient occurs [4]. This result is shown in Figure 2.24. The addition of droop has minimal effect on the linear portion of the lift polar but delays stall and results in a higher maximum lift coefficient. Burnazzi and Radespiel [7] investigated the effect of various droop angles on the maximum lift coefficient. The results of this are shown in Figure 2.25. This shows that increasing the droop angle increases the maximum lift coefficient the angle of attack up to a maximum angle of attack of 30° after which the lift coefficient reduces.

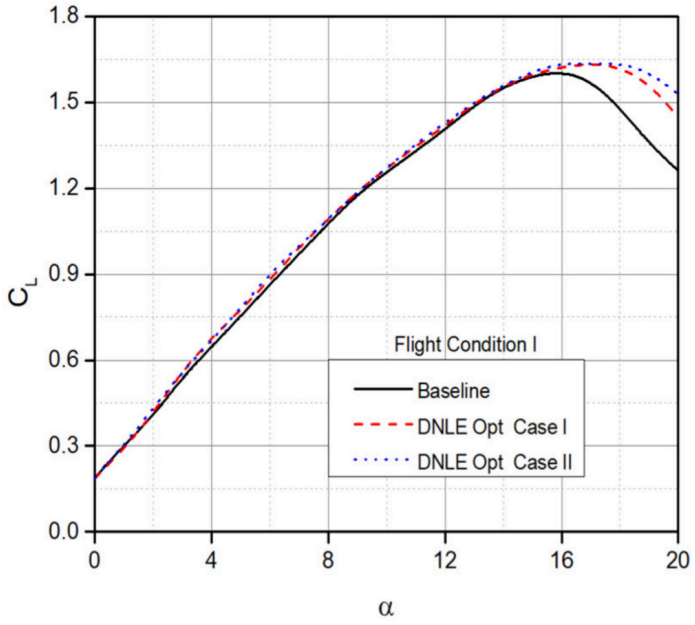

Figure 2.24: Lift polar for two different leading edge droop configurations and the baseline wing [4]

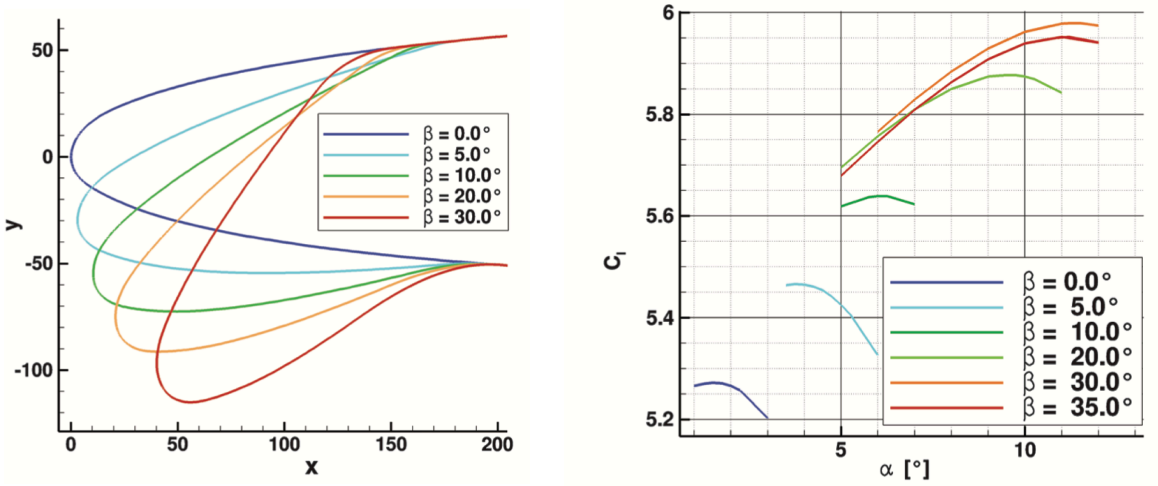

(a) leading edge geometry

(b) Lift Polar

Figure 2.25: Leading edge geometry and corresponding lift polar for various droop angles for a configuration with leading edge droop and an active Coandă flap [7]

Burnazzi and Radespiel [7] also looked at the effect of leading edge radius on the effectiveness of a droop system. This is shown in Figure 2.26. This shows that increasing the leading edge radius results in an increase in the maximum lift coefficient and maximum lift angle of attack up to a maximum leading edge thickness factor of 1.6.

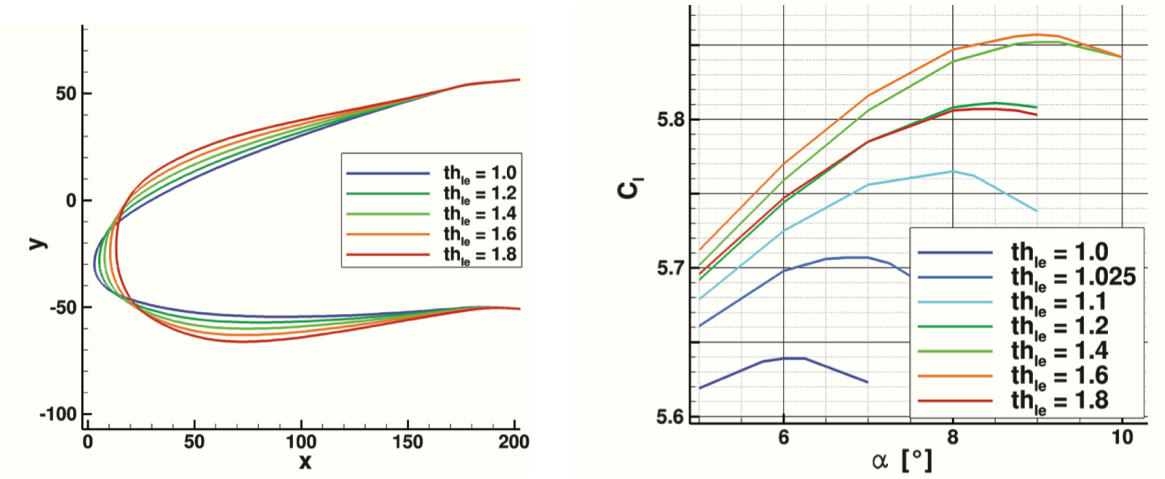

(a) leading edge geometry

(b) Lift Polar

Figure 2.26: Leading edge geometry and corresponding lift polar for a droop nose with an angle of 10° with various leading edge radii [7]

It is clear that droop has significant potential in terms of increasing the maximum lift coefficient in general and therefore may be able to better deal with the increased wing incidence angle that is induced by propeller swirl or nacelle effects. Moreover, Burnazzi and Radespiel [7] and Bashir et al. [4] found that for every given lift coefficient the airfoil with droop produced lower drag than the clean airfoil. This is particularly the case at higher angles of attack as is shown in Figure 2.27. Moreover, Jirásek and Amoignon [16] found that while a conventional vented Kruger flap is able to produce higher maximum lift coefficients the drag penalty is far higher than for a droop nose.

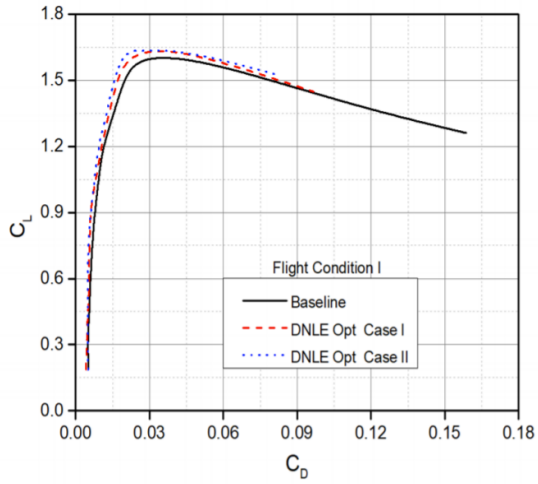

(a) Drag coefficient as a function of lift coefficient for a clean airfoil and airfoil with droop [4]

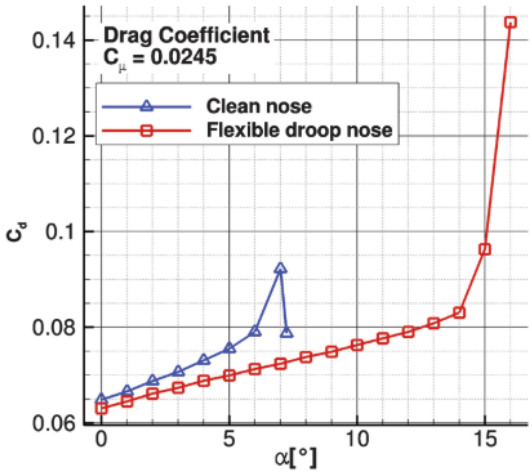

(b) Drag coefficient as a function of angle of attack for a clean airfoil and airfoil with droop [7]

Figure 2.27: Lift-drag polar and drag polar for different leading edge droop configurations and baseline wings

While Figure 2.27 shows that not only does the addition of droop increase the wing lift coefficient it also produces less drag across the positive angle of attack range. This results in an increase in lift over drag and therefore efficiency across a range of lift coefficients. Despite this fixed droop is rarely applied in operational aircraft. The A400M features limited droop that is isolated to the region close to the propeller [30] and other concepts that apply droop as a high lift device employing wing morphing. The SFB 880 being one such example of a future concept that employs a morphing leading edge to produce droop. There is limited research into the drooped airfoils in cruising conditions however Burnazzi and Radespiel [7] show that a droop nose increases the nose down pitching moment and therefore may increase the aircraft trim drag in cruise. In addition to this droop may have some adverse effects at higher Mach numbers.

2.4.4. Reflections on Wing and Nacelle Modification

Nacelle strakes seem to offer an effective way to suppress the boundary layer growth resulting from the nacelle vorticity and as a result are effective in delaying stall. They are particularly effective when considering the propeller off condition however have little effect on the maximum achievable lift coefficient in the case with the propeller on. This result is therefore perhaps not particularly useful as the goal of the research is to maximise high lift performance and therefore the off-design condition where the propeller is inoperative is not of particular interest.

Changing the nacelle vertical position can change the lift coefficient in both the powered and unpowered case. Lowering the nacelle powers up the nacelle vortices delaying separation. Moving the propeller to a position above the centre line of the wing offers the possibility of increasing the wing lift by maximising the high dynamic pressure flow over the wing. The ideal position to place the propeller is dependent on the design angle of attack. Moving the propeller away from the wing centre line results in a drag penalty in cruise condition.

Droop is effective in efficiently increasing the wing maximum lift coefficient and the angle of attack corresponding to that maximum lift coefficient. The use of droop is able to reduce the magnitude of the leading edge pressure peak and therefore is able to reduce boundary layer growth and delay the onset of stall. It has however only had limited application to propeller wing interaction problems. Applying, droop to address the boundary layer growth problem that occurs as a result of the presence of the nacelle may give

There have been a variety of leading edge modifications and nacelle modifications aimed at improving the performance of a propeller-wing system however there are relatively few that look specifically at improving the improve high lift performance and those that do lack experimental validation The modifi-

cations that do relate to high lift performance are often very limited in scope, often focusing on mitigating a specific deficiency that was encountered with their concept through the application of a specific technique rather than looking at how the performance can be maximised. Techniques like droop have been applied to several propeller wing aircraft concepts however there is limited information on how it impacts the propeller wing interaction effects.

This page is intentionally left blank

3

Research Questions and Thesis Scope

This section outlines the knowledge gap that will be investigated and based on this gap the research questions that will be answered. Finally, the limitations of the project will be explored.

3.1. State of the Art and Knowledge Gap

Literature shows that the interactions between a nacelle and wing in a tractor configuration introduce multiple local flow phenomena that alter the wing performance. The nacelle modifies the wing pressure distribution, changes the local inflow conditions at high angles of attack and introduces vortices. These interactions can cause boundary layer growth and ultimately local flow separation that can negatively impact the high angle of attack performance. The nacelle-wing interactions result in a reduction in maximum lift coefficient and angle of attack. While there are studies that investigate these wing and nacelle effects they are limited and rely heavily on numerical methods that are not directly validated using experimental methods. Additionally, the studies that do cover wing nacelle do not isolate the wing nacelle problem, focusing on their impact on full aircraft configurations rather than isolating the impact through the use of a simple wing and nacelle. This makes it difficult to gain an understanding of the mechanisms that influence the performance of a propeller-nacelle-wing system as the influence of other parts of the aircraft (particularly the fuselage) complicate the interaction effects making the problem more complex. This can make it difficult to draw general conclusions regarding how the propeller-nacelle-wing system performance can be maximised.

The impact of a propeller on wing performance is treated more extensively in literature. The combination of the high dynamic pressure behind the propeller and the propeller swirl causes significant changes in the wing loading distribution. Additionally, to the large scale flow changes to the lift distribution, the propeller also introduces changes in the wing boundary layer. It introduces turbulence and velocity to the wing boundary layer that can make it more resistant to stall. The wing also influences the propeller performance. The way in which the propeller effects interact with the nacelle effects is less well studied. The high energy propeller wake likely suppresses the negative impacts of the nacelle-wing interactions however to what extent is not clear with no clear consensus between studies.

The use of multiple propellers causes more of the wing to be blown and therefore increases the possible positive effect on the wing high angle of attack performance. The stall behaviour and lift distortion that result from the presence of multiple propellers are not substantially different from those observed in the single propeller case and therefore it seems likely that the majority of the conclusion regarding the propeller-nacelle-wing interactions in the case with a single propeller will also be applicable in a case with multiple propellers.

The use of nacelle strakes to generate vortices that can suppress the boundary layer growth. Their use is documented in both literature and has been implemented in real-world aircraft. The position of the nacelle strake is however quite critical in determining its effectiveness. Similarly changing the nacelle vertical position to improve high angle of attack performance has been extensively investigated

and is widely implemented on turboprop aircraft however the nacelle location also impact the propeller interactions and therefore the ideal position is complex to determine. Droop is effective in increasing the wing maximum lift coefficient and angle of attack. Drooping the leading edge increases the wing effective camber and better aligns the leading edge with the free stream flow reducing the leading edge pressure peak. There is limited research investigating the effect of droop on propeller-nacelle-wing interactions. While some studies have investigated the use of leading edge and nacelle modifications to address aerodynamic issues encountered by propeller-nacelle-wing systems most studies only consider a single concept to address the negative interaction effects rather than approaching the problem systematically.

Based on this research a knowledge gap is identified. When considering propeller-nacelle-wing systems at high angles of attack the majority of literature focuses on the influence of the propeller on the wing performance and behaviour. Research into the influence of the nacelle on the wing performance is considerably more limited. Nacelle interaction effects have an almost exclusively negative impact on wing performance. Additionally, the nacelle's impact on performance is easier to address particularly through modifications to the wing and nacelle geometry than those introduced by the propeller. The impact of phenomena like swirl are particularly challenging to address as they are inherent propellers and perhaps more importantly are also not constant with advance ratio and therefore thrust setting or the specific propeller being used. Understanding and addressing the impact of the nacelle on the high angle of attack performance of the propeller-nacelle wing system can yield performance improvements across a wide variety of conditions and configurations. This study will therefore focus on nacelle-wing interactions. Similarly, there is a knowledge gap regarding how the propeller influences these nacelle-wing effects.
The aim of the study is to understand the impact of the nacelle on the high angle of attack both with and without the influence of a propeller and then look at how and to what extent the wing and nacelle geometry can be modified such that the negative interaction effects outlined in Section 2.1 can be mitigated.

3.2. Research questions

The goal of the thesis will be to gain an understanding into the extent to which the high angle of attack performance of a propeller-nacelle-wing can be increased through the use of wing leading edge and nacelle modifications that aim to mitigate the nacelle-wing interaction effects. In order to reach meaningful conclusions about this clear research objectives shall be defined. The scope of this research is summarised by the following research question:

How can wing leading edge and nacelle geometry be modified to reduce the negative effects of propeller-nacelle-wing interactions to improve high angle of attack performance for an aircraft with leading edge mounted propellers?

In order to address this research question, the research is split into two parts. The first part aims to understand the nacelle-wing interaction problem. The second part will consider techniques that can be applied to mitigate negative impacts associated with nacelle integration through the use of wing and nacelle modification. Each of these parts has a series of sub-questions that must be evaluated.

3.2.1. Part One

The main sub-question that should be answered in this first part is: **How does the presence of a nacelle influence the high angle of attack behaviour of a wing?** Based on the results of the literature survey the influence of the nacelle was more detrimental than the effects of the propeller on the wing performance. Moreover, the propeller off condition is a relevant condition for concepts such as distributed propulsion that may not use all propellers in all flight regimes and as such the propeller off condition may be limiting. The focus of this question will be on how does the presence of the nacelle influence the wing boundary layer and stall behaviour. How limiting are the nacelle effects in terms of maximum lift coefficient and angle of attack? This is a particularly important question given the limited

research into this area and the fact that some studies have indicated that this effect can have a large impact on the performance of the total propeller-nacelle-wing system.

Although the focus of the study will be on nacelle interaction effects the impact of the propeller cannot be ignored. This gives rise to the next sub-question which will be: **What is the effect of the propeller on the high angle of attack performance of the nacelle-wing system?** In order to answer the above research question, it must be assessed to what extent does propeller interaction mitigates the influence of the nacelle on the wing performance. An understanding of which effects become dominant in terms of dictating the high lift performance and which effects are suppressed in the combined system. Any new effects that result from the complete system should also be considered. An understanding of the interaction effects in a propeller-nacelle-wing system and having a sense of the origin of the effects is important to allow for mitigation techniques to be targeted. It must be determined which nacelle effects are key in dictating the performance of the propeller-wing-nacelle system and which have lower importance in this configuration to allow for critical assessment of the results of the design study.

3.2.2. Part Two

Once the problem is well understood the next part addresses concepts to mitigate the effects that can be tested based on the insight gained. This concept testing aspect of the research gives rise to two further sub-questions.

The first of these sub-questions is: **What nacelle and leading edge modifications can be used to mitigate or suppress the undesirable high angle of attack performance characteristics introduced by the nacelle?** A number of modifications will be considered. Firstly, how the wing leading edge profile can be modified to reduce its sensitivity to induced angle of attack effects resulting from the nacelle. This can be accomplished through the use of techniques such as droop. In addition to this, the effect of adding a fillet to the nacelle-wing junction shall be considered to reduce interaction between the nacelle and wing boundary layers.

The next question to be addressed is: **To what extent can the performance gains achieved in the propeller off configuration translate to a performance increase once the propeller is installed?** This question is closely related to the second sub-question. The extent to which the modifications will increase the performance of the propeller influences the nacelle-wing system will likely determine how far the modifications can influence the performance of the propeller-nacelle-wing system and therefore allows the overall usefulness of the modifications to be assessed critically. The introduction of additional interaction effects arising from the propeller interacting with the nacelle must be considered to ensure that the modifications do not introduce undesirable effects in the presence of the propeller.

The final sub-question that will be considered is: **How do any modifications that increase high angle of attack performance impact cruise performance?** The effect of any modification on performance at lower angles of attack and at higher Reynolds numbers must be considered to judge if the modification will be efficient when implemented in an aircraft. As was seen in Section 2.4.2 modifying the nacelle height is effective in increasing high lift performance but leads to a significant drag rise that can be limiting. Therefore the impact of the modifications in conditions that are representative of the majority of the flight profile should be evaluated.

3.3. Scope

In order to make the research feasible in the time frame required for a master's thesis and to ensure that the research remains focused limitations should be imposed on the scope. In this way, the research questions can be answered as efficiently as possible within the resource constraints imposed. This section will outline and explain the decisions that are made regarding the scope of the research.

3.3.1. Wing System Complexity

To reduce the complexity of the problem, the investigation will be carried out on a model without a flap deployed. While this is not a likely configuration when considering the maximum lift performance of

a theoretical propeller aircraft the added complexity of modelling a wing with a flap and the additional interactions introduced by adding another body into the already complex system will make the research too complex to be achievable. Additionally the use of a flap adds another variable to the problem (flap position) which will require further modelling to give meaningful results. It is hoped that the results from the single will still have some relevance to the case where a multi-element wing is considered however this will be a topic for future research. The implications of this choice are further discussed in Section 4.1.

3.3.2. Modelling Limitations

Answering the research questions requires the evaluation of several geometries and each of these geometries will require assessment in different conditions (with and without propeller at multiple angles of attack) to assess the viability of each of the modified geometries as well as several simulations to validate and understand the model. This means that in order to make this study feasible within the context of a master's thesis. The resource usage per evaluation use should be minimised as far as possible. This will require the limitation of the number of conditions that are tested and will limit the accuracy of the simulations to only what is required to answer the research questions such that the project is feasible in the time frame and with the resources available. To this end, the majority of the work shall be carried out using numerical methods rather than physical testing with the use of wind tunnel testing limited primarily to validate the simulations. Further details of the approach that is used and the modelling assumptions and simplifications that are used are outlined in Chapter 4.

3.3.3. Decision not to Perform Optimisation

As the goal of the study is to look at the feasibility of using nacelle and wing modifications to increase the performance of a propeller-nacelle-wing system rather than achieving the maximum possible performance no numerical optimisation techniques will be applied with the focus instead being placed on concept design an evaluation for potential rather than necessarily results. Some limited optimisation may be required in order to assess this potential (for instance modifying a concept to ensure that it is properly aligned and does not simply separate) however iteration is to be limited as much as possible to once again ensure that the research is feasible within the required time frame.

3.3.4. Metrics

To assess the level to which the research goals are met some key metrics and conditions will be defined. Due to the nature of CFD simulations which will be used for the majority of this study it is not straightforward to obtain a full angle of attack sweep that would be necessary in order to determine the maximum lift coefficient. A single design point will therefore be used. A point should be selected that exhibits the phenomena that are of interest, close to the maximum lift angle of attack and can be considered representative of a high angle of attack condition. The performance change at this condition will be the key metric to be assessed. The primary variable of interest is lift coefficient. lift to drag ratio shall also be considered to determine the relative efficiency of any concepts and finally, the modifications shall be assessed qualitatively as given that no optimisation is performed it is critical to understand if the concept achieves to what extent the modifications achieve their goals and if unintended consequences limit the performance. It is hoped that conclusions that are made in this condition will have wider applicability at other angles of attack.

3.4. Problem Approach

The problem as outlined in the research questions in Section 3.2 is decomposed into two key parts. The first aspect involves the understanding of the problem and how the propeller-nacelle-system influences the wing high angle of attack performance. The second element involves carrying out a design study into how the high angle of attack performance can be improved by the use of modifications.

The first of these parts will primarily aim to generate further understanding of the key flow phenomena that influence the high angle of attack performance and therefore largely aims at answering the first and second sub research questions. This understanding will be generated using a combination of wind tunnel results and a CFD model and therefore will also involve the development and validation of this model. The second element of the study will involve generating and testing hypotheses of how the key

flow phenomena generated in the first part can be addressed. This study will exclusively use CFD. This design study will involve modifying the wing geometry and testing it using the validated CFD approach.

This page is intentionally left blank

I

Validation and Problem Definition Experiment

This page is intentionally left blank

4

Methodology and Validation Approach

This chapter outlines the numerical and experimental setups that will be used to define and understand the propeller-nacelle-wing problem as well as describing the validation approach for the numerical model.

The experimental data is used to identify key flow phenomena present in the propeller-nacelle-wing system and validate the numerical to ensure it demonstrates similar flow behaviour. The numerical model is then used to generate additional understanding regarding the interaction effects. the results of these two models combined will be used in order to answer part one of the research question.

4.1. Model Configuration Choices

To address the research questions, a model must be created. The selection of this model configuration will be critical in determining the applicability of the conclusions and the feasibility of the study. This section will outline the configuration that is chosen as well as the motivation behind these decisions.

The configuration that will be used to evaluate the impact of the propeller-nacelle on the wing high angle of attack performance consists of a single propeller, nacelle mounted to the leading edge of the wing (dimensions of this model can be found in Appendix A). Although the context of the study also concerns multiple propeller configurations including concepts such as distributed propulsion, based on the results in Section 2.3 the conclusions that are valid in the single nacelle and propeller case will still apply to a case with multiple nacelles and propellers. Simplifying in this way makes it easier to draw conclusions and will reduce the time required to evaluate every possible configuration.

Similarly, the study will only the flap retracted case. While the flap will have a strong influence on the interaction effects it is not deemed feasible to incorporate its effects within the scope of a master's thesis project. When considering high angle of attack performance one normally considers a wing with high lift devices deployed however the flap significantly complicates the interaction effects by introducing another component to the already very complex system and would require significant amounts of additional research in order to evaluate its impact. The decision not to include a flap is a major but necessary limitation of the study therefore this limitation should be considered when critically when reflecting on the results and conclusions. Conclusions regarding the nacelle high pressure region and increase in local angle of attack effects described in Sections 2.1.1 and 2.1.2 respectively will still be applicable in the presence of a flap as these effects primarily concern the leading edge portion of the wing and therefore will still alter the performance when a flap is fitted. Modifications that address these issues in the flap retracted case are therefore still relevant to a multi-element configuration however these conclusions must still be assessed critically. The influence of nacelle vortex bursting inducing flap stall described in Section 2.1.3 cannot be studied using this model.

In order to complete this study the multiple evaluations of multiple configurations in different conditions will be required. In addition to this understanding of both the on surface and off surface flow structures

is required. Achieving this aim exclusively through the use of full scale or even wind tunnel testing is deemed infeasible due to the large number of configurations and measurement techniques that would be required. A hybrid approach is therefore used where the combination of numerical methods and wind tunnel test to validate the model are performed to answer the research questions in this first part.

4.2. Experimental Setup

To allow the numerical model to be used for development and analysis, it must be validated to ensure it reasonably represents real-world physics. In order to accomplish this validation data from a wind tunnel test campaign will be used. The data from this wind tunnel test shall also be used to generate some initial insight into the influence of the propeller and nacelle on the high angle of attack performance. This chapter describes the methodology and instrumentation used to generate the wind tunnel data.

4.2.1. Wind Tunnel Description

Validation data for the numerical model was collected at the Delft University of Technology Low Turbulence Tunnel (LTT) pictured in Figure 4.1. The LTT is a closed-throat single-return wind tunnel with a contraction ratio of 17.8 allowing for turbulence levels of between 0.015% and 0.7% [35]. The tunnel features interchangeable test sections with a height of 1.25m, length of 2.6m and an inlet width of 1.8m and an outlet width of 1.821m. The discrepancy between the inlet and outlet width is calibrated to ensure that there is no pressure gradient between the inlet and outlet of test section as a result of boundary layer growth. Each test section features a flush-mounted turntable.

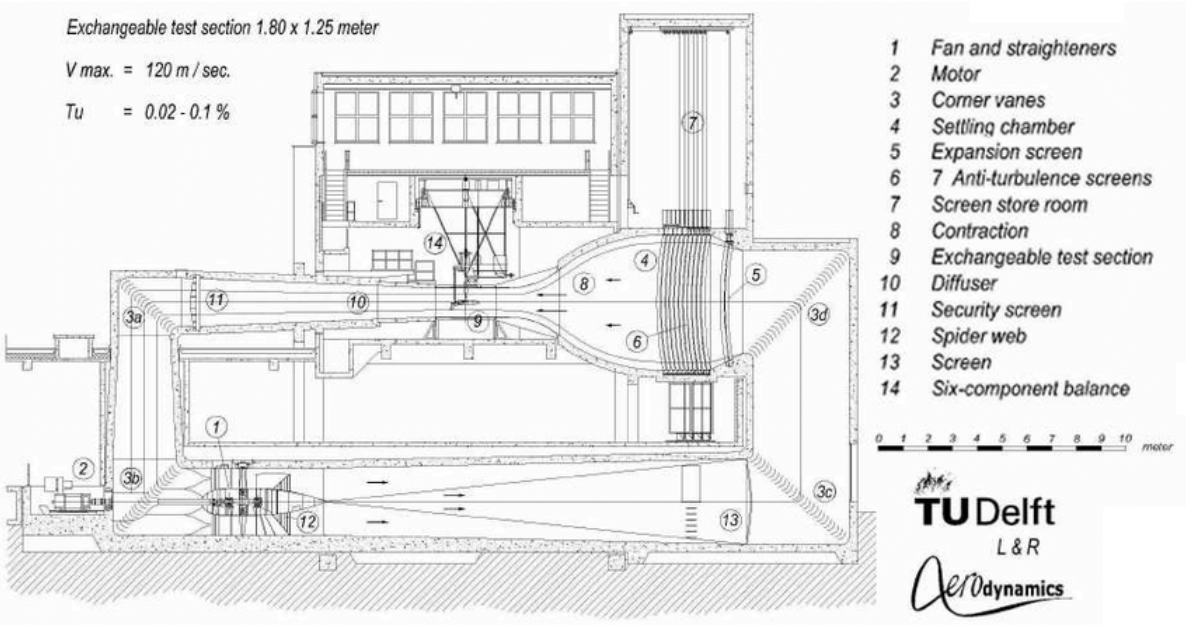

Figure 4.1: Diagram of the Delft University of technology Low Turbulence Tunnel

4.2.2. Model Description

The model used is based on the NLF-Mod22(B) airfoil originally designed and characterised by Boermans and Rutten [5]. This is a natural laminar flow airfoil featuring a 30% chord fowler flap and a sharp cove. The model consists of a wing with a chord of 0.3m and a span of 1.2m onto which up to 3 nacelles and propellers can be mounted. The wing was mounted vertically in the test section and secured to the turntables. The main element of the wing was clamped at both the top and bottom of the tunnel using shim plates and clay to smooth the transition. The wing flap is attached to the trailing edge of the wing using 6 brackets indicated in Figure 4.2. The gaps at the top and bottom of the flap were sealed to the wall using high-speed tape in order to prevent leakage at the walls.

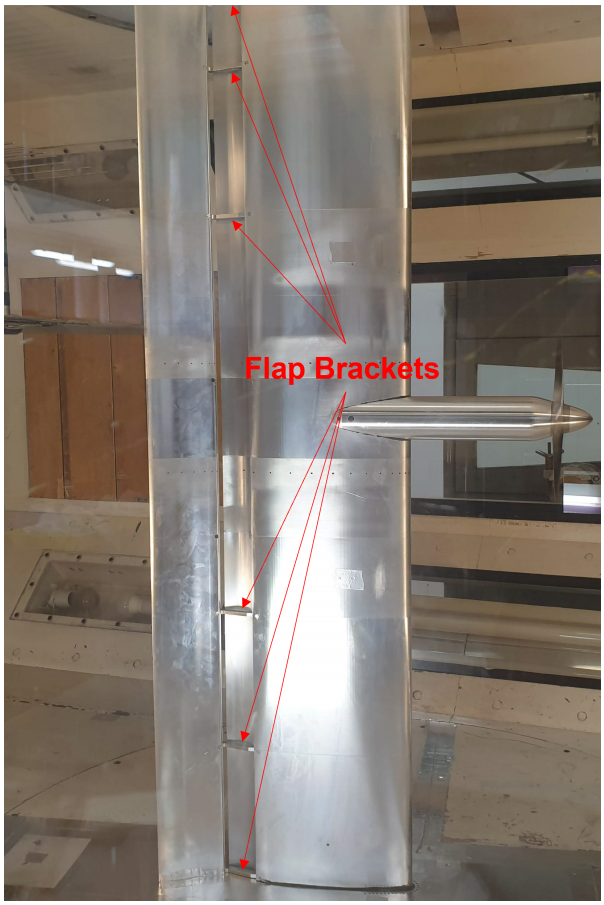

Figure 4.2: Photo of the pressure side of the wind tunnel model mounted in the test section at the LTT with the flap brackets indicated

A single nacelle is used for the purposes of this experiment. This nacelle contains an electric motor. The TUD-XPROP-S is used as the propeller. This propeller is the scale version of the Delft University of Technology XPROP and has been extensively characterised by amongst others van Arnhem et al [38]. The six bladed propeller had a setting angle of 30° and was run at two different advance ratios (J = 0.8 and J = 1.0) which correspond to the maximum propeller thrust coefficient achievable by this setup ($T_c = 1.05$) and maximum efficiency ($T_c = 0.45$) respectively. See Figure 4.3 for details.

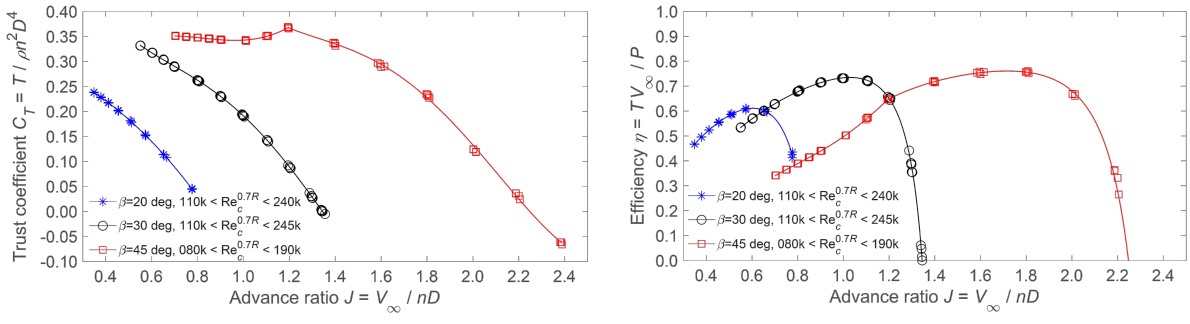

(a) Thrust Coefficient Plot

(b) Efficiency Plot

Figure 4.3: TUD XPROP experimental thrust coefficient and efficiency curves for the isolated propeller [34] (unpublished internally distributed data discussed by Van Arnhem et al [38])

The wind tunnel was run at a free stream velocity of 30 m/s for all tests corresponding to a Reynolds number of roughly 588,000. This is relatively low when considering transport aircraft however it was

selected based on the limitations of the motor that was used to drive the propeller in the wind tunnel model and a desire to run the propeller at advance ratios corresponding to the propeller maximum efficiency and a higher thrust coefficient. Additionally, these low Reynolds numbers while perhaps not representative of cruise are more relevant when considering high angle of attack performance which is typically most relevant during the take-off and landing portions of the flight envelope. Finally, these low Reynolds number conditions are limiting in terms of separation and therefore this can be considered as almost the worst-case scenario and as such will most clearly illustrate the aerodynamic challenges introduced by propeller-nacelle-wing interactions.

4.2.3. Instrumentation

A variety of instrumentation is used to assess the wing performance and allow for comparison with simulations. The wing is fitted with two rows of pressure located at 71.1mm on either side of the wing centre-line. This places the two pressure taps in the wake of the propeller and allows for assessment of the asymmetry introduced by the propeller wake. Each set of pressure taps consists of 31 taps located on the wing main element and a further 14 on the flap. The location of these pressure taps is indicated in Figure 4.4. The static pressure is measured at each of these locations using an external pressure scanner.

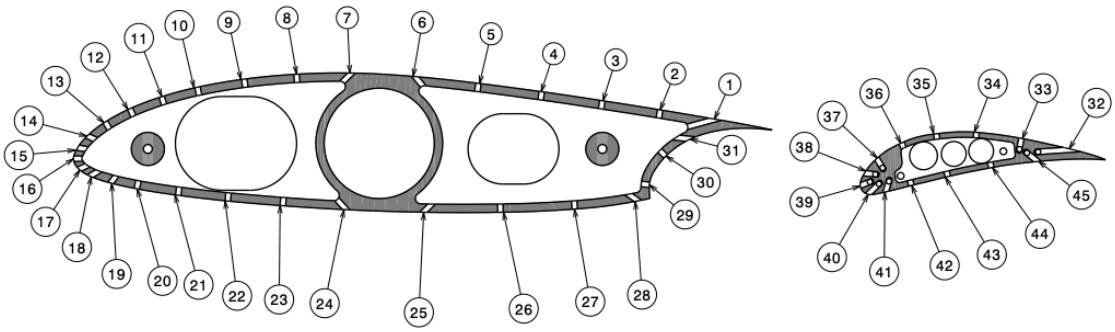

Figure 4.4: Wing pressure tap locations and numbering for the upper row of wing pressure taps

In addition to the local pressure data, oil flow visualisation will be applied to the wing in order to show surface flow phenomena. These images can be compared on a qualitative level to computational simulations. Unfortunately, as the model used is a pre-existing model and was not designed with testing at the LTT in mind it was not possible to capture balance data and therefore total wing forces are unavailable.

As well as the instrumentation integrated into the model a number of external measurement techniques are applied. A wake rake with static and total pressure probes shown in Figure 4.5 is positioned one chord length (0.3m) behind the wing trailing edge in the zero angle of attack position. This wake rake can be translated vertically and horizontally by ±0.19m. The wake rake will be translated to ensure a 3mm spatial resolution in the region behind the wing. These measurements can be used to analyse the flow structures behind the wing as well as giving an estimate of the wing drag by looking at the velocity deficit at the wake rake plane.

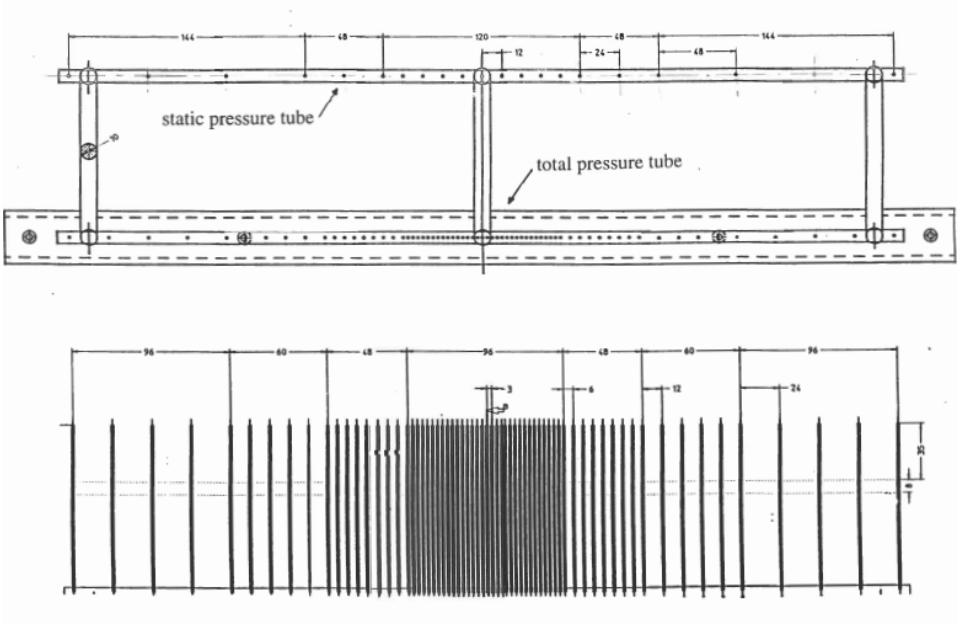

Figure 4.5: Diagram showing the wake rake dimensions and configuration [5]

Finally, a manually operated static pressure probe will be used. This probe is traversed across the wing span at a single chord-wise location in order to give an indication of the wing spanwise loading distribution. The data from all of these instruments can then be used for the validation and verification of numerical methods.

4.2.4. Experimental Strategy

A number of different configurations were tested over the course of the campaign. these configurations are detailed in Table 4.1. The configurations that are most important for this study are indicated in green. In addition to this, the four initial concept leading edge extension configurations discussed below are highlighted in yellow.

Configuration Number	Flap Deflection [deg]	Gap [%]	Overlap [%]	LEx	Nacelle	Propeller	Blade Pitch [deg]
1	0	-	-	-	Off	Off	-
2	15	2	8	-	Off	Off	-
3	30	3	0	-	Off	Off	-
4	30	3	0	-	On	Off	-
5	30	3	0	-	On	On	45
6	30	3	0	-	On	On	30
7	15	2	8	-	On	On	30
8	15	2	8	-	On	Off	-
9	0	-	-	-	On	Off	-
10	0	-	-	-	On	On	30
11	0	-	-	LEx1	On	On	30
12	0	-	-	LEx1	On	Off	-
13	0	-	-	LEx2	On	Off	-
14	0	-	-	LEx2	On	On	30

Table 4.1: Wind Tunnel Test Matrix

Given the decision to focus the study on looking at the case with flap retracted Configurations 9 and 10 will be the most relevant for validation purposes (highlighted in green). For each of these configurations, an angle of attack sweep is conducted and wing pressure tap measurements recorded. In addition to this oil flow visualisation and wake rake data is captured for 3 angles of attack. These are 0,

10 and 13°. These angles of attack are selected as they offer an understanding of the flow structures in the case that the wing is fully attached, close to the maximum lift coefficient and finally after the maximum lift coefficient. These points are selected such that as far as possible the wing behaviour is captured completely with as few points as possible.

In addition to the 10 unmodified wing cases outlined above, two leading edge modifications (highlighted in yellow) are tested through the use of 3D printed add-ons. These two leading edge extensions (LExs) aimed to improve the wing high angle of attack performance and are shown in figure 4.6a and 4.6b (scale drawings can be found in Appendix B). The two LExs are designed for different purposes, LEx1 attempted to reduce the interference effects between the nacelle and leading edge of the wing through the use of a fillet. It aims to smooth the junction and therefore reduce the interaction between the nacelle and wing boundary layers. LEx2 aimed to make the wing more resilient to the changes in angle of attack induced by the propeller and nacelle by increasing the leading edge radius.

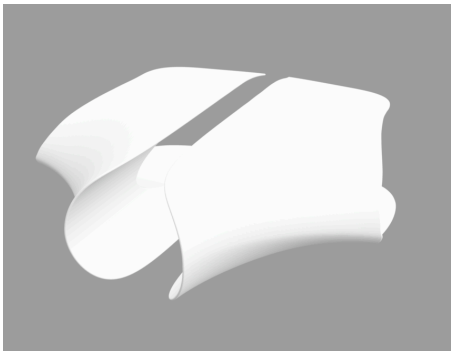

(a) Nacelle fillet Leading edge extension (LEx1)

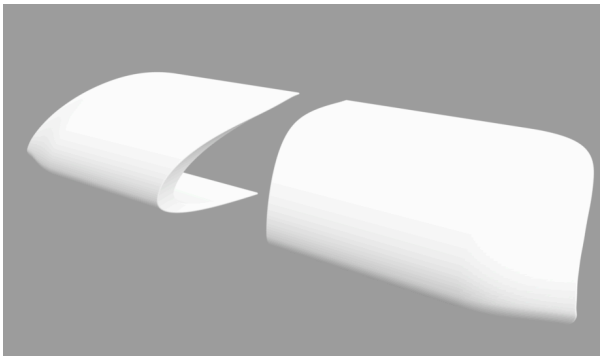

(b) Leading edge radius increase Leading edge extension (LEx2)

Figure 4.6: Render of the two leading edge extensions that are tested

These two leading edge extensions are 3D printed and attached to the wing using high-speed tape. Unfortunately, due to minimum thicknesses when 3D printing the leading edge extensions a small step was present. Attempts were made to smooth this step using tape were reasonably successful however the transition was still not perfect and as such it introduces some uncertainty regarding which effects are a result of the intended geometry and which are the result of the step it introduces. The results were intended as a first look into the use of leading edge extensions to improve high angle of attack performance however due to the model deficiencies mentioned previously and a lack of data further analysis using other modelling techniques will be necessary in order to draw firm conclusions about the effectiveness of these devices.

4.3. Numerical Setup

This section gives an overview of the numerical modelling setup that will be used for the majority of the study. It will cover the modelling assumptions and design choices.

4.3.1. Numerical Model Description

The goal of the study is to investigate the high angle of attack performance and the interaction effects between the propeller nacelle and wing. These effects are by their nature three dimensional and dominated by viscous effects, therefore the use of lower-order numerical models such as panel codes or inviscid flow solvers is considered infeasible. As such the study will be completed using higher-order Computational Fluid Dynamics (CFD) methods.

To validate the numerical simulation, such that conclusions can be drawn based on the simulation results, a comparison will be made to wind tunnel data. In order to facilitate this, the wind tunnel model and test section geometry will be recreated in CFD. The model is shown in Figure 4.7. By faithfully recreating the tunnel geometry and flow conditions in this way the results of this simulation can be

directly compared to data collected in the wind tunnel.

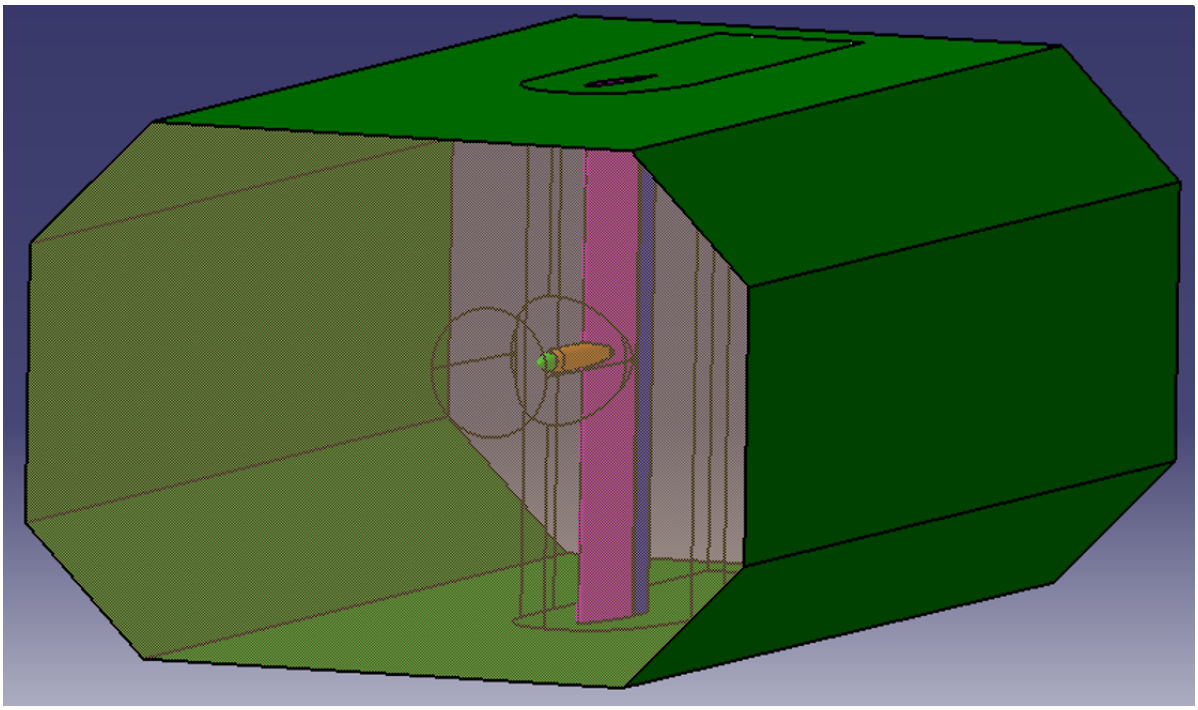

Figure 4.7: CAD model of the wing and wind tunnel tests section that is used for numerical simulations

The mesh that is used has roughly 230 million cells with multiple levels of cell refinement. The mesh is refined in the region around the wing and in the wake behind it. Additionally, several local refinement regions are applied in order to aid in resolving the separated flow structures. The far-field mesh has a maximum cell size of 50mm with reducing down to 1mm in the local refinement regions. This mesh was iterated upon in order to achieve steady state convergence

To validate all the configurations that will be required to answer the research questions outlined in Section 3.2 a total of 4 configurations will need to be validated to facilitate the design study. These configurations are described in Table 4.2.

Config number	Angle of attack [deg]	Propeller
1	10	No
2	10	Yes
3	0	No
4	0	Yes

Table 4.2: Specification of the CFD simulations that will be needed in order to validate all of the configurations that are necessary to answer the research questions

As multiple configurations are being considered, carrying out a numerical angle of attack sweep is not feasible and will likely not provide a significant amount of additional information regarding the wing high angle of attack performance given that the wing is already characterised in the wind tunnel. A single angle of attack of 10° was therefore selected for this study. This angle of attack was chosen as this point is relatively close to the maximum lift angle of attack and exhibits the undesirable high angle of attack behaviour around which the study focuses. Additionally, this angle of attack was specifically selected as extensive wing wind tunnel data and propeller performance data is available at this angle of attack allowing the numerical model to be effectively validated. The approach of using a single angle of attack will not allow for a conclusion to be drawn regarding the wing maximum lift coefficient and angle of attack but will allow the wing high angle of attack performance to be assessed critically. It is assumed that changes in the in wing performance and qualitative changes to the wing stall and lift

behaviour at an angle of attack of 10° will also result in a change in the performance at the maximum lift angle of attack. Finally, typically aircraft do not operate at the maximum lift point as the risk of entering a lift breakdown condition is large therefore this condition is considered more representative of the high angle of attack conditions experienced by a real aircraft in a typical flight. A second angle of attack of 0° will also be considered when assessing the 'cruise' performance. This condition is not of relevance to assessing the high angle of attack performance and will not be extensively analysed however, it is useful as a reference to allow for comparison of the impact of different geometries in conditions outside the design condition.

The conditions used for the numerical model are matched to the wind tunnel model flow conditions. This is done to ensure that the model can be validated with experimental. Without validation data the behaviour of the model at different Reynolds numbers cannot be validated.

4.3.2. Numerical Solver Settings

The nature of the project requires multiple iterations therefore in order to make this design study feasible within the allotted time frame run times should be minimised. In order to achieve this a Reynolds-averaged Navier-Stokes (RANS) model is selected. While both large eddy simulation (LES) and direct numerical simulation (DNS) will likely model the physics better as they resolve (part of) the turbulence numerically the run times for these types of simulation are prohibitively computationally expensive.

The use of a RANS model requires the selection of a turbulence model as the turbulence physics is only approximated. The selection of this model is important to ensure accurate modelling of the problem. A Spalart-Allmaras (one-equation) model was selected as it was specifically designed for these types of external flow modelling applications and is effectively able to model the boundary layer flow with lower computational resource use than two-equation models [1].

Steady-state simulation is chosen to make up the majority of the study in order to minimise the computational time required. Moreover, as was described in Chapter 2 the effects that are most influential and detrimental to wing high angle of attack performance in the presence are likely captured by a time-averaged result.

The ANSYS Fluent solver is chosen for the purposes of this analysis as there is experience within the department with using this software package for solving these types of problems and as it is a commercial CFD code it is relatively straightforward to use and has reasonably stable convergence properties.

4.3.3. Propeller Modelling

While the focus of the research is on mitigating the negative impacts of nacelle wing interaction effects there is a requirement to assess the impact of the propeller on these effects. As is described in Chapter 2. While there are some transient effects that result from propeller wing interactions these mostly concern the periodic injection of velocity and turbulence into the boundary layer. Given that the focus of the study is on high angle of attack performance the flow is expected to become completely turbulent close to the wing leading edge therefore this effect is likely to have a small impact on the overall wing interactions. As the goal of the study is to understand nacelle effects and there is a desire to use steady-state simulations to reduce the required computational resource, the fulle propeller is not modelled. As such the propeller will be modelled through the use of an actuator disc model based on previous transient simulations of the propeller. This approach is applied quite widely in propeller wing interaction studies [17][18][15].

The non-uniform inflow field has a large impact on the propeller performance as was described in Section 2.2.3 which in turn impacts the wing performance, creating a closely coupled system. Coupling the actuator disc model to the solver or correcting the propeller loading to account for the influence of the non-uniform inflow adds significant complexity to the simulations. The decision was therefore taken not to couple the propeller and wing. The primary goal of the study is to investigate the nacelle effects on wing performance therefore the propeller model is only intended to give an understanding of how a

propeller might influence the nacelle-wing interaction effects, the accurate modelling of the propeller is not a key aim. While the simulations will likely not give an accurate representation of the overall high angle of attack performance of the propeller-nacelle-wing system, the influence of the key phenomena of swirl and the high dynamic pressure wake on the nacelle-wing interactions can be assessed. Moreover, the wing configuration that is used has a relatively long nacelle and therefore the mutual interaction effect is likely less strong than in a more closely coupled systems as such the influence of this choice is likely less significant. The validation of the propeller cases is particularly important as the differences in the propeller wake as a result of the mutual interactions must be reflected on critically and considered when analysing any geometric modifications.

The propeller will be implemented as an actuator disc using the Fluent fan boundary condition. This model assumes that the propeller is an infinitely thin pressure discontinuity with an imposed tangential and radial velocity distribution. This model was chosen as it is relatively simple to implement within fluent and does not require the use of a user-defined function. The simplified actuator disc model is implemented within the Fluent solver and allows the user to prescribe a pressure jump as a function of the local axial velocity. The tangential and radial velocity is prescribed based on the radial position. This data is generated based on previous tests performed on the TUD XPROP. The pressure jump is defined based on the propeller thrust curve. The propeller rotation rate is fixed and the thrust is defined for a given axial inflow velocity; the thrust is then divided by the disc area to give the disc averaged pressure jump. A polynomial is fitted to the propeller data and inputted into Fluent. The pressure jump is solely a function of the inflow axial velocity and therefore no correction is made for the angle of attack changes as a result of the inflow tangential velocity component. The pressure jump as a function of the inflow axial velocity is given in Figure 4.8. The radial and tangential velocity components that define the swirl velocity are prescribed as a function of the propeller radius. These velocity components are similarly fit with a polynomial which are presented in Figure 4.9. Fluent limits the user to a sixth-order polynomial when modelling the tangential and radial velocity therefore there is some discrepancy between the actual velocity profiles and those that are used by fluent. Overall there are a number of key deficiencies in the propeller modelling and an exact match between the propeller model and experimental data however this simplified model will give some initial understanding of how propeller might influence nacelle-wing interaction effects. While this is not ideal the time and resource constraints that are inherent to the master's thesis project have made more advanced numerical simulations impossible.

Figure 4.10 shows the streamlines behind the isolated numerical propeller model described above. Overall the model can introduce an increase in axial velocity and introduce swirl to the flow.

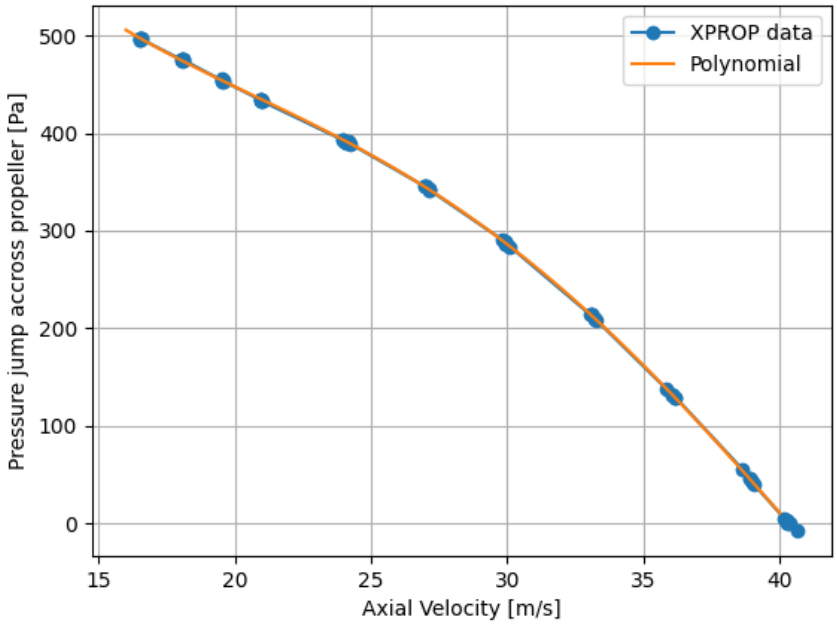

Figure 4.8: Plot of the propeller disc pressure jump as a function of the inflow axial velocity with the polynomial used by fluent indicated (adapted from unpublished internally distributed data produced by Van Arnhem as part of his PhD thesis [37])

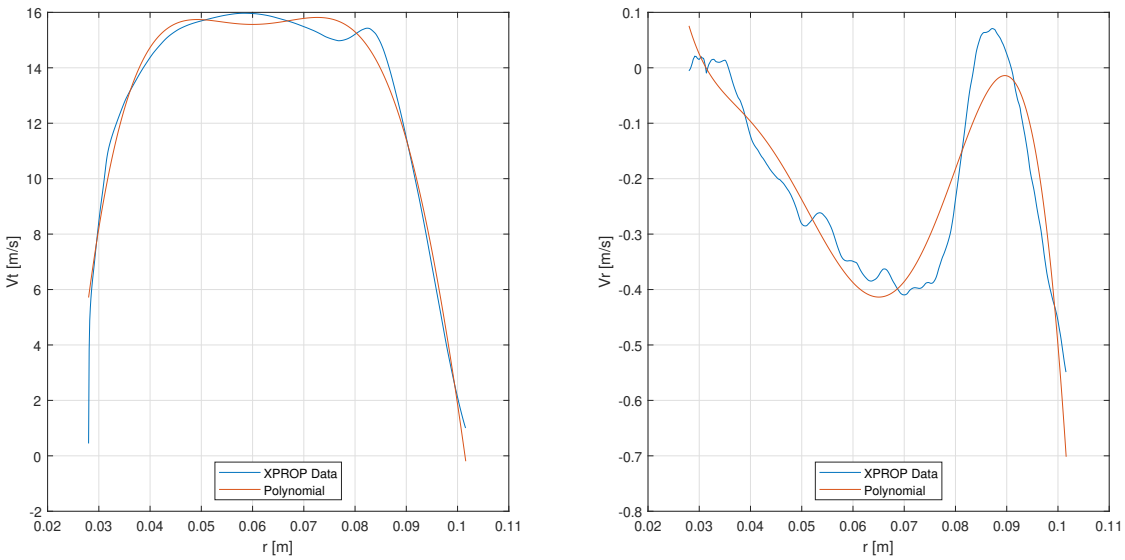

(a) Tangential Velocity Plot

(b) Radial Velocity Plot

Figure 4.9: Plot of the disc averaged tangential and radial velocity as a function of the radius velocity with the polynomial used by fluent indicated (adapted from unpublished internally distributed data produced by Van Arnhem as part of his PhD thesis [37])

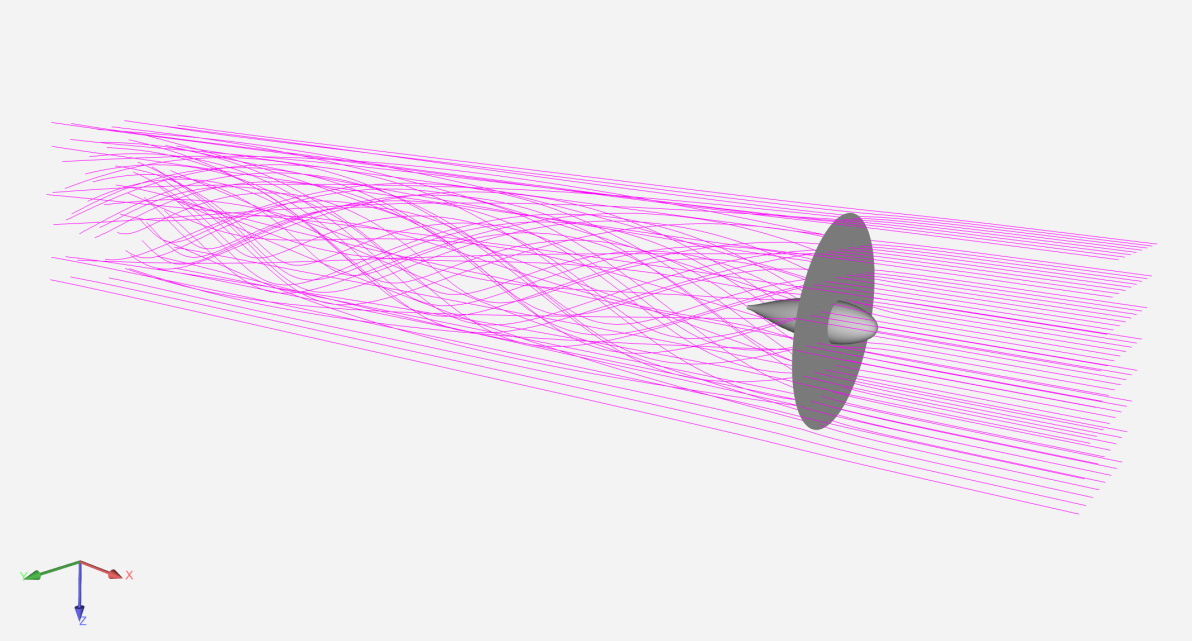

Figure 4.10: The streamlines on the isolated numerical propeller model

4.4. Validation Approach

Unfortunately, the validation experiment does not contain many repeats therefore statistical comparison between the CFD and experimental data is not possible. Therefore the validation will largely involve the qualitative comparison of CFD and wind tunnel data.

4.4.1. Oil Flow Visualisation Comparison

Perhaps the most interesting comparison that can be made between the CFD and wind tunnel results is to compare the oil flow visualisation images with the line interval convolution (LIC) images generated in CFD. The surface flow structures can be compared. This is largely a qualitative comparison with the flow structures, their locations and separation line locations compared. This will give the clearest indication of how well the numerical model captures the real flow phenomena.

4.4.2. Pressure Tap Comparison

Pressure tap data collected at the target angle of attack (10°) can be compared with pressure data at the same location in CFD. The data can be plotted together in the same plot and the pressure coefficient magnitudes compared and pressure distribution features compared.

Discrepancies between the CFD and experimental pressure data can be explored by looking at the oil flow visualisation comparison. Small discrepancies in the location of flow structures could result in a significant discrepancy in the pressure distribution. The proximity of the pressure taps to the nacelle/ propeller, a region which has significant 3D effects, makes it likely that the pressure taps will be influenced by local flow phenomena.

4.4.3. Wake Rake Comparison

In a similar manner to the pressure tap data, the total pressure at the wake rake plane location in CFD can be compared to the experimental data. In this way the flow structures behind the wing can be compared. Some indication of how well the off surface flow structures are modelled can be obtained.

This page is intentionally left blank

5

Experimental Results, Validation of The Numerical Model and Problem Characterisation

This chapter will discuss the initial results that were obtained from the wind tunnel test campaign. Additionally, it will cover the validation of the numerical model by comparing it to the wind tunnel data. Finally, this chapter will present the additional problem insight from the validated model. Conclusions can then be drawn on the impact of the propeller-nacelle system on the wing high angle of attack performance.

5.1. Wind Tunnel Test Results

This section covers the results from the wind tunnel tests carried out at the LTT between the 10th and 21st of May 2021. The results are presented and some initial conclusions are drawn where possible.

5.1.1. Nacelle-wing Interaction Effects

Figure 5.1 shows the local lift, drag and moment coefficient polars based on the data from the two rows of pressure taps placed either side of the nacelle. The presence of the nacelle has minimal impact on the lift coefficient at low angles of attack. The lift curve slope is the same in the linear regime. At angles of attack above 4°, as viscous effects become significant, the case with nacelle shows a reduction in lift coefficient compared to the clean wing. Close to and beyond the maximum lift coefficient, the behaviour becomes more complex in the case with the nacelle. Significant asymmetry is observed and in the case of the starboard set of pressure taps substantial changes in behaviour between angles of attack with the lift coefficient even rising to above the maximum lift coefficient at an angle of attack of above 18°. This behaviour is attributed to the 3D nature of the flow in the region close to the nacelle and therefore it is difficult to draw conclusions from the local pressure data.

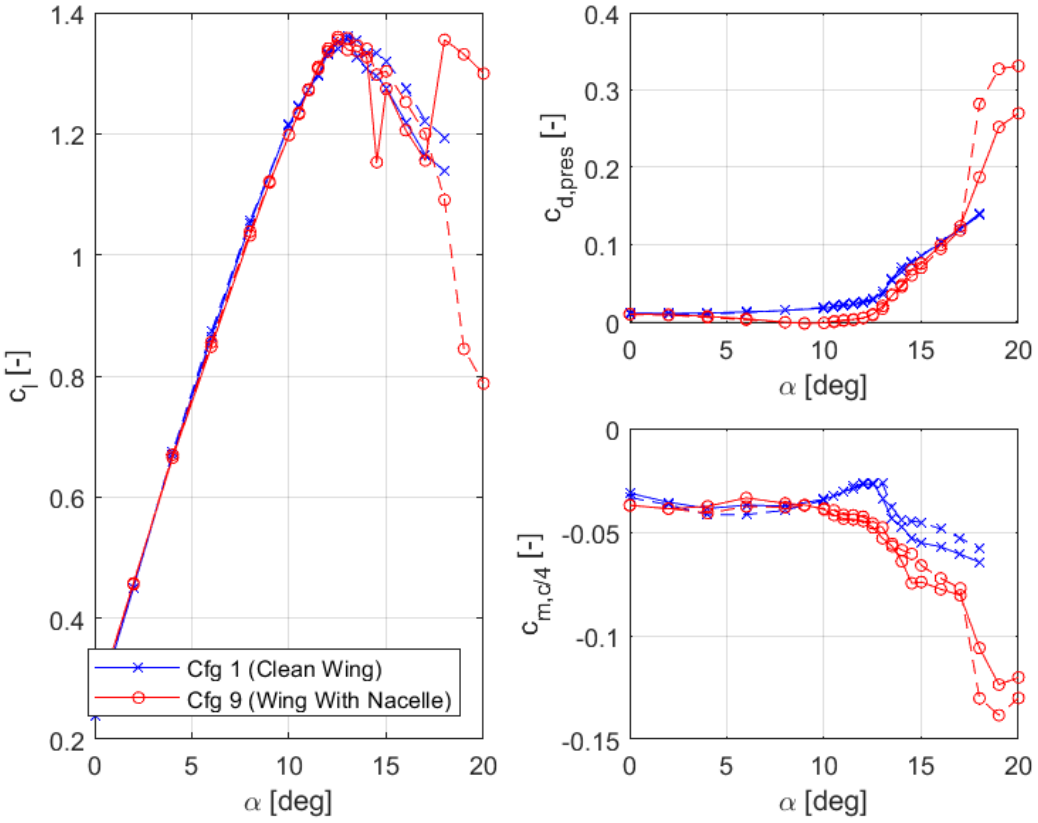

Figure 5.1: Local Lift, drag and moment coefficient polars for the NLF-Mod22(B) with and without nacelle, solid line = starboard side, dashed line = port side

Figure 5.2 shows the local pressure coefficient from the pressure taps for an angle of attack of 10°. In the case with the nacelle attached an increase in the magnitude of the leading edge pressure peak can be observed. This increase in pressure peak is characteristic of the increased local flow incidence effect described in Section 2.1.2. The mid-portion of the airfoil is offloaded in comparison to the clean wing with the aft portion of the wing once again being more loaded than in the clean wing case. Interpreting this pressure distribution is difficult in isolation as the pressure is measured at two single chord-wise locations and the flow adjacent to the nacelle is dominated by 3D effects.

Figure 5.3 shows the wing surface flow. The region behind the nacelle shows a clear flow lateral expansion consistent with the effects described in Section 2.1.1 suggesting the presence of a higher pressure region behind the propeller nacelle. The flap and trailing edge in the region behind the nacelle remain attached for longer. In addition to this, the regions either side of the flow expansion show a forward movement of the wing separation line which is consistent with the boundary layer accumulation effect observed by Qiu et al [28]. Figure 5.3 shows that the pressure taps are located in the region that experiences significant 3D variation. The presence of the flow separation adjacent to the nacelle likely explains the reduction in suction observed in Figure 5.2 with the increase in trailing edge suction potentially the result of the increased flow attachment in the high-pressure region. The size and location of these 3D structures introduced by the nacelle have a large effect on the measure pressure coefficient and therefore the calculated performance coefficients. The complex flow structures are likely responsible for the erratic behaviour of the lift coefficient in the post-stall.

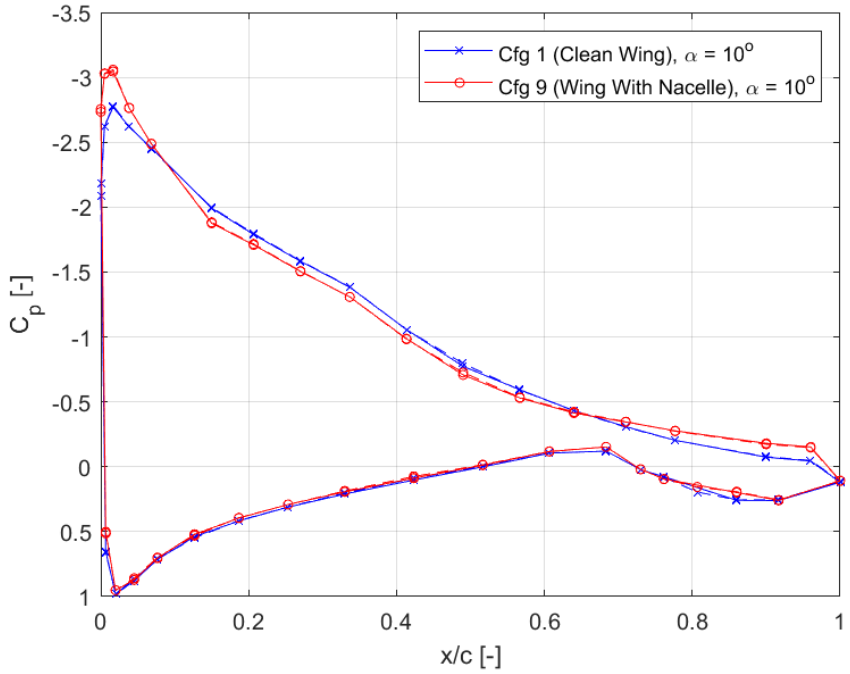

Figure 5.2: Pressure coefficient distribution for the NLF-Mod22(B) with and without nacelle at an angle of attack of 10°, solid line = starboard side, dashed line = port side

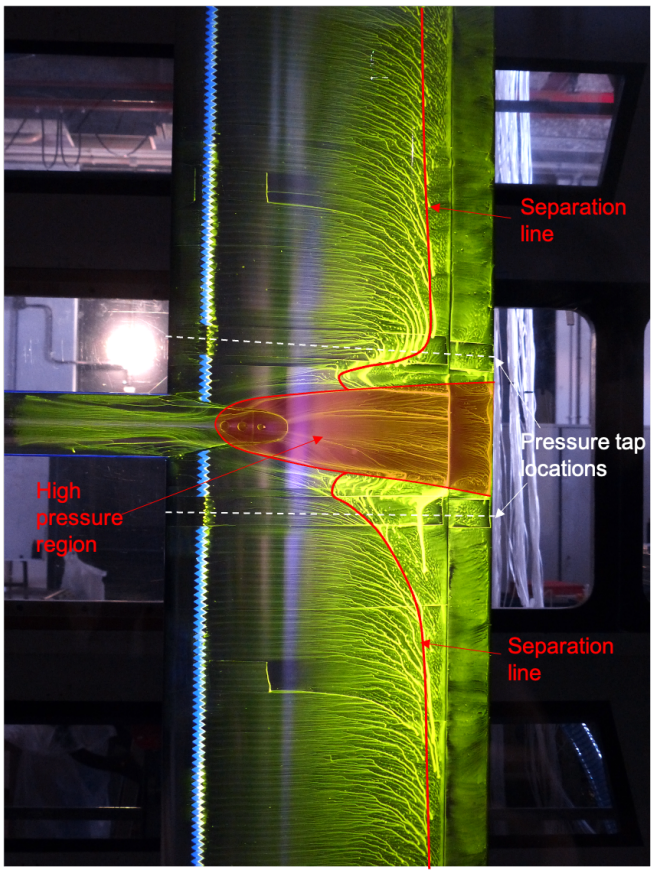

Figure 5.3: Annotated oil flow visualisation for the NLF-Mod22(B) with nacelle at an angle of attack of 10°

Figure 5.4 shows the wake behind the wing. The presence of the nacelle distorts the uniform wake distribution behind the clean wing, two large regions of lower total pressure are clear either side of the wing centre line. These regions likely originate from the two areas of the separation describe previously. The centre portion of the wake shows a slightly higher dynamic pressure compared to the case without nacelle that is likely a reflection of the less loaded and therefore unseparated region directly behind the nacelle. Overall the presence of the nacelle seems to result in a net reduction in the wake total pressure which is indicative of an increase in drag. Figure 5.1 shows that the addition of a nacelle reduces the local drag coefficient at all angles of attack below the maximum lift angle. While locally the pressure distribution leads to a lower pressure drag the wing removes more energy from the flow and therefore almost certainly has a higher wing drag.

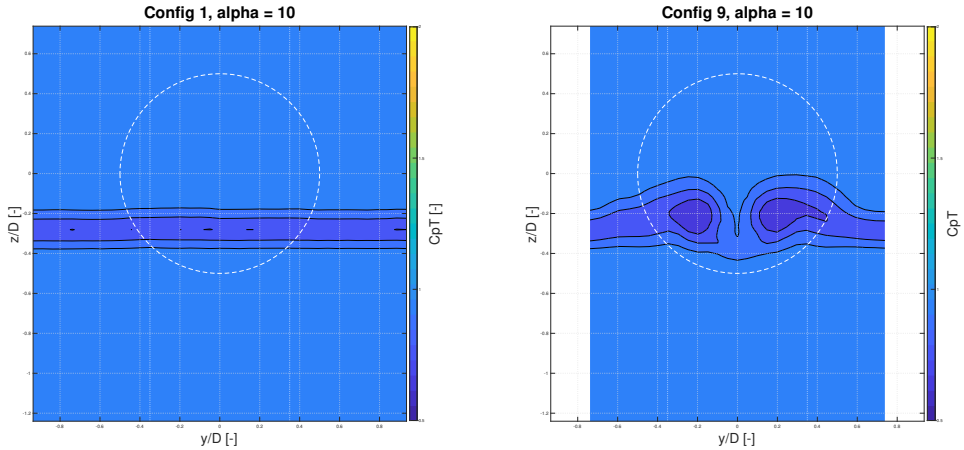

Figure 5.4: Comparison of wake rake measurements one chord length behind the wing for the case with (Config 9) and without (Config 1) nacelle for the NLF-Mod22(B) at an angle of attack of 10°

Unfortunately, no balance data is available for this test and therefore it is not possible to quantify the wing lift and drag coefficients however the presence of the separation either side of the nacelle and the offloaded region behind the nacelle suggests that the presence of the nacelle likely reduces the wing lift coefficient. This combined with the increase in wing drag implied by Figure 5.4 suggests an overall reduction in wing efficiency and therefore a reduction in the high angle of attack performance due to the presence of a nacelle. Addressing these negative interactions is likely to yield an improvement in performance.

5.1.2. Propeller-Nacelle-wing Interaction Effects

The addition of a propeller slipstream alters the interaction effects significantly. Figure 5.5 shows the local lift, drag and moment polars for the wing with and without propeller. The high dynamic pressure wake results in an increase in the slope of the lift curve polar and results in an increase in local lift coefficient at virtually all positive angles of attack. The propeller swirl introduces large differences between the sides. The up-going blade side is offset relative to the down-going side. This effect is due to the differences in induced angle of attack described in Section 2.2.1. The swirl effect also results in a difference in the maximum lift angle of attack, the up-going blade side has a lower maximum lift angle of attack and the down-going blade side experiences a higher maximum lift angle of attack compared to the case without propeller.

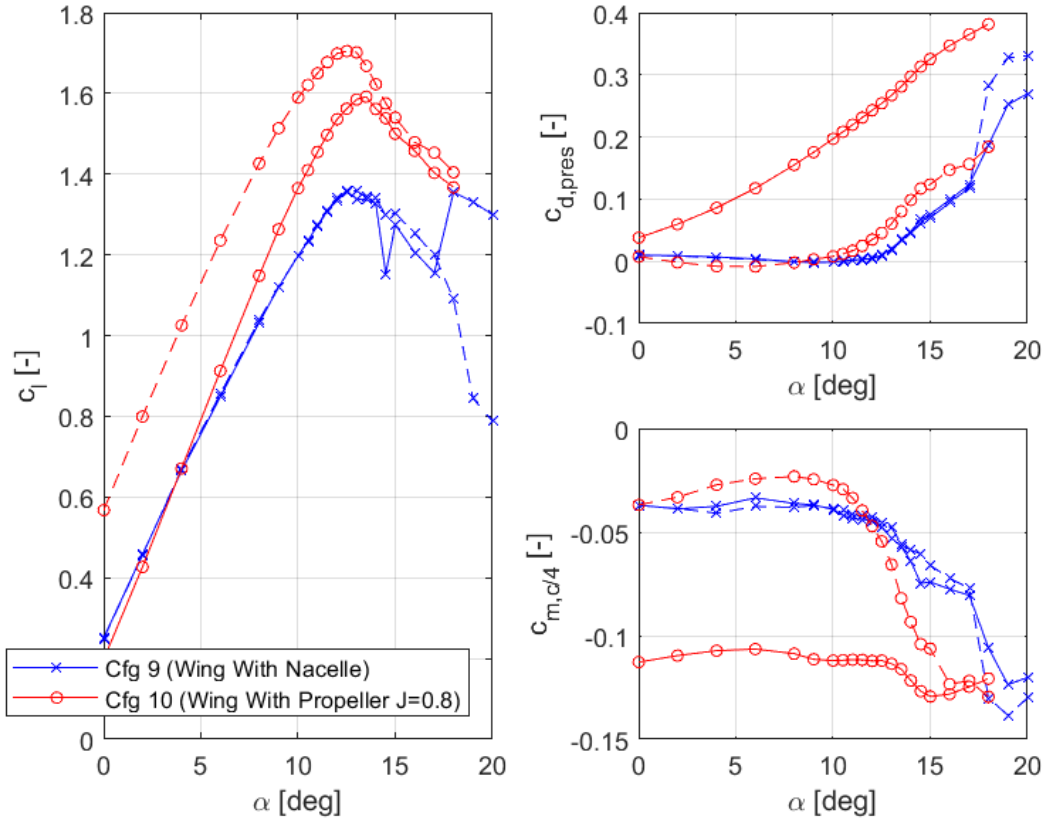

Figure 5.5: Local Lift, drag and moment coefficient polars for the NLF-Mod22(B) with nacelle, with and without propeller, solid line = (down-going blade) starboard side, dashed line = (up-going blade) port side

Figure 5.6 shows the local pressure coefficient from the pressure taps for an angle of attack of 10°. The presence of the propeller once again leads to significant asymmetry in the distribution. The up-going blade side shows a significant increase in the leading edge pressure peak which is consistent the higher induced angle of attack as a result of the propeller swirl. The down going blade side shows a minimal pressure peak which is indicative of a lower angle of attack. Both sides show a stagnation pressure coefficient that is greater than one as a result of the increased dynamic pressure introduced by the propeller. In general, the pressure distribution is very different to the case without propeller.

Figure 5.7 shows the wing surface flow structures through the use of oil flow visualisation. The influence of the propeller wake is clearly visible, the propeller clears much of the oil from the region influenced by its wake. This is indicative of the higher dynamic pressures in the propeller wake resulting in higher surface shear stresses and therefore more oil transport in the propeller wake. The influence of the wing on the propeller wake is also apparent. The wake shears towards the down-going blade side (top in this image) of the wing as was described in Section 2.2.3. While the wake is sheared to the down-going side the streamlines in the wake clearly bend towards the up-going which is consistent with the bulk rotation of the upper wake. Either side of the propeller wake the separation line moves forward in a similar way to what was observed in the propeller off case. This also seems to cause the propeller wake region to contract slightly. This separation likely limits the maximum performance of the propeller-nacelle-wing system.

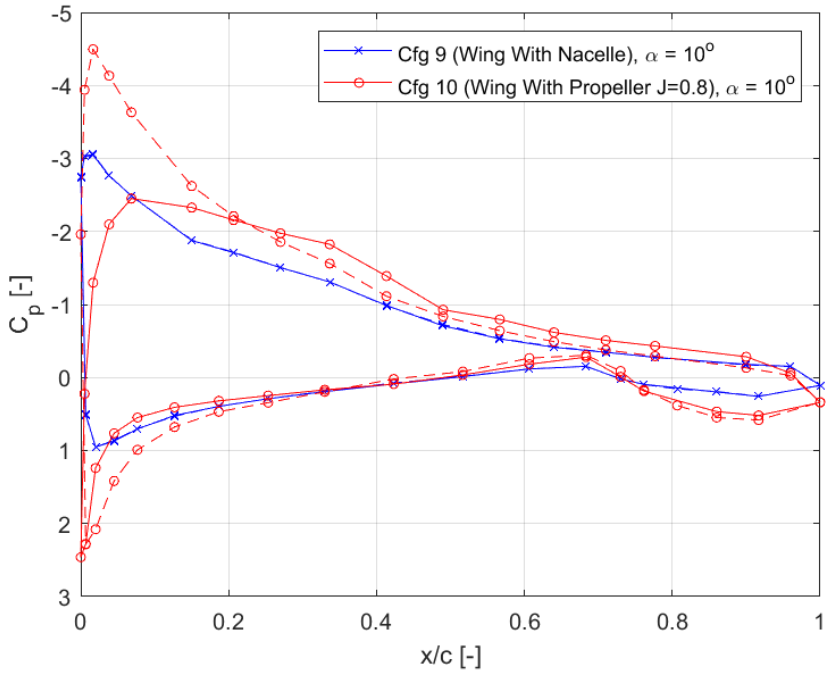

Figure 5.6: Pressure coefficient distribution for the NLF-Mod22(B) with nacelle, with (Config 10) and without propeller (Config 9) at an angle of attack of 10°, solid line = starboard (down-going blade) side, dashed line = port (up-going blade) side

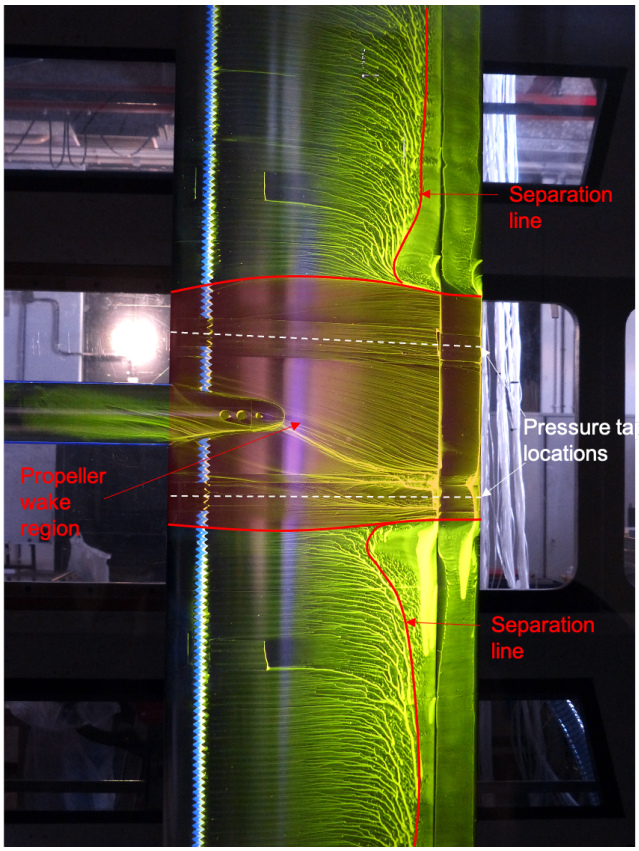

Figure 5.7: Annotated oil flow visualisation for the NLF-Mod22(B) with nacelle and propeller (J = 0.8) at an angle of attack of 10°

Figure 5.8 shows the total pressure distribution one chord behind the wing. The characteristic T shaped propeller wake described in Section 2.2.3 is clear from this figure. The propeller injects higher dynamic pressure into the wake making it difficult to make an accurate assessment of its impact on the wing drag from these wake rake plots.

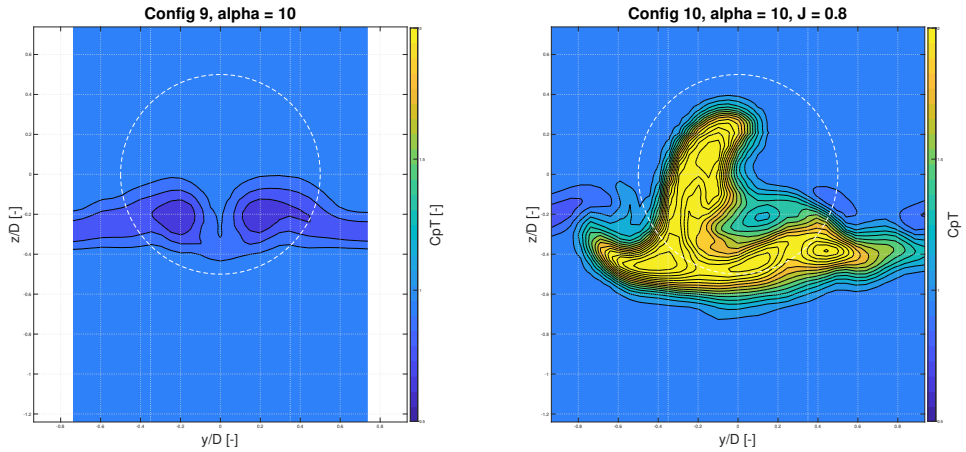

Figure 5.8: Comparison of wake rake measurements one chord length behind the wing for the case with nacelle, with (Config 10) and without (Config 9) propeller for the NLF-Mod22(B) at an angle of attack of 10°

5.1.3. Leading Edge Extensions

In addition to the basic configurations, two initial leading edge modifications described in Section 4.2.4 were assessed. These modifications were developed early on in the development process and therefore these results only represent an initial look at how the propeller wing interaction effects can be modified.

Figure 5.9 shows the pressure coefficient distribution for the wing with nacelle and with nacelle and each of the two LExs at an angle of attack of 10°. The leading edge extensions, unfortunately, cover the pressure ports on the front portion of the wing meaning that the pressure distributions with the LExs is only partial. At this higher angle of attack it can be seen that there is some additional loading on the aft portion of the wing. This results in an increase in partial lift coefficient (cl': lift computed using only the rear pressure taps) at high angles of attack as is shown in figure 5.10. Because of the covered pressure taps, it is hard to determine the significance of these results and what they mean in terms of answering the research questions of improving the wing high angle of attack performance.

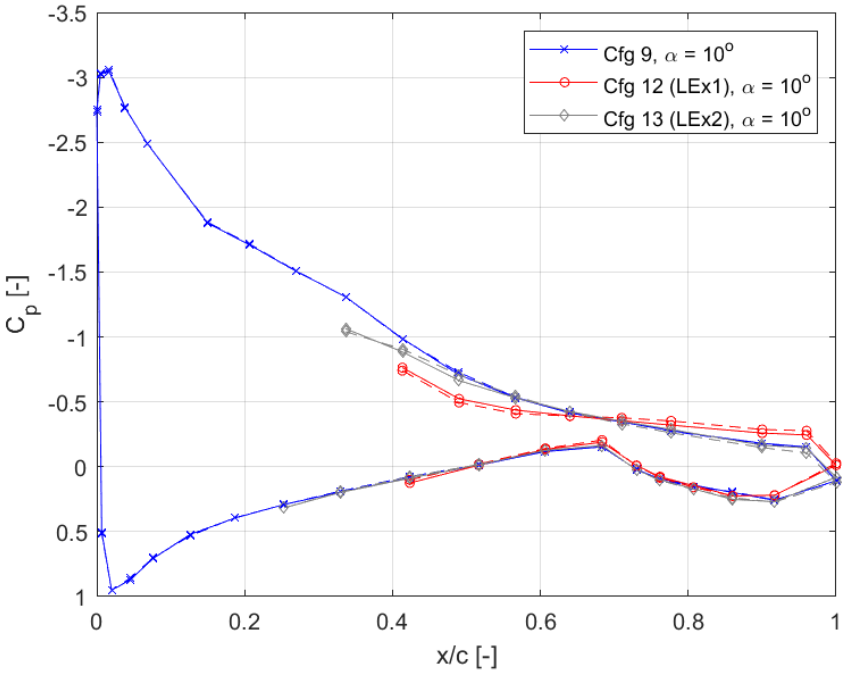

Figure 5.9: Pressure coefficient distribution for nacelle off, nacelle on, nacelle on with LEx1 and nacelle on with LEx2 at an angle of attack of 10° and a flap deflection of 0°, solid line = starboard (down-going blade) side, dashed line = port (up-going blade) side

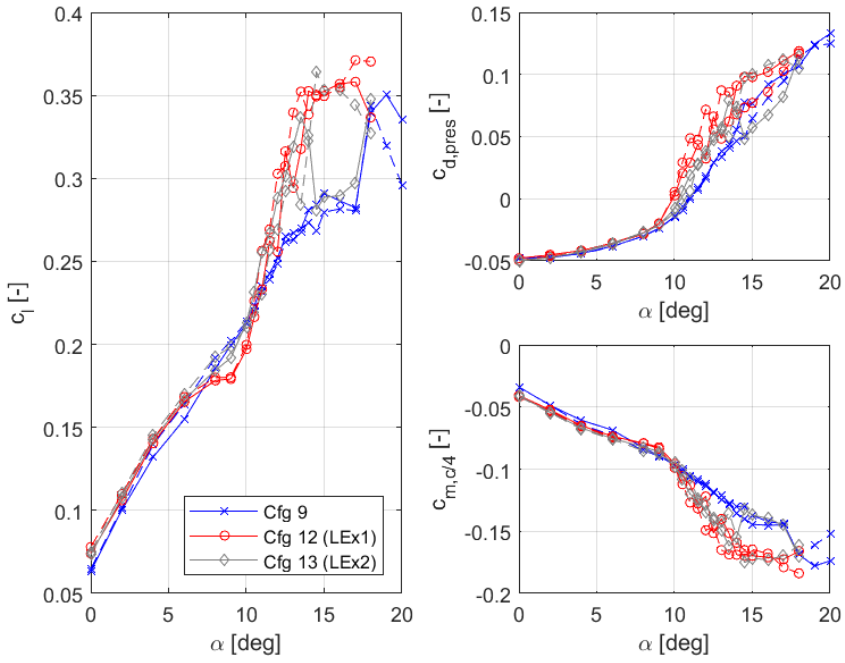

Figure 5.10: Lift, drag and moment polars for nacelle off, nacelle on, nacelle on with LEx1 and nacelle on with LEx2 with a flap deflection of 0°, solid line = starboard (down-going blade) side, dashed line = port (up-going blade) side

Oil flow visualisation images at the same angle of attack as the pressure coefficient distribution shown in figure 5.9 are presented in figure 5.11. Both LExs introduce some differences in terms of stall behaviour. Far away from the nacelle LEx1 seems to result in movement of the stall line aft. The starboard (upper)

portion of the wing seems to remain attached much closer to the nacelle compared to the port (lower) side. This significant asymmetry was not observed in the pressure tap measurements presented in figure 5.10. The reason for this discrepancy is not clear however it is worth noting that for LEx1 clay was used to try to smooth the transition between the 3D printed LEX and the wing. This clay seemed to interact with the fluid used for the oil flow visualisation causing it to become more viscous. Figure 5.11b shows this in that in some locations the brush strokes are still visible. This makes it difficult to draw conclusions from this oil flow image. The interactions with the clay led to the decision not to use this clay for the flow visualisations of LEx2. LEx2 appears to result in a substantial change in the growth of the stall region behind the nacelle. The stalled flow that occurs directly behind the nacelle seems to reduce in size suggesting that the more tolerant leading edge is better able to mitigate the induced angle of attack. However, the LEx also introduces an additional region of separated flow that appears to form in the region behind where there is chord discontinuity as a result of the LEx being an add on rather than being smoothly integrated into the airfoil. Due to the close proximity of the two stall regions produced it seems likely that these regions influence each other and therefore understanding to what extent the reduction in size of the stall region near to the nacelle is the result of the LEx improving the local flow and what is the result of interactions between structures is difficult. In addition to this, both LExs show evidence of a laminar separation bubble. Installing the LExs required the removal of the trip strips and therefore allows for the formation of these types of structures. This change in the transition location and boundary layer development also influences the development of the stalled flow. Finally, the blend between the LEx and the wing was not smoothed perfectly and therefore the surface finish was not the same as the unmodified wing model. The combination of these modelling deficiencies mean that these results alone are not able to produce answers regarding the second part of the research question however they do give some initial insight that can be used to inform future design decisions.

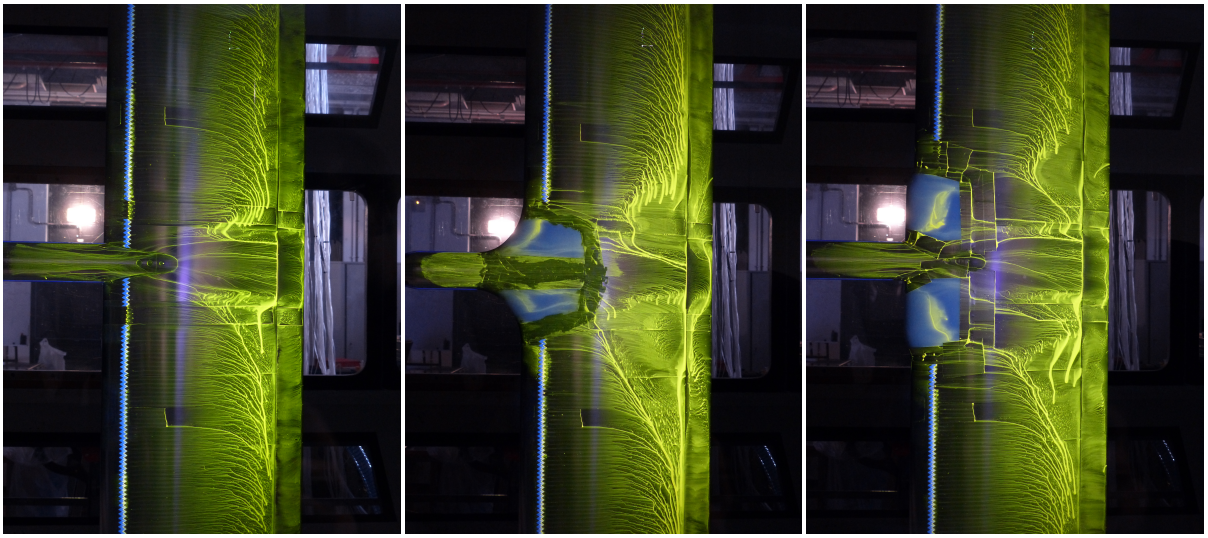

(a) Propeller off (b) Propeller off, LEx1 (c) Propeller off, LEx2

Figure 5.11: Oil flow visualisation for the cases with propeller off, propeller off and LEx1 and propeller off and LEx2 at an angle of attack of 10°

Figure 5.12 shows the pressure distribution without and with each of the two LExs in the case with the propeller on. It is noticeable that in the down-going blade case the loading in the of the aft portion of the airfoil is virtually identical to that seen in the case of the wing without LEx in the case of the up-going blade side both LExs appear to result in a slightly more aft loading of the airfoil. this is most obvious in the case of LEx2. The partial lift coefficient for both of these cases is shown in figure 5.13. From this figure the increase in aft loading results in a higher maximum partial lift coefficient on the up-going blade side. However, the LEx modifications seem to have minimal effect at lower angles of attack. Once again it is difficult from this limited data to draw conclusions about how effective the modifications have been in increasing the high angle of attack performance due to the limited data.

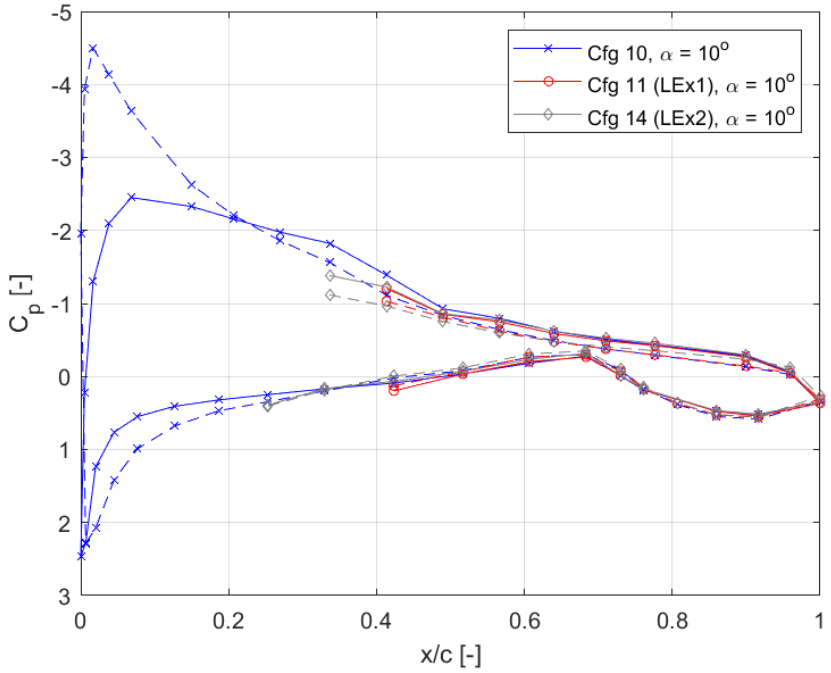

Figure 5.12: Pressure coefficient distribution for the prop-on, prop-on with LEx1 and prop-on with LEx2 at an angle of attack of 10° and a flap deflection of 0°

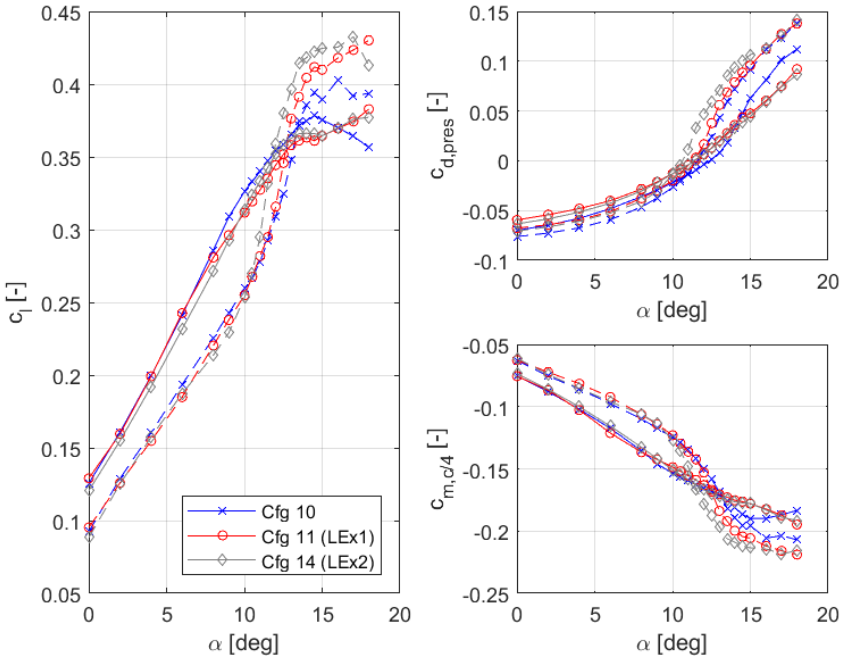

Figure 5.13: Lift, drag and moment polars for prop-on, prop-on with LEx1 and prop-on with LEx2 with the flap set at 0° for J = 0.8

Figure 5.14 shows the oil flow visualisation images for the wing with and without each of the two LExs in the case with the propeller on. In this case, the issues with the oil flow visualisation mixing with the clay are much worse as these measurements were performed later resulting in much of the span not flowing correctly the oil also clearly has a different texture and appearance to the other cases. This

makes drawing any meaningful conclusions from this image impossible. LEx2 on the surface does not appear to result in a significant change in the propeller slipstream behaviour however it does result in a growth of the separated regions that form at the edge of the slipstream. this is consistent with the behaviour observed previously at the chord discontinuity. The chord discontinuity augments the separation that forms at the edge of the slipstream. Understanding the significance of this result is therefore hard to determine.

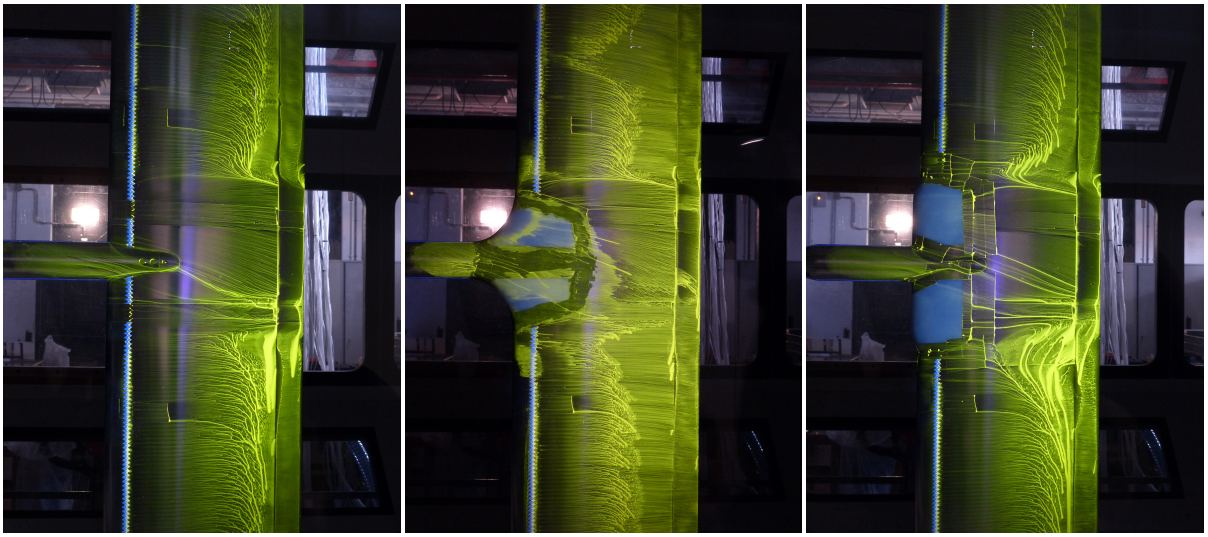

(a) Propeller on (b) Propeller on, LEx1 (c) Propeller on, LEx2

Figure 5.14: Oil flow visualisation for the cases with propeller on, propeller on and LEx1 and propeller on and LEx2 at an angle of attack of 10°, J = 0.8

Figure 5.15 shows the span wise pressure distribution over the wing with and without propeller and with each of the two leading edge extensions fitted. This distribution is intended to be representative of the lifting distribution across the span of the wing. Moreover, the probe data for LEx2 does not follow the trend observed for the clean wing or LEx1 case. This is expected to be the result of the incorrect execution of the measurements. Finally, an additional check was performed by comparing the static pressure measured by the probe at the wing pressure tap line with the result obtained by interpolating the wing pressure taps. While this shows a similar trend between configurations (in terms of the relative pressure coefficient for each configuration) the pressure tap interpolation consistently underpredicts the static. This may be the result of the interpolation used as the pressure distribution between pressure taps was assumed to be linear. In addition to this, the probe itself may alter the flow over the wing resulting in lower pressures.

The probe measurements for the baseline wing and LEx1 show some key trends. In the propeller off, configuration a clear increase in static pressure can be observed behind the nacelle, This increase in pressure is aggravated by the presence of the fillet leading edge extension. This is logical as the fillet alters the wing leading edge and therefore reduces the leading edge suction resulting in a higher pressure behind the nacelle. In the propeller on case, a region of reduced static pressure is observed in the region behind the propeller. This is the result of the high dynamic pressure produced by the propeller resulting in higher lift on the wing. A reduction in static pressure is present on the up-going blade side due to the swirl reducing the effective angle of attack consistent with what was observed in figure 5.13. Two peaks can be observed in the pressure distribution. One at the edge of the blade on the up-going blade side and one behind the nacelle. The reason for these peaks is not well understood at this time and will require further analysis. The presence of LEx1 once again reduces the static pressure in the region in a similar way to the propeller off condition. In order to further understand this result, further comparisons with simulations will be required.

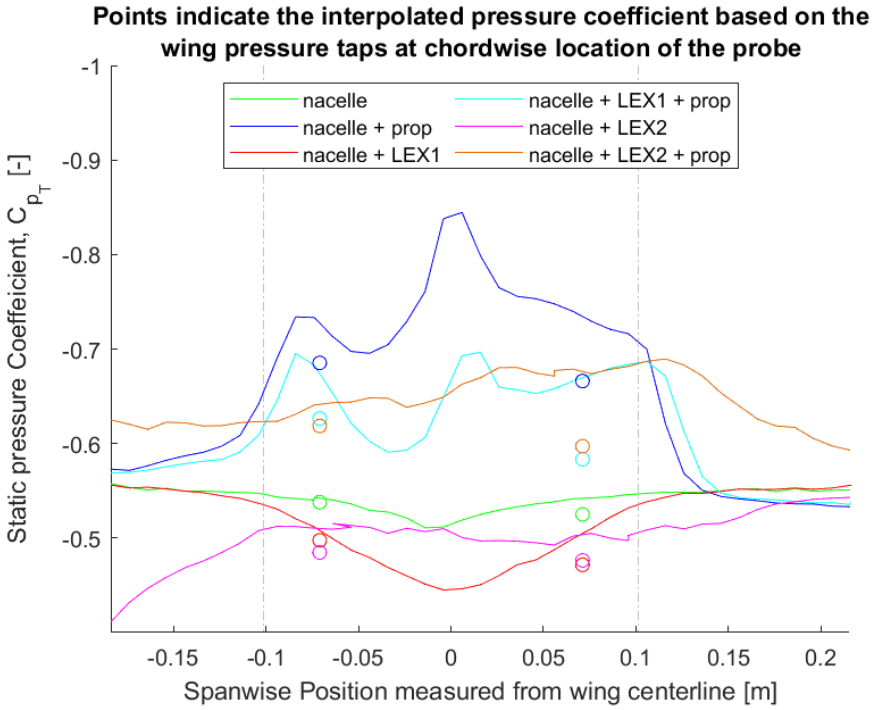

Figure 5.15: Span wise pressure coefficient distribution at location of approximately 45% of the chord with the corresponding pressure coefficient interpolated from the pressure ports. For an angle of attack of 0° and a flap deflection of 0°. The dotted lines indicate the edge of the propeller.

Figure 5.16 shows the total pressure contour downstream of the wing in the region behind the propeller for the case with propeller off, with and without the LEx1 at an angle of attack of 10°. Additionally, a comparison between these two contours is presented. The case with the fillet LEx1 attached shows a growth of the low total pressure region either side of the nacelle.

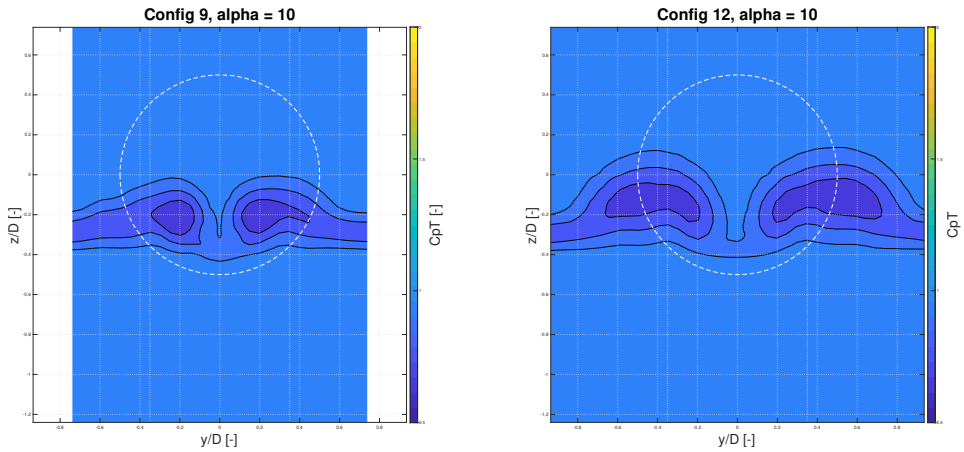

Figure 5.16: Total pressure contour plot based on wake rake measurements for the case with nacelle and the case with nacelle and LEx1 at an angle of attack of 10°

The final measurement technique that was applied to the two initial leading edge extensions was the use of a wake rake positioned behind the wing. Figure 5.17 shows the total pressure contour for the case without propeller, with and without LEx2 at an angle of attack of 10°. It shows the presence of large low-pressure regions that are consistent with the locations of the chord discontinuity and suggests the presence of vortices. Additionally, the low-pressure region corresponding to the nacelle vortices is reduced. Understanding this result will require additional analysis to determine if this is due to the LEx shape or if it is the result of interactions with the chord discontinuity vortices.

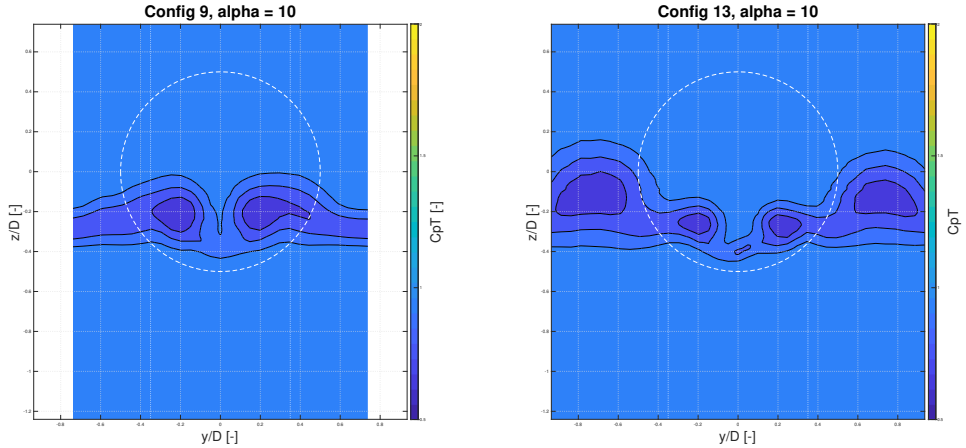

Figure 5.17: Total pressure contour plot based on wake rake measurements for the case with nacelle and the case with nacelle and LEx2 at an angle of attack of 10°

Figure 5.18 shows the total pressure contour for the case with propeller with and without LEx1 at an angle of attack of 10°. The added complexity introduced by the propeller makes interpreting the results more difficult. Further analysis is likely required in order to u8understand how the LEx impacts the wing performance. Looking at the whole region behind the wing has a lower dynamic pressure than without the LEx. This suggests higher drag. Understanding whether this is the result of the LEx geometry

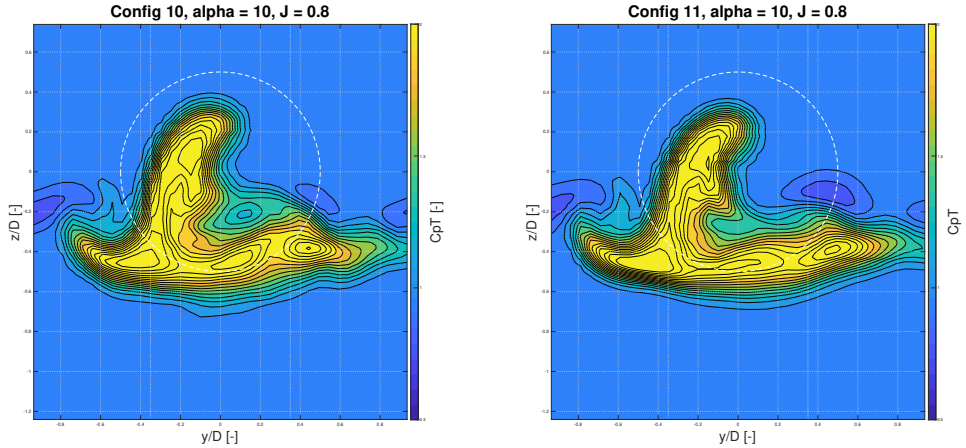

Figure 5.18: Total pressure contour plot based on wake rake measurements for the case with propeller on and the case with propeller on and LEx1 at an angle of attack of 10°

Figure 5.19 shows the total pressure contour for the case with propeller with and without LEx2 at an angle of attack of 10°. The presence of the decreased dynamic pressure region resulting from the chord discontinuity is still clear with the propeller on. Once again overall it appears that the total pressure behind the wing in the case with the LEx mounted is lower than in the case of the unmodified wing however further analysis is once again necessary.

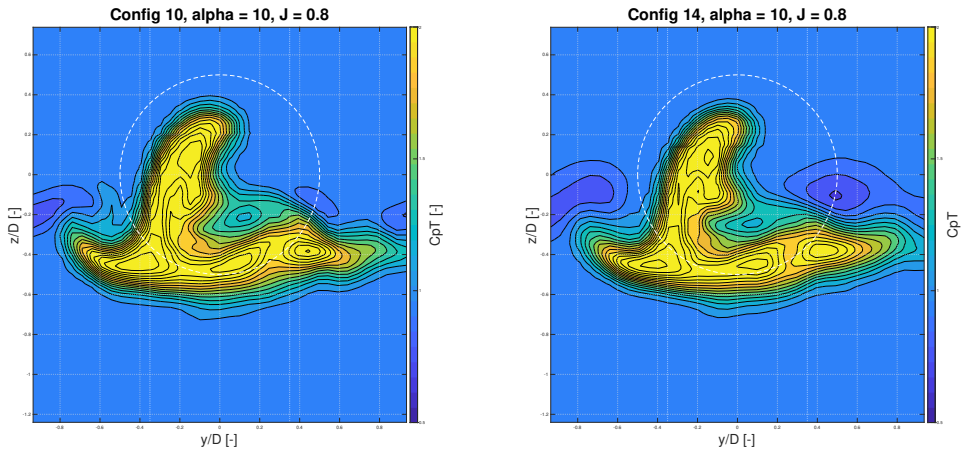

Figure 5.19: Total pressure contour plot based on wake rake measurements for the case with propeller on and the case with propeller on and LEx2 at an angle of attack of 10°

Overall, the results of this preliminary investigation into the effectiveness of leading edge and nacelle modifications is largely inconclusive. The combination of model limitations and time constraints when evaluating these options makes the result difficult to interpret. This data alone is insufficient to answer the research question and therefore further analysis will be required. These results can nonetheless be used to inform future development steps.

5.2. Numerical Model Validation

This section will outline the steps taken to validate the numerical model. The comparisons between the CFD results and the wind tunnel data will be made and discrepancies addressed.

5.2.1. Nacelle-Wing Model

Figure 5.20 shows a comparison between the wind tunnel and CFD pressure data. Overall the match between the model and the experimental data is good, with both showing similar distributions. The magnitude of the leading edge pressure peak is almost identical however the CFD data shows an additional local suction peak. The nature of the pressure taps means that the pressure is only measured at discrete locations the local pressure peak seen in CFD is unlikely to be measurable on the wind tunnel model. The other discrepancy that is observable is towards the trailing edge of the wing main element CFD predicts slightly more loading however the discrepancy is small. This is likely the result of the influence of the 3D cross flow structures identified previously. Small differences in the location of these structures change the chordwise pressure distribution significantly. Achieving a perfect match in this region between CFD and the wind tunnel model is difficult particularly given the asymmetries observed in the wind tunnel surface flow.

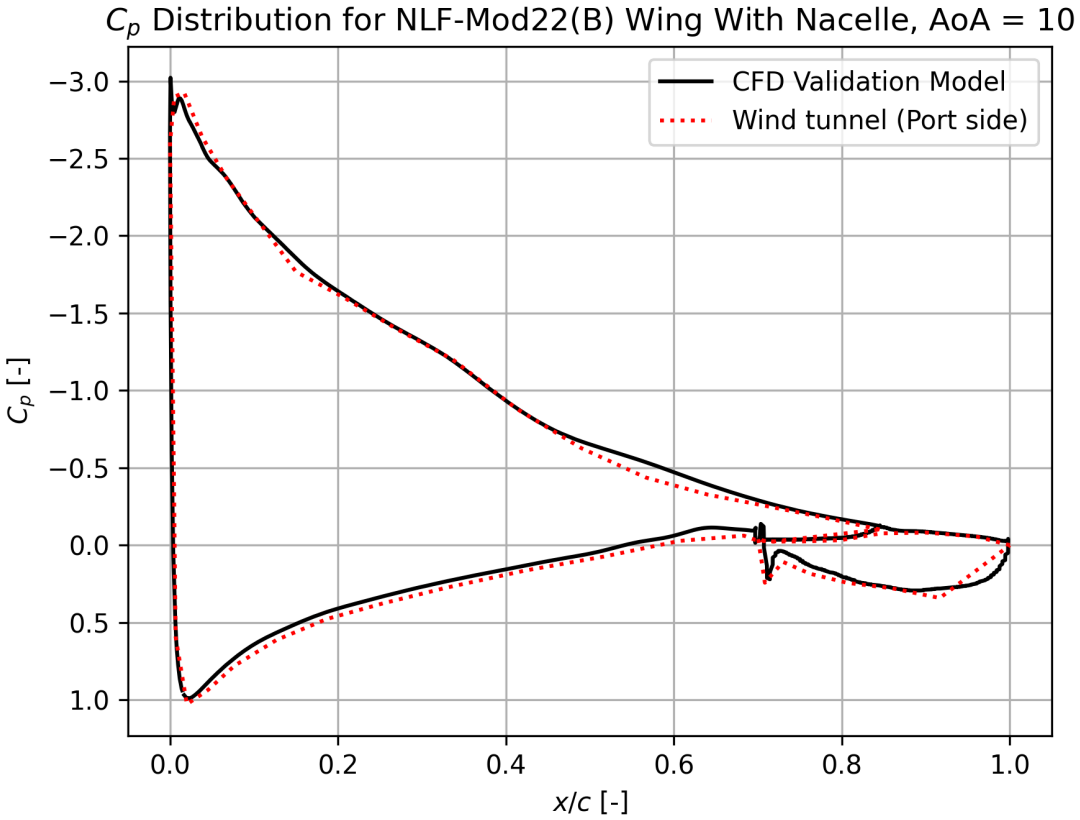

Figure 5.20: Comparison of the pressure coefficient distribution between the wind tunnel model port side pressure taps data and the corresponding location in CFD at angle of attack of 10°

Figure 5.21 shows a comparison of the experimental oil flow and the CFD wing shear stress Line Integral Convolution (LIC) images coloured by the wall shear magnitude in order to approximate the oil flow colouring. Overall comparing the two images it is clear that CFD predicts the key flow features accurately. The local flow direction shows the streamline expansion directly behind the nacelle is well captured by the CFD model. In addition, the streamline distortion that results from the presence of the flow separation is apparent in CFD with the flow curving as a result of the recirculating regions. The wind tunnel results do not show the same flow reticulation as the relatively low shear stresses in this region prevents the oil from being transported forwards but the flow does locally bend towards the leading edge which is indicative of reversed flow. The location of the wing stall line does show some discrepancy with the CFD model predicting that the main element stall occurs slightly later than what is seen in the OFV. This discrepancy is likely the result of a number of differences between the two models. The wind tunnel model flow is tripped using a zig-zag strip. The strip introduces vorticity that breaks down into turbulent flow and therefore the exact transition location is hard to determine. This effect is not present in the numerical model which is tripped at the leading edge and therefore the boundary layer turbulence is likely different. Moreover, the wing surface roughness and the effect of the oil itself on the fluid is not the same between the two models, these effects cannot be modelled in CFD easily and are therefore not considered. The differences in surface quality once again will lead to variations in the boundary layer evolution. Finally, even if the boundary layer were identically modelled in CFD you would expect to see some variation between the LIC and OFV in terms of the location of the stall line. The mass of the oil used means that very small wall shear forces cannot transport it resulting in some discrepancy in terms of the actual location of flow separation. In addition to this, the oil is impacted by gravity and therefore in regions of low shear stress the oil will tend to bend downwards in a way that is not modelled in CFD which removes the influence of gravity. Overall the match is deemed to be acceptable, the numerical model shows all of the key flow features and seems to accurately show the surface flow features introduced by the interactions between the wing and nacelle.

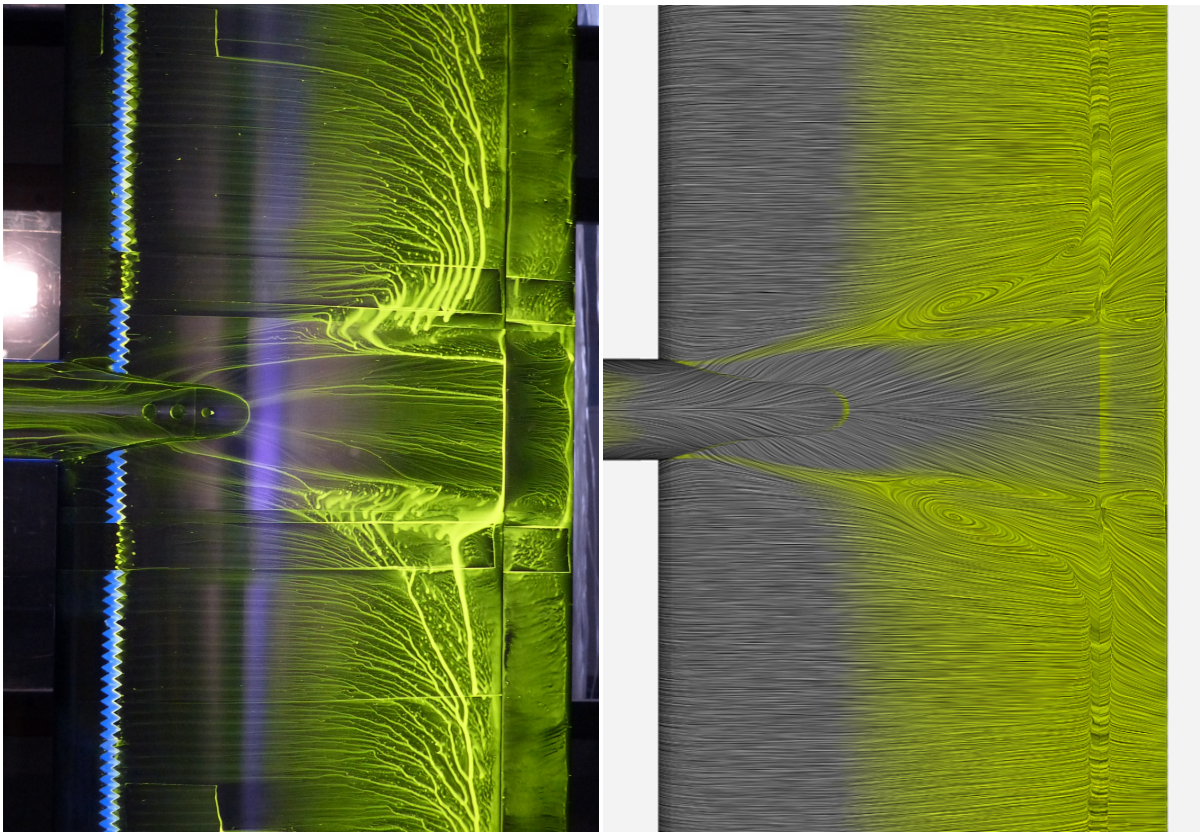

(a) Wind tunnel OFV (b) CFD wall shear LIC

Figure 5.21: Comparison of the CFD and wind tunnel surface flow field for wing with nacelle at an angle of attack of 10°

Figure 5.22 shows a comparison of the total pressure distribution at the wake rake plan located one chord length behind the trailing edge of the wing. Comparing the total pressure distribution similar structures are observed with two regions of loss that originate from the two regions of increased separation adjacent to the nacelle. In the CFD case however, the structures are far less diffuse than in the wind tunnel case. There are a number of reasons for this. As a RANS model is used the CFD model turbulence dissipation is not resolved but rather modelled which can lead to discrepancies in the persistence of turbulent structures [31]. In addition to this, the wake rake also introduces some uncertainty. The resolution of the wake rake probes is far lower than the resolution achieved by CFD and therefore some uncertainty is introduced due to interpolation. The wake rake is also positioned close to the wing (only one chord length behind) the trailing edge and therefore the flow at the wake rake plane may not be aligned with the probes which are only able to measure the total pressure contribution that is parallel to the probes and as such measurement errors are introduced. Additionally, it is possible that the upstream blockage that the wake rake introduces may impact the wing performance.

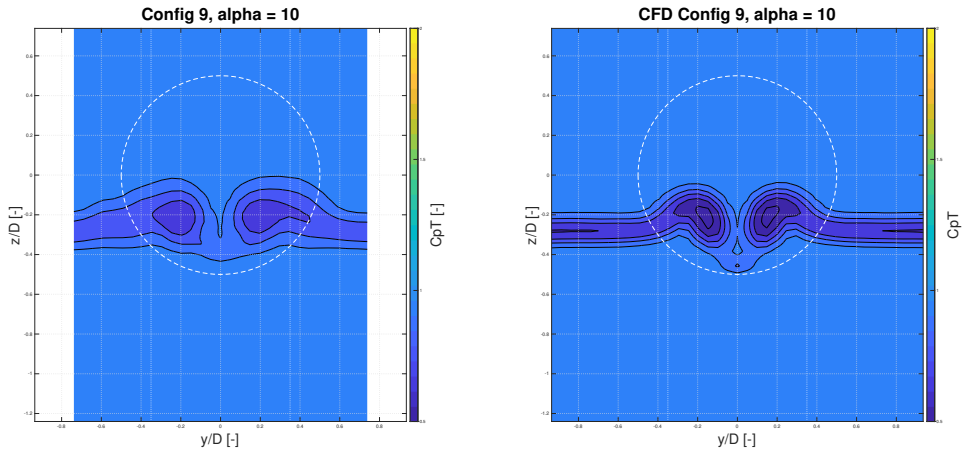

Figure 5.22: Comparison of the CFD and wind tunnel total pressure distribution at the wake rake plane for wing with nacelle at an angle of attack of 10°

5.2.2. Propeller-Nacelle-Wing Model

Figure 5.23 shows a comparison of the port and starboard pressure data 71.1mm from the wing centre line. The loading distribution is broadly similar at the pressure tap locations with CFD showing the same reduction in suction on the down-going blade side and increase in suction on the up-going blade side as a result of swirl. Some discrepancy can be observed in the magnitude of the leading edge pressure coefficient in both cases but particularly in the case of the down-going blade side. This discrepancy likely results from the differences between the behaviour of the CFD actuator disc propeller model and the real XPROP-S fitted to the wind tunnel model. The non-uniform disc loading introduced as a result of the propeller blade angle of attack is not modelled by the actuator disc model. The increase in blade loading on the down-going blade side described in Section 2.2.3 is not modelled and therefore the velocity induced by the propeller on the down-going blade side is lower than that produced by the wind tunnel propeller. In addition to this, the fan boundary condition used assumes a uniform axial loading across the whole disc. The pressure jump was prescribed based on the propeller thrust divided evenly over the disc and therefore locally the induced velocity will differ from the real propeller.

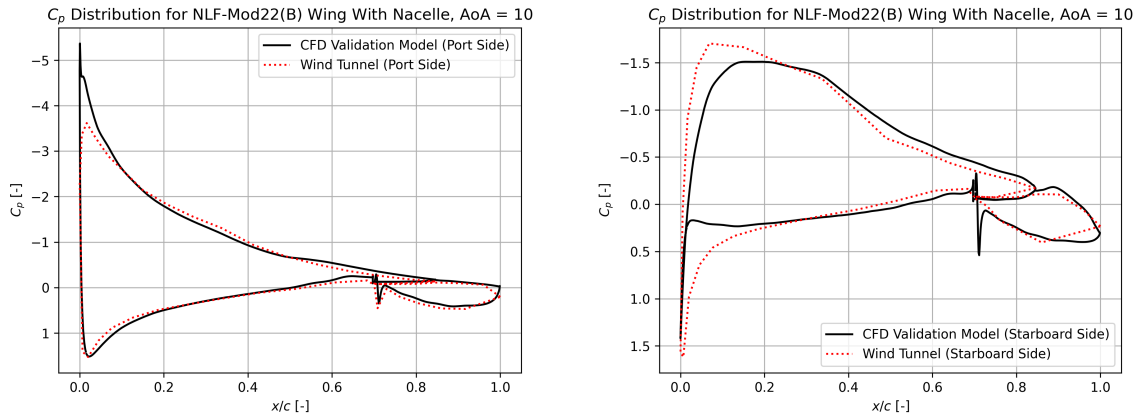

(a) Port side (up-going blade side)

(b) Starboard side (down-going blade side)

Figure 5.23: Comparison of the pressure coefficient distribution between the wind tunnel model port and starboard side pressure taps data and the corresponding location in CFD at angle of attack of 10°, propeller advance ratio J = 1.0

Figure 5.24 shows a comparison between the oil flow images in the wing tunnel and LIC images generated from CFD. It is worth noting that no oil flow data was collected at an advance ratio, J of 1.0 and therefore the oil flow images are of a propeller operating at J = 0.8. This difference in advance ratio means that even assuming that the CFD model was to perfectly model real-world physics significant differences would be expected. The lower advance ratio and thrust coefficient result in a lower dynamic

pressure propeller wake and differences in the ratio of axial and tangential velocity at any given point in the wake changing how it will interact with the wing. Overall, the CFD model shows the same key flow features. It shows the region of influence of the propeller wake surrounded by two regions where the flow separation line moves forward. The swirl in the propeller wake introduces a spanwise flow component to the flow that seems to behave in a similar way to the case without the propeller. The port side behaviour is complex and likely the result of interactions of the combined propeller-nacelle system on the wing. In addition to this, the wind tunnel result from the oil flow suffers from the same deficiencies in terms of the influence of gravity and the lack of oil transport at lower shear stresses that was described previously therefore discrepancies in the flow direction in regions of low shear are not unsurprising. Overall while the wing surface flow field is far from identical comparing CFD and the wind tunnel data this is unsurprising given the low fidelity propeller model and the differences in conditions, the flow structures are largely similar and therefore this is likely sufficient to allow for an understanding of the influence of a propeller on the nacelle-wing interactions effects and for use as part of a comparative study.

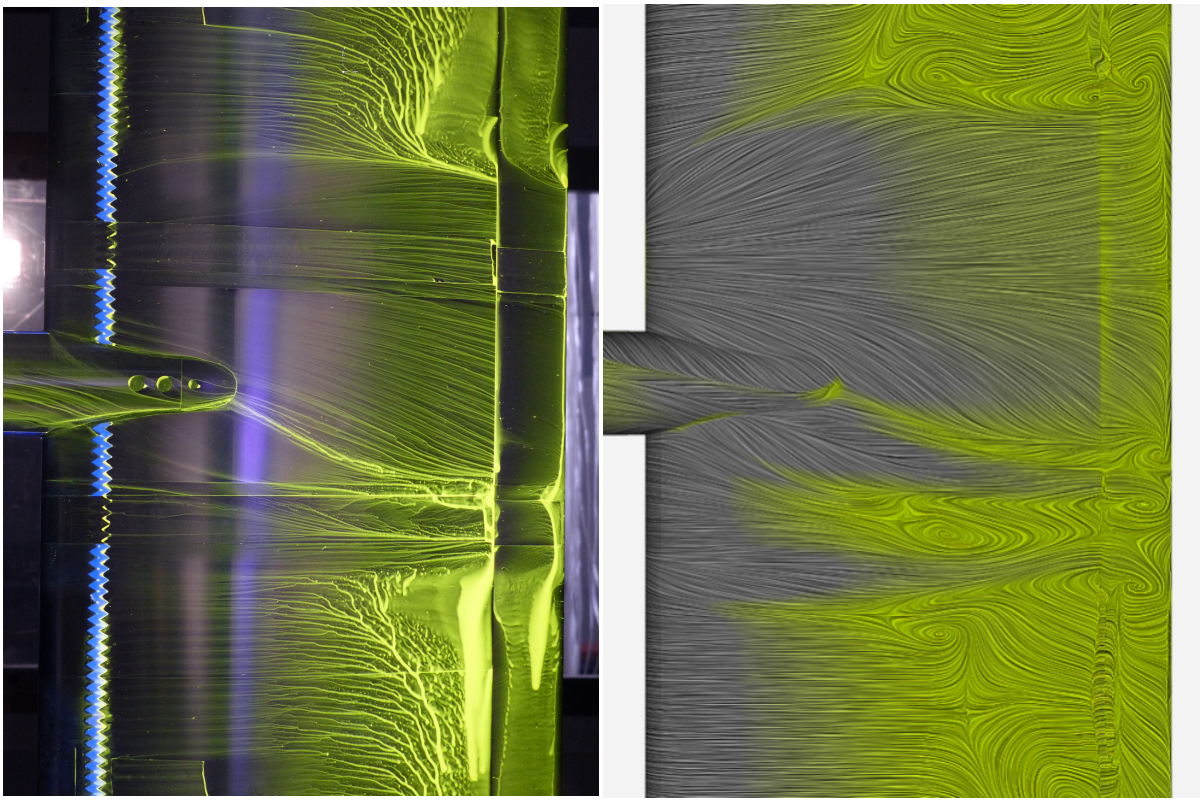

(a) Wind tunnel OFV (J = 0.8)

(b) CFD wall shear LIC (J = 1.0)

Figure 5.24: Comparison of the CFD and wind tunnel surface flow field for wing with nacelle a propeller at an angle of attack of 10°

Figure 5.25 shows the comparison of the CFD and wind tunnel total pressure distribution at the wake rake plane located one chord length behind the wing trailing edge. There is a substantial discrepancy between the total pressure distribution generated by CFD and what was measured in the wind tunnel. Both distributions show the characteristic inverted T distribution however the shape and location of the various structures is very different. Additionally, the magnitude of the increase in dynamic pressure in the wake resulting from the propeller is lower than was seen in the wind tunnel. When interpreting these discrepancies it is, however, important to note there is a difference once again between the advance ratio and therefore the thrust coefficient between the two cases. This will have an impact on both the magnitude of the total pressure increase in the wake a the thrust is lower and the ratio between axial and tangential velocity is different. In addition to the discrepancies in the condition, the differences could also be the result of the of the CFD model deficiencies, particularly in terms of the way turbulence dissipation is modelled in RANS. Similarly to what was observed when analysing the on surface flow,

CFD shows a much stronger separation adjacent to the propeller wake.

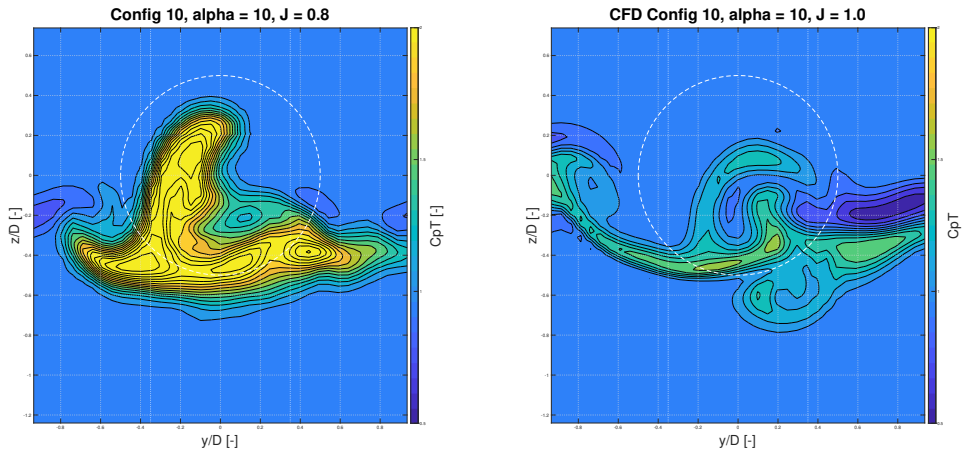

Figure 5.25: Comparison of the CFD and wind tunnel total pressure distribution at the wake rake plane for wing with nacelle and propeller at an angle of attack of 10°

5.2.3. Zero Degree Angle of Attack Condition

To meet the research objectives, the impact of the propeller-nacelle-wing interactions and any modifications applied to the geometry at lower angles of attack should be assessed. This case should also be validated however as the focus of the research question is on high angle of attack performance this case is considered less important and therefore the evaluation activities are more limited.

Figure 5.26 shows a comparison of the pressure distributions at zero angle of attack. Overall the distributions are similar in shape however the CFD model seems to consistently overpredict the pressure coefficient. It is not clear exactly why this occurs but it is perhaps a systematic error present in the CFD data introduced by for example differences in the boundary layer measurements or limitations in the point accuracy of the pressure measurements. Such a systematic error is likely not as apparent at higher angles of attack as a result of the larger changes in pressure introduced by the wing and therefore the errors are relatively smaller. The other discrepancy observed is on the lower side, just in front of the cove, CFD predicts suction in this region however the wind tunnel pressure distribution does not reflect this. Considering the airfoil shape (shown in Figure 4.4) it is not unsurprising that there is suction on the lower surface close to the cove on the main element at low angles of attack given the curvature in this region. No oil flow or other data was collected for the wing lower side and therefore analysis of this discrepancy is not straightforward.

Figure 5.27 shows a comparison of the pressure distribution either side of the nacelle with propeller. As was observed at higher angles of attack the propeller swirl induces an increase in local angle of attack on the up-going blade side and a reduction in angle of attack on the down-going blade side. Comparing the CFD and wind tunnel results a number of discrepancies become apparent. In both cases, the suction close to the leading edge is significantly overestimated particularly in the case of the lower side. It is not entirely clear why this occurs however, one potential reason could be discrepancies in the local swirl angle between the propeller model and XPROP-S changing the flow incidence at the pressure tap location. Aside from the region close to the leading edge the pressure distribution is well matched. On the port side, close to the trailing edge of the main element suction is once again seen on the lower surface in CFD but not in the wind tunnel data. Unlike in the case without the propeller this is likely the result of the limited pressure tap resolution not capturing the local pressure well which seems likely due to the 'clipped' leading edge pressure distribution.

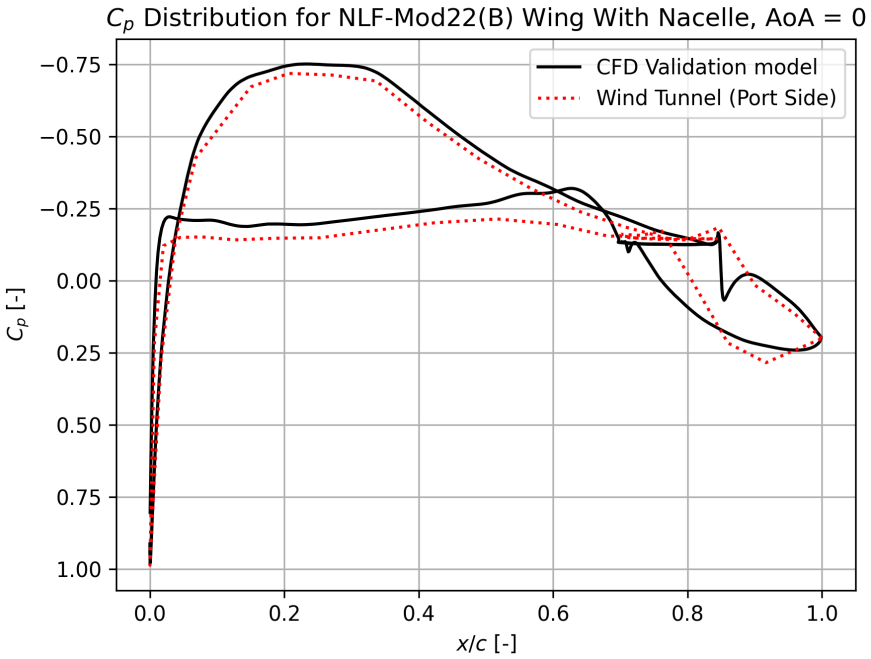

Figure 5.26: Comparison of the pressure coefficient distribution between the wind tunnel model port side pressure taps data and the corresponding location in CFD at angle of attack of 0°

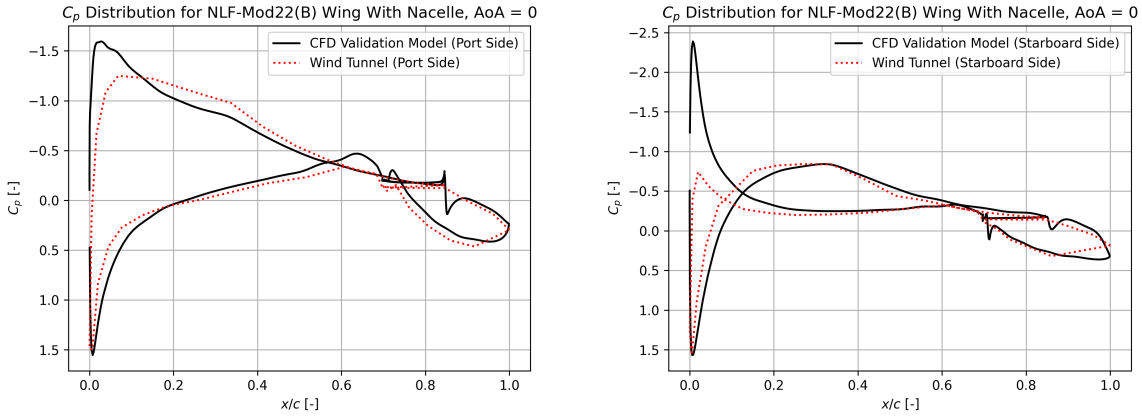

(a) Port side (up-going blade side)

(b) Starboard side (down-going blade side)

Figure 5.27: Comparison of the pressure coefficient distribution between the wind tunnel model port and starboard side pressure taps data and the corresponding location in CFD at angle of attack of 0°, propeller advance ratio J = 1.0

Figure 5.28 shows a comparison of the CFD wall shear and wind tunnel OFV. As this is a relatively simple case the structures are relatively simple. The nacelle has a relatively small impact however the CFD does accurately model the small amount of flow expansion seen directly behind the nacelle and the stall region that forms on the wing trailing edge. As was hoped this condition does not show much in the way of negative interactions effects as a result of the nacelle and therefore should be able to give a good understanding of to what extent the modifications that will be evaluated in the design study will influence the condition where the 'cruise' like condition where the nacelle is less detrimental to performance.

Figure 5.29 shows a comparison of the surface flow between CFD and the wind tunnel. At 0° attack the flow structures are well modelled. The high dynamic pressure wake results in a region of higher surface

shear which is clearly represented in CFD. There is some discrepancy in the shape of the wake region which is likely the result of the different propeller advance ratio and differences in loading between the actuator disc and real propeller. Similarly to the case with propeller, a noticeable structure is shed from the nacelle that results in a small increase in separation at the flap trailing edge similar to the case without propeller however as a result of the propeller swirl the structure is significantly deformed. The propeller model seems to be reasonably representative at these lower angles of attack conditions. There are differences in the shear close to the wall but these are more likely a result of the way the post-processing is applied rather than reflecting a genuine difference in the behaviour.

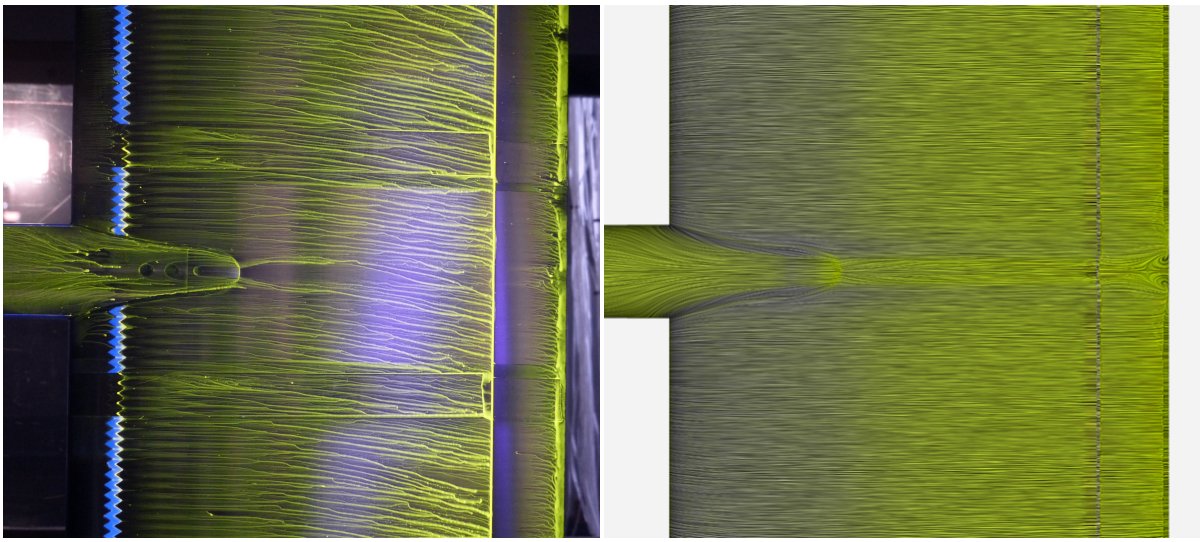

(a) Wind tunnel OFV (J = 0.8) (b) CFD wall shear LIC (J = 1.0)

Figure 5.28: Comparison of the CFD and wind tunnel surface flow field for wing with nacelle at an angle of attack of 0°

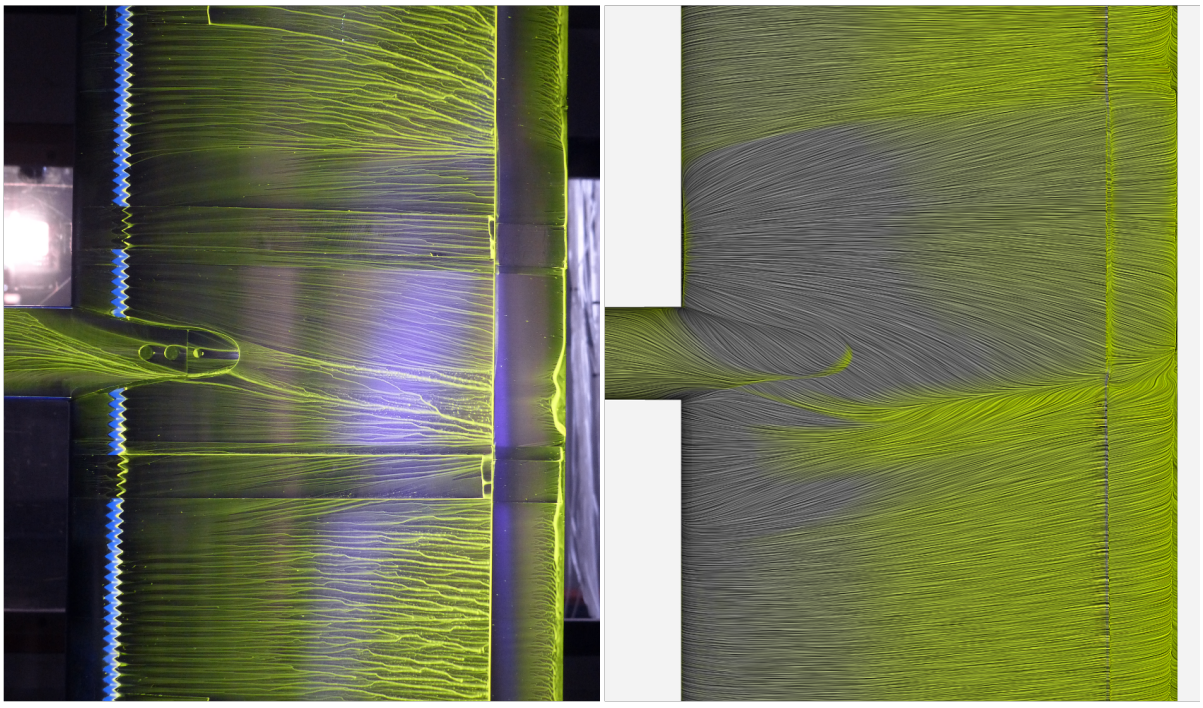

(a) Wind tunnel OFV (b) CFD wall shear LIC

Figure 5.29: Comparison of the CFD and wind tunnel surface flow field for wing with nacelle and propeller at an angle of attack of 0°

Figure 5.30 gives a comparison of the wake shape between CFD and the wind tunnel. Overall the shape is matched quite closely. The nacelle locally produces a small region of low total pressure however the distortion introduced is unsurprisingly much smaller than at higher angles of attack. The wake in CFD is much less diffuse than what was measured in the wind tunnel. The cause of this could be the result of the way turbulence dissipation is modelled in CFD however it may also be the result of the influence of the wake rake on the flow that was discussed previously.

Figure 5.31 shows the wake shape with the propeller. That shape is similar in both cases with the wake being sheared as a result of interacting with the wing however at these low angles of attack the influence of the wing circulation is small and as such the wake does not for the T-shaped distribution seen at higher angles of attack. The total pressure seen in CFD is lower than that observed in the wind tunnel however this is a result of the discrepancy in advance ratio described previously.

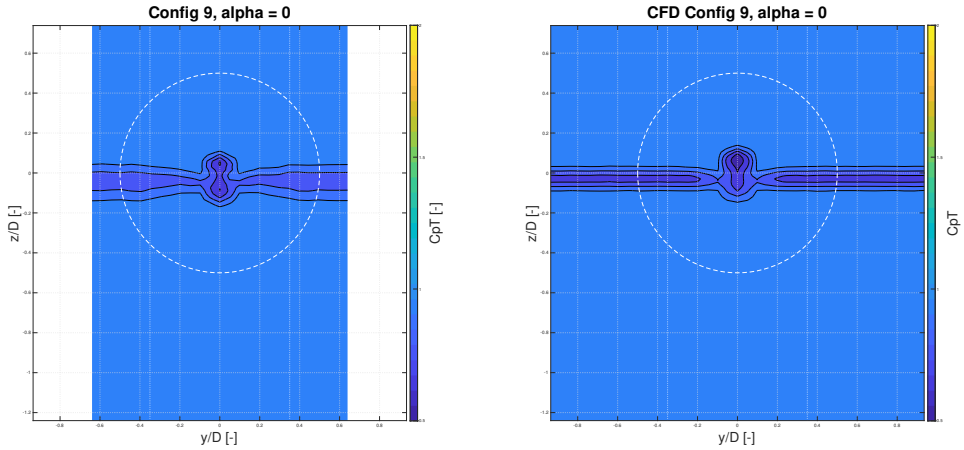

Figure 5.30: Comparison of the CFD and wind tunnel total pressure distribution at the wake rake plane for wing with nacelle at an angle of attack of 0°

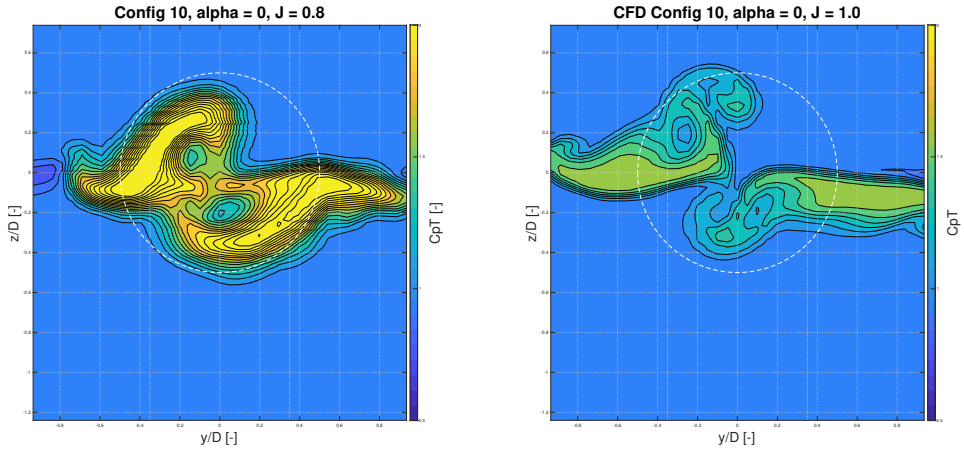

Figure 5.31: Comparison of the CFD and wind tunnel total pressure distribution at the wake rake plane for wing with nacelle and propeller at an angle of attack of 0°

5.3. Numerical Model Analysis

The nature of the wind tunnel measurement techniques used means that very little can be determined about the off surface flow structures and some variables could not be measured in the wind tunnel. The numerical model, therefore, gives additional information regarding the interactions present in the

propeller-nacelle-wing system that will help to inform the design study process. This section will present some analysis of the CFD results and compare these results to literature. The results presented in this chapter combined will be used to answer the two primary research questions that are considered in this part and will inform the approach that will be used to tackle the part two research questions.

5.3.1. Nacelle-Wing Interaction Effects

Figure 5.32 shows the pressure distribution on the upper surface of the wing in the vicinity of the nacelle. A number of clear effects are visible. The centre line of the wing is offloaded towards the wing leading edge showing the high-pressure region described in Section 2.1.1. This sets up a clear spanwise pressure gradient that is responsible for the flow expansion is observable in the streamlines. In addition to this, Figure 5.32 shows a stronger leading edge pressure peak in the vicinity of the nacelle. While this pressure peak increases local suction it also causes the flow to have to overcome a stronger adverse pressure which can lead to boundary layer growth.

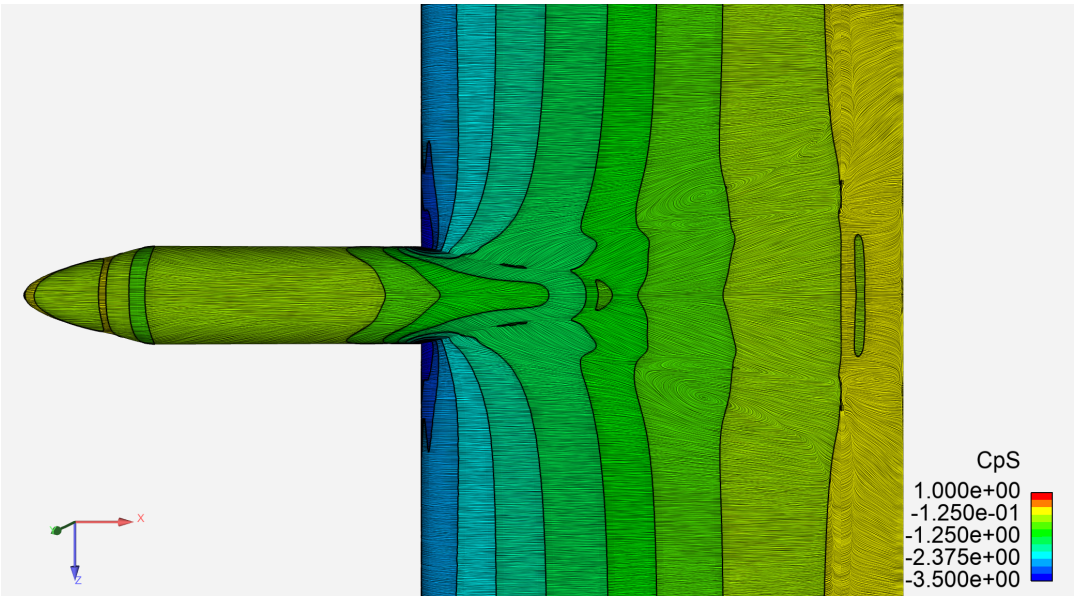

Figure 5.32: Static pressure coefficient distribution behind the nacelle for the wing with nacelle at an angle of attack of 10°

Figure 5.33 shows the surface flow in the vicinity of the nacelle in more detail with the local flow direction indicated. These arrows clearly show the way the flow expands behind the nacelle as well as showing the patches of reversed flow that are indicative of flow separation that form either side of the nacelle. These arrows also show the streamline convergence that results from the cross flow component and leads to boundary accumulation as was described by Qiu et al [28].

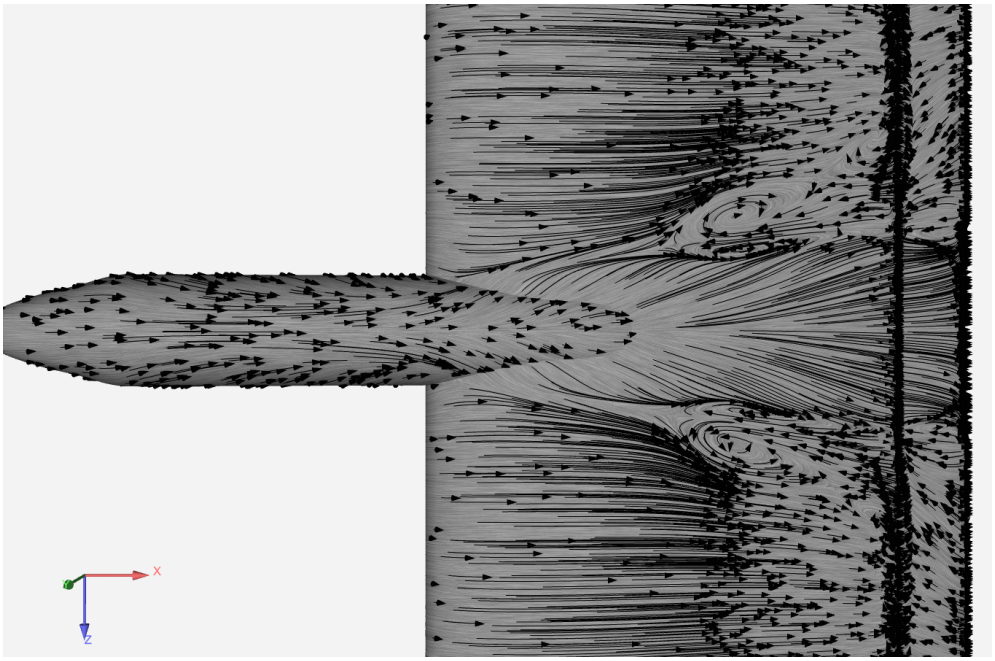

Figure 5.33: Surface flow field with arrows to indicate local flow direction for the wing with nacelle at an angle of attack of 10°

Total pressure coefficient slices shown in Figure 5.34 give an indication of the wing boundary layer development in the vicinity of the nacelle. It shows that the boundary layer at the edge of the flow expansion region is considerably thicker than in the rest of the wing. This low energy, thick boundary layer is less able to overcome the wing adverse pressure gradient and ultimately leads to the separation described previously. The thicker boundary layer seems to originate from the nacelle-wing junction. This region is the region where the wing experiences the greatest induced local angle of attack and sees the interaction of the wing and nacelle boundary layer. The cross flow also leads to boundary layer accumulation, pulling the nacelle top surface and wing centre boundary layer outwards leading to further growth of the local boundary layer. Which of the above effects is dominant in causing the local wing separation is unclear however addressing this boundary layer growth will be key to increasing the wing high angle of attack performance. The high-pressure region and resulting cross flow distribution are however fairly inherent to the installation of a nacelle therefore addressing the induced angle of attack seems more likely to yield results.

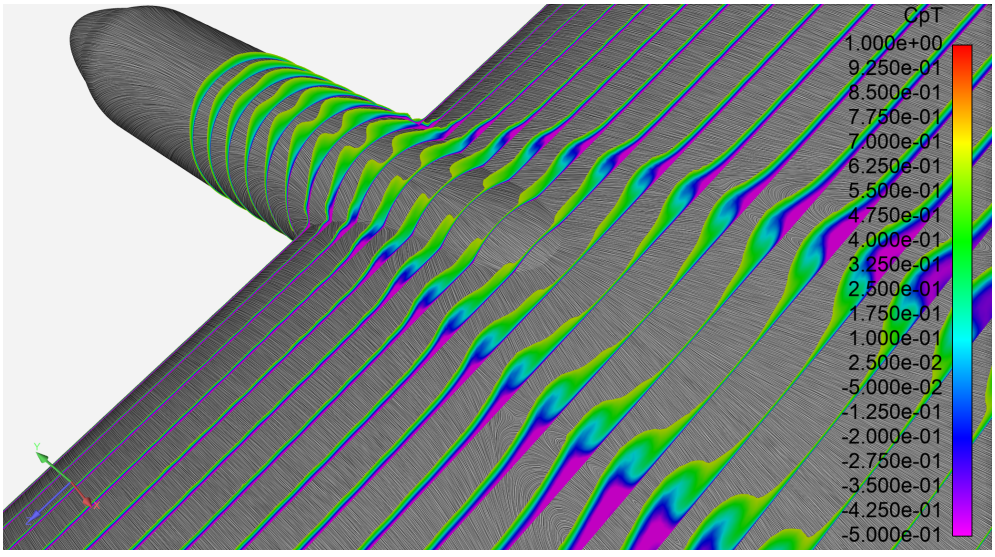

Figure 5.34: Total pressure coefficient slices in the vicinity of the nacelle for the wing with nacelle at an angle of attack of 10°

Figure 5.35 shows the presence of the nacelle vorticity described in Section 2.1.3 however it is clear that the vorticity, in this case, is weak and not very persistent. The structures do not reach the wing trailing edge and therefore it seems unlikely that these structures will play a significant part in determining the wing high angle of attack performance. The vortex bursting effects are therefore likely not limiting in this configuration. Behind the wing the two regions of separated flow are wrapped into two weak vortices. These are likely secondary structures that result from the lift distortion introduced by the presence of the nacelle rather than the structures directly shed from the nacelle described in Section 2.1.3.

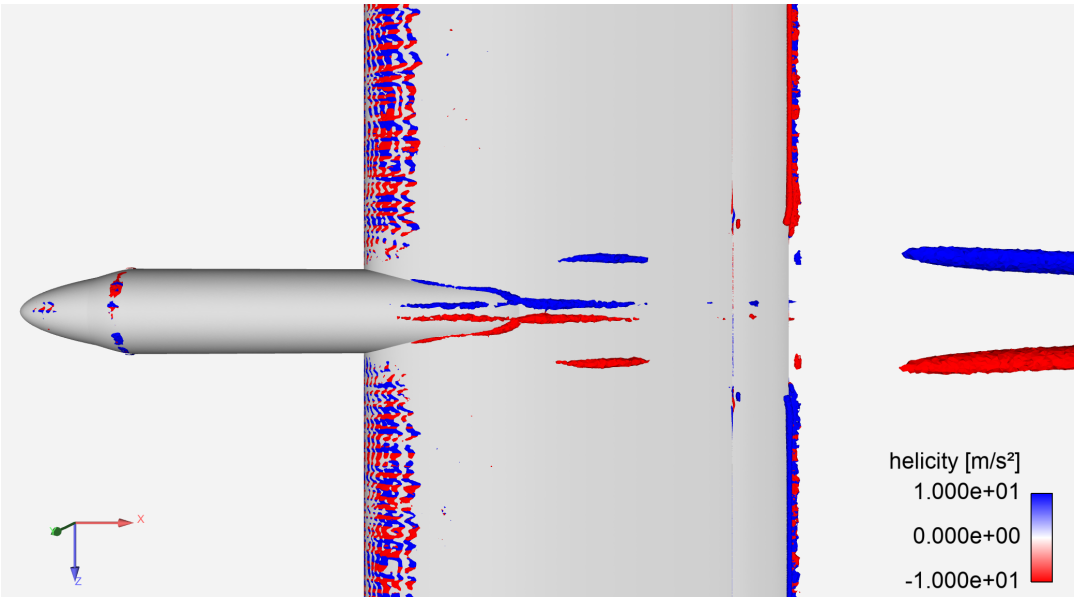

Figure 5.35: Q-criterion iso surfaces coloured by helicity in the vicinity of the nacelle for the wing with nacelle at an angle of attack of 10°

Figure 5.36 shows the off surface streamlines in the vicinity of the nacelle along with the regions of separated flow. The off surface streamlines show as was described previously that the regions of separated flow seem to originate in the region close to the nacelle wing junction. The flow in this region experiences higher local angles of attack as a result of the nacelle blockage. In addition to this, the off surface streamlines show that while the flow does expand behind the nacelle, this phenomenon is limited to a region that is relatively close to the wing surface. Flow further from the surface seems to be mostly aligned in the flow direction.

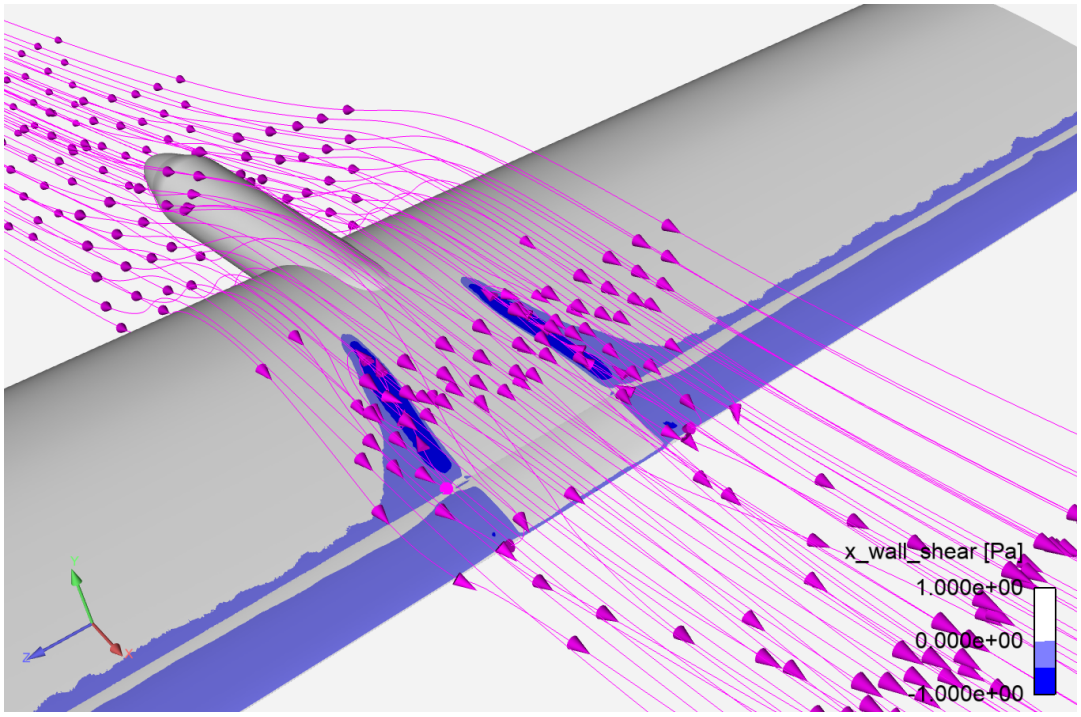

Figure 5.36: Streamlines showing the off surface flow on upper surface of the wing with nacelle at an angle of attack of 10°

5.3.2. Propeller-Nacelle-Wing Interaction Effects

The pressure field with the actuator disc present is rather more complex than when considering just the nacelle in isolation. Figure 5.37 shows that the region behind the propeller on average seems to exhibit greater suction than in the case without propeller. This is apparent from the way the iso-contours bend rearwards in the region influenced by the propeller. In addition to this, the influence of swirl is immediately apparent at the leading edge. The up-going blade side sees much higher leading edge suction than was observed in the case without the propeller. Similarly, the down-going blade side shows a reduction in leading edge suction as a result of the induced angle of attack. Aside from these larger scale effects a number of smaller structures seem to have an impact on the surface pressure distribution. The port side of the wing shows surface flow structures that are similar to those introduced by the nacelle in isolation. The presence of the nacelle results in a region of higher pressure forming that, in turn, leads to flow expansion. The starboard side shows a region of flow expansion. The downwash introduced by the propeller results in a region with higher pressure than the surrounding region resulting in the formation of a spanwise pressure gradient that, in turn, induces a cross flow component. Adjacent to the propeller wake two regions of separation form. These flow structures are likely the result of a similar mechanism to the one that was observed in Section 5.3.1 however do not seem to be caused by the nacelle wing interactions.

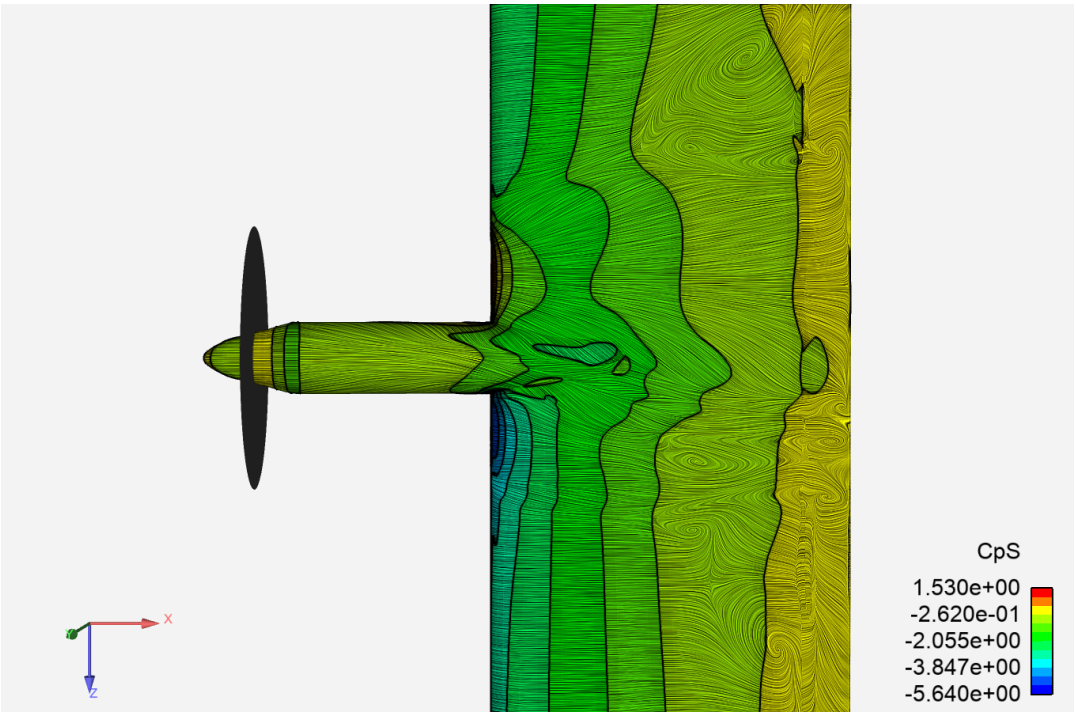

Figure 5.37: Static pressure coefficient distribution behind the nacelle for the wing with nacelle and propeller at an angle of attack of 10°, advance ratio: J = 1.0

Figure 5.38 shows the local flow direction on the wing surface. This image clearly illustrates the complex nature of the flow in the presence of the propeller particularly on the port side of the wing a series of regions of reversed flow are visible indicating the complex separation behaviour.

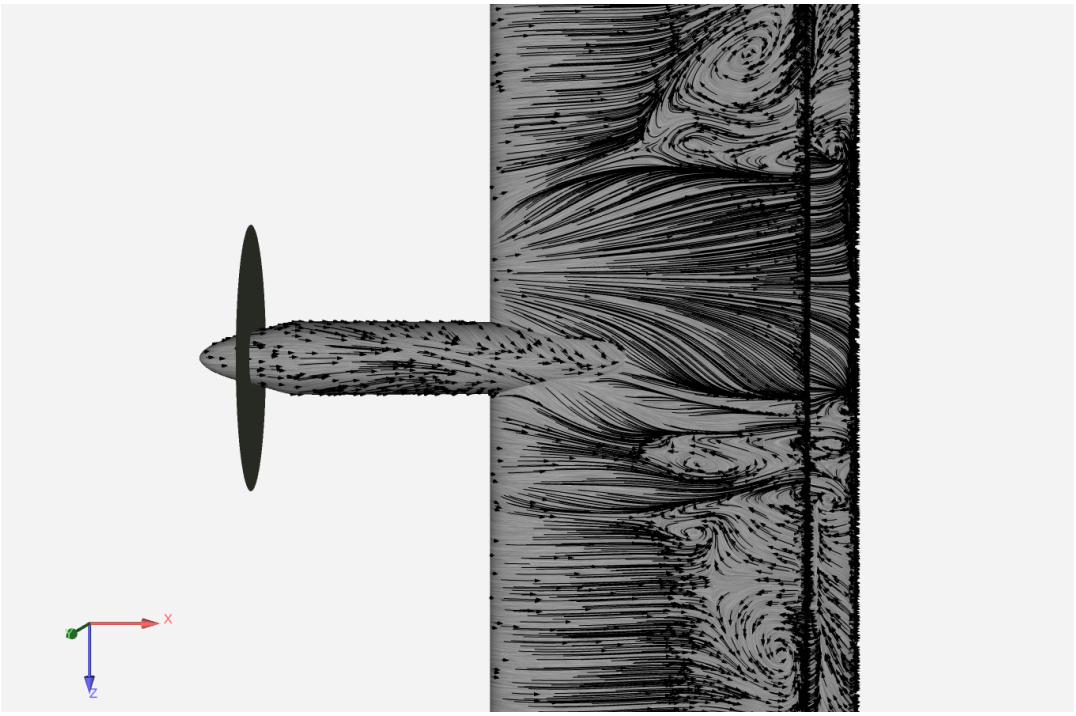

Figure 5.38: Surface flow field with arrows to indicate local flow direction for the wing with propeller and nacelle at an angle of attack of 10°, advance ratio: J = 1.0

Figure 5.39 shows total pressure slices close to the nacelle and propeller. The high dynamic pressure

wake is apparent. The wing distorts the wake substantially. The bulk wake rotation causes it to shear as it interacts with the wing. The flow separation either side of the wake is apparent and is perhaps more severe than in the propeller off case. Somewhat counter-intuitively the flow separation seems to be worse on the down-going blade side which experiences lower induced angles of attack.

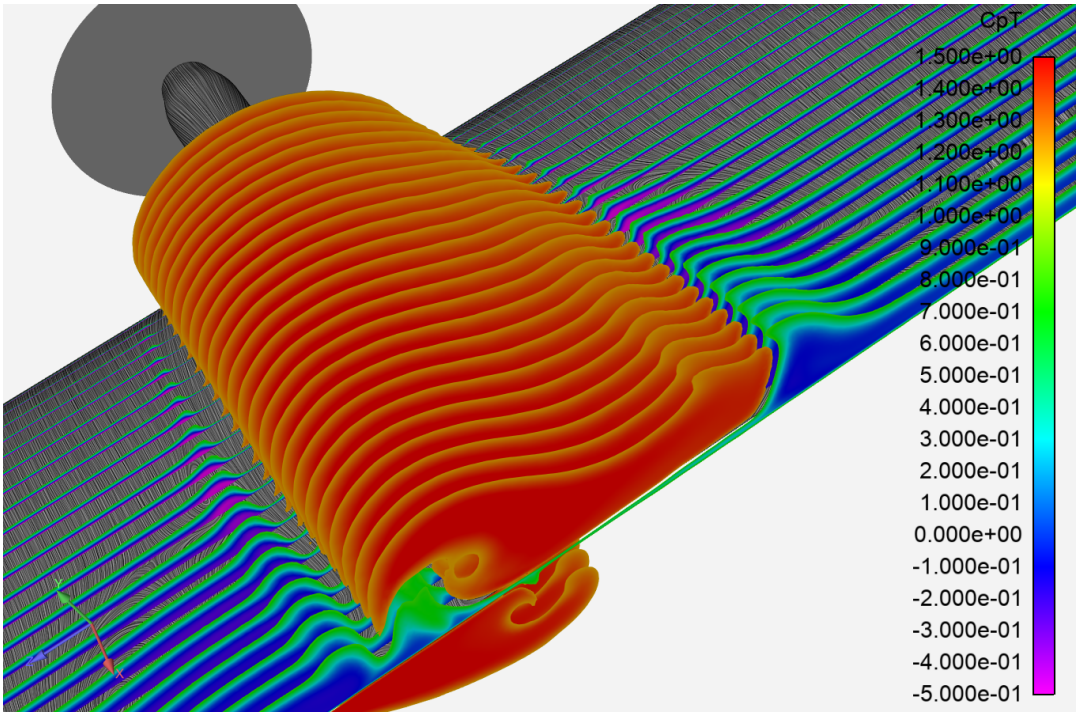

Figure 5.39: Total pressure coefficient slices in the vicinity of the nacelle for the wing with nacelle and propeller at an angle of attack of 10°, advance ratio: J = 1.0

In order to better understand the negative interactions present in the propeller-nacelle-wing system Figure 5.40 shows the same region but with a filter applied to remove the high dynamic pressure wake. This image shows not only the two large separation regions adjacent to the propeller wake but also shows two regions of thickened boundary layer that originate from the nacelle that are reminiscent of the structures discussed in Section 5.3.1 however rather than forming either side of the nacelle propeller swirl causes the structures to be transported towards the port side. Figure 5.41 shows that the combination of the nacelle wing junction flow, nacelle top surface separation and boundary layer accumulation induced by the cross flow component result in the formation of two regions of thickened boundary layer.

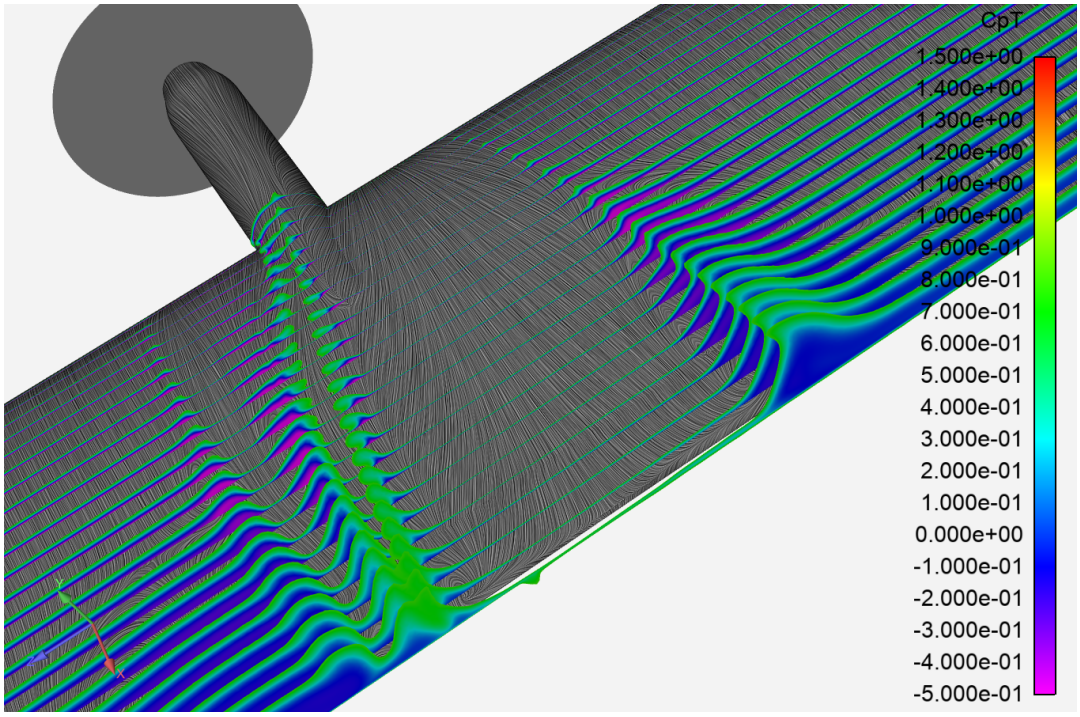

Figure 5.40: Total pressure coefficient slices with a filter applied to remove the propeller wake in the vicinity of the nacelle for the wing with nacelle and propeller at an angle of attack of 10°, advance ratio: J = 1.0

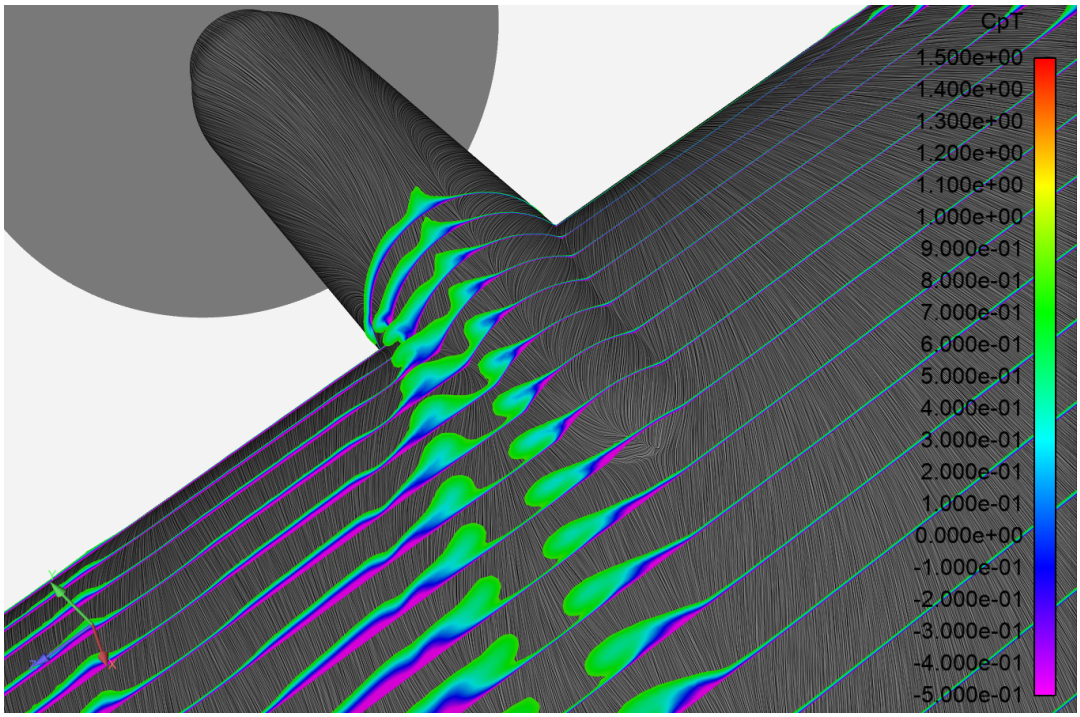

Figure 5.41: Total pressure coefficient slices with a filter applied to remove the propeller wake in the vicinity of the nacelle for the wing with nacelle and propeller at an angle of attack of 10°, advance ratio: J = 1.0

Figure 5.42 shows the vorticity produced by the propeller-nacelle-wing system. The propeller rotation leads to the formation of root vortices. In this model the vorticity takes the form of a distributed vortex sheet however in the case of a real propeller it is likely that these structures would form at the root of each propeller blade. In addition to this, a vortex is shed from the upper surface of the nacelle as was

described in Section 2.1.3. A number of vortical structures form as a result of the interactions between the rotating propeller wake, irrotational flow and the wing, the most prominent of these is located on the starboard side of the nacelle. It is hard to determine what if any impact these vortices have on the surface flow structures.

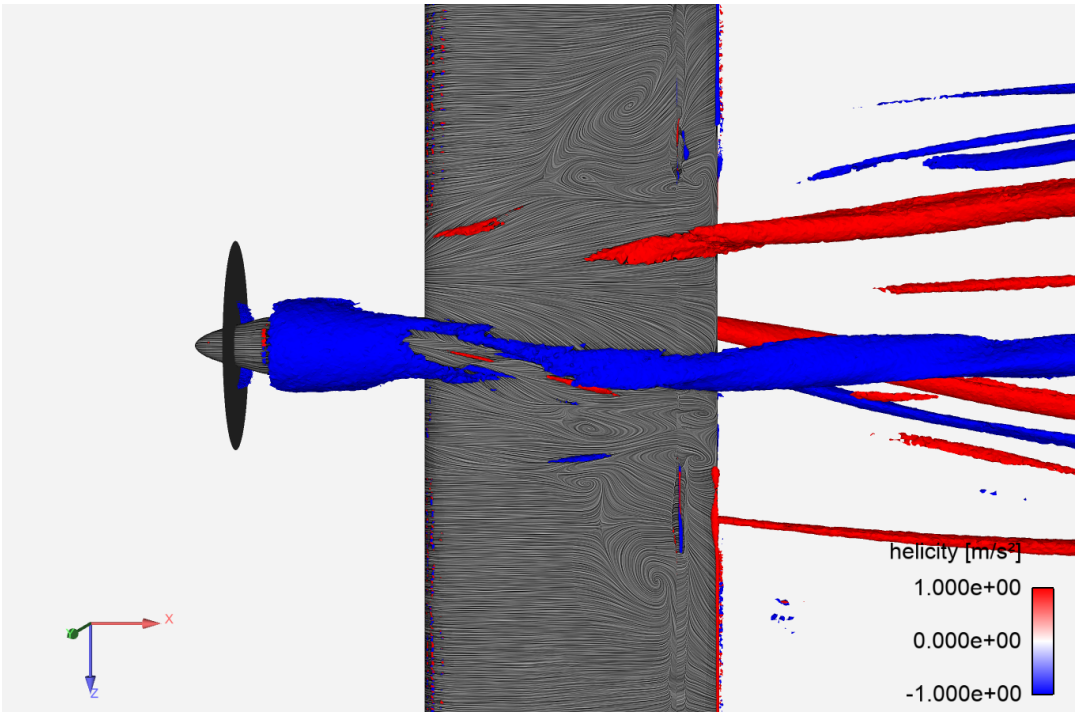

Figure 5.42: Q-criterion iso surfaces coloured by helicity in the vicinity of the nacelle for the wing with nacelle and propeller at an angle of attack of 10°, advance ratio: J = 1.0

Figure 5.43 gives an indication of the off-surface flow and shows where the various regions of separated flow draw from in the case with the propeller. This image further illustrates what was outlined previously. The two outer separated regions raw primarily from the flow outside the vicinity of the nacelle. The nacelle flow does however influence the separation at the trailing edge behind the nacelle and coalesces with the structures formed on the port side. The off surface flow in the presence of the propeller wake shows a strong swirling component while the flow at the root is influenced less by the swirl as a result of the tangential velocity distribution that is prescribed to it (see Figure 4.9a).

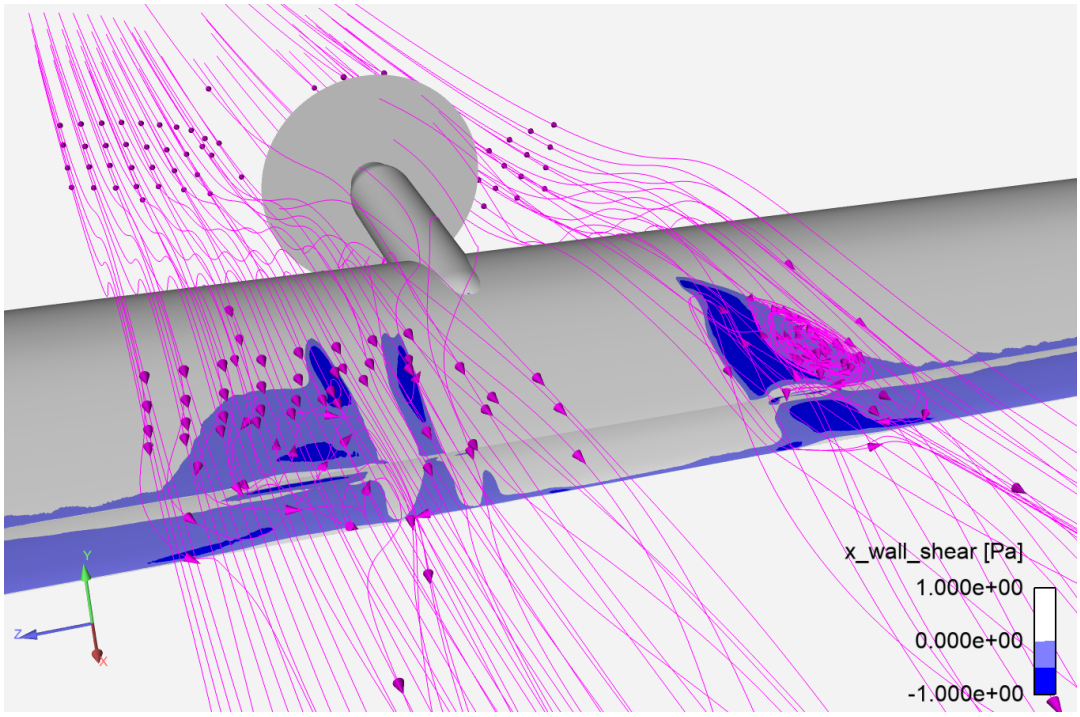

Figure 5.43: Streamlines showing the off surface flow on upper surface of the wing with nacelle and propeller at an angle of attack of 10°, advance ratio: J = 1.0

5.4. Conclusions Regarding Validation and Problem

Propeller-nacelle-wing problem is reasonably well modelled by the RANS simulation model that was created. The case without propeller is well matched, exhibiting near-identical pressure distributions and surface flow structures. The relatively low fidelity propeller matches less well as a result of the modelling deficiencies. Validating this condition is also more difficult as there is no direct comparison between the CFD model and wind tunnel test data. Despite the simplified propeller model used and difficulties in validating the model completely, it does exhibit similar behaviour to the wind tunnel data, with all the key flow structures present. The actuator disc implementation appears to give a good estimate of the impact of a propeller if not necessarily the TUD-XPROP-S. Given that the focus of the study is on nacelle wing interaction effects this is deemed acceptable to answer the research goals. The CFD model's predictive ability of real-world physics at 0° angle of attack is unsurprisingly as good or better than at 10° and therefore is considered suitable to evaluate the research questions.

The presence of the nacelle introduces a number of negative interaction effects. The induces an increase in the local angle of attack that may make the wing locally more prone to stall. In addition to this, the nacelle creates a higher pressure region that results in a spanwise flow expansion behind the nacelle leading to boundary layer accumulation. These effects combined with the nacelle junction flow leads to the formation of two separation regions either side of the nacelle. Addressing these regions of separation will likely yield performance improvements at high angles of attack and therefore will form the basis of the design study.

The nacelle effects also seem to be present in the case with the actuator disc fitted. In addition to this, two regions of separated flow form either side of the propeller wake that appear to be unrelated to the nacelle-wing interaction effects and are likely the result of interactions between the swirling propeller wake and the wing boundary layer.

Overall, the two separation regions towards the wing trailing edge that seem to originate from the nacelle-wing wing have an impact on the overall high angle of attack performance. The separated flow region leads to a reduction in suction in both the propeller on and off condition. Addressing this effect will therefore be key to achieving the research goals. It is hypothesised that this effect can be

addressed by either distributing the boundary layer growth that originates at the nacelle wing junction or by reducing the leading edge pressure peak that is generated by the induced local angle of attack.

II

Modification Design Study

This page is intentionally left blank

6

Design Study Methodology

Now that the modelling approach has been validated and the impact of the nacelle on the wing high angle of attack performance determined the second aspect of the research question can be considered. This aspect concerns the last three research questions outlined in Section 3.2, the use of geometric modifications to improve the high angle of attack performance of the propeller-nacelle-wing system. This chapter outlines the design study methodology that will be applied in order to this problem.

6.1. Development Model description

The design study will be completed exclusively through the use of the validated CFD model. While the wind tunnel results of some preliminary modifications were presented in Chapter 5 this is not practical for the majority of the design study as the costs, lead times and availability of wind tunnel resources make this an impractical method to evaluate and iterate new geometry concepts. Moreover, the nature of the wind-tunnel model used meant that geometric modifications could only be accomplished through the use of add-ons, significantly limiting the available design space.

While the solver and wing model will remain the same as the ones used to validate the CFD approach some simplifications will be applied to the far-field region. The complex wind tunnel test section geometry is replaced with a simpler rectangular cross-section. Additionally, the wall boundary conditions will be changed. The no-slip walls that were used in the validation model to simulate the wind tunnel walls will be replaced with symmetry conditions at the wing connection points and slip conditions for the remaining walls. This is done to reduce computation time and to remove the influence of the wind tunnel walls on the wing performance. The wing in this simpler domain is shown in Figure 6.1. While physically the development model has a larger domain a less refined mesh can be used close to the walls as the junctions and wind-tunnel walls do not need to be resolved and therefore the development has a lower overall cell count.

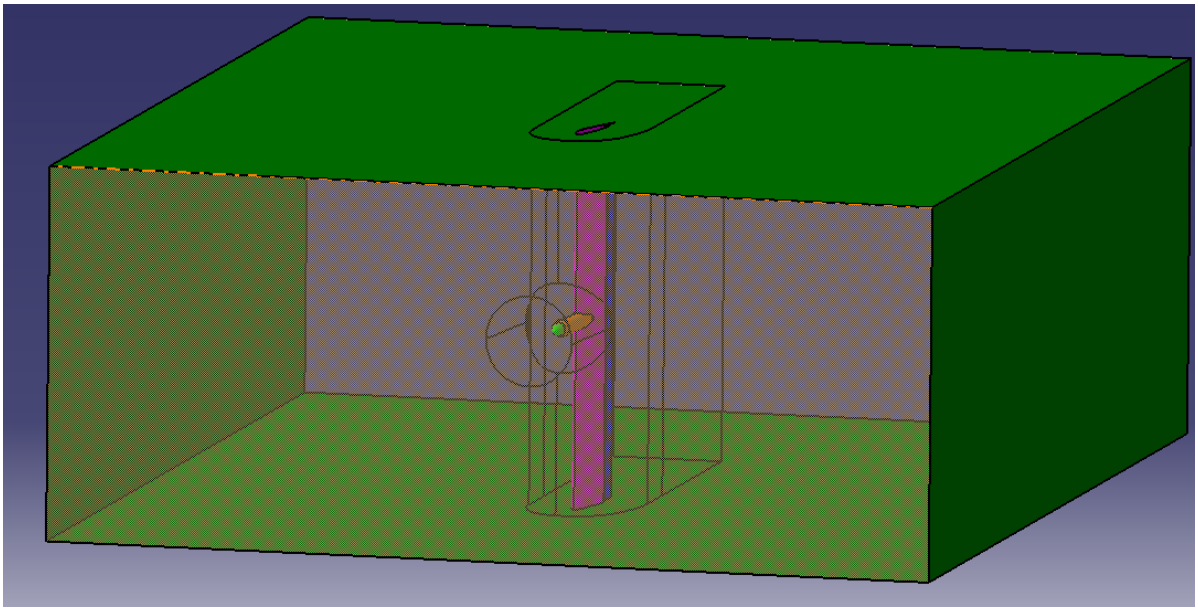

Figure 6.1: CAD model of the wing and domain that is used for numerical simulations

Before the design study can be completed the impact of the changes must be assessed. A comparison must be made between the validation model results and the development model results. While there will be significant change between these two models close to the wall region the impact of these changes on the propeller-nacelle-wing interactions should be considered and understood. The changes are unlikely to substantially alter the propeller region however any changes must be considered critically in order to be able to get a clear indication of what effects are the result of geometry changes and which are the result of changes to the model introduced for the development study.

6.2. Problem Approach

In order to answer the research questions, a number of key steps should be completed. Once the verification is completed the model without wind-tunnel walls can be used.

Based on this development model two key modifications will be tested. These concepts aim to address the propeller-nacelle-wing interaction effects in two distinct ways and therefore it will to some extent address the feasible design space. Based on literature, wind tunnel and baseline CFD results it was determined in Chapter 5 that the presence of a nacelle results in the early onset of stall in the region directly adjacent to it as a result of the nacelle wing interaction effects leading to boundary layer growth. This study will aim to address this through two different methods. The wing pressure peak shall be reduced in the region close to the nacelle in order to make the wing more tolerant to the local increase in induced angle of attack caused by the presence of the nacelle. The second approach attempts to reduce the interaction between the nacelle and wing to prevent separation from forming. The method by which these goals will be explored is elaborated below.

6.2.1. Droop

The first approach that is assessed is droop. The wing leading edge is angled downwards in the region close to the nacelle with the aim to better align it with the increases in effective angle of attack induced by the nacelle and propeller swirl and therefore reduce the leading edge pressure peak. This modification should reduce the strength of the adverse pressure gradient in the region close to the nacelle to slow boundary layer growth. This has the effect of delaying wing stall as is outlined in Section 2.4.3. In addition to this, the droop aims to make the wing span-wise pressure distribution more uniform and therefore help to reduce the wing cross-flow component and resultant boundary layer accumulation. This modification aims to increase the wing's tolerance to the higher local angles of attack that are introduced by the presence of the nacelle (see Section 2.1.2) and the propeller swirl (see Section 2.2.1).

It is hoped that the addition of droop will not only be able to address the separation introduced by the nacelle but will also be able to target and reduce the separation resulting from the propeller-wing interactions that appear to be unrelated to the nacelle. The use of droop will likely result in an increase in high angle of attack performance as was described in Section 2.4.3 however the option should also be assessed qualitatively basis to determine to what extent the droop impacts the effects that are introduced by the nacelle. Additionally, the use of droop may prove detrimental at lower angles of attack therefore the efficiency of this modification at different points in the flight envelope.

The first 20% of the wing chord in region directly influenced by the propeller will be drooped This value is chosen as typically the wing spar is positioned at this chord wise location [32] and therefore this modification could theoretically be applied to an existing aircraft without significant structural modification. The leading edge will be drooped by an angle of 10° as this is roughly the local angle of attack change introduced by the presence of the nacelle as is shown in Figure 6.2. While this is likely not the optimal droop angle will give a reasonable indication of the effectiveness of fixed droop to improve the high angle of attack performance of a propeller-nacelle-wing system. The droop is applied to a region of the leading edge that is 140% of the propeller diameter and then smoothly blended back to the original wing profile. This is selected based on preliminary wind tunnel results which indicated that this should be sufficient to cover the entirety of the leading edge that is directly influenced by the propeller wake and therefore should be sufficiently large to properly assess this modification in the limiting case with a propeller. The decision was taken not to extend the droop across the entire span as it is intended to specifically mitigate the propeller-nacelle-wing interaction phenomena and not to alter the performance of the entire wing. The drooped wing geometry is shown in Figures 6.3 and 6.4.

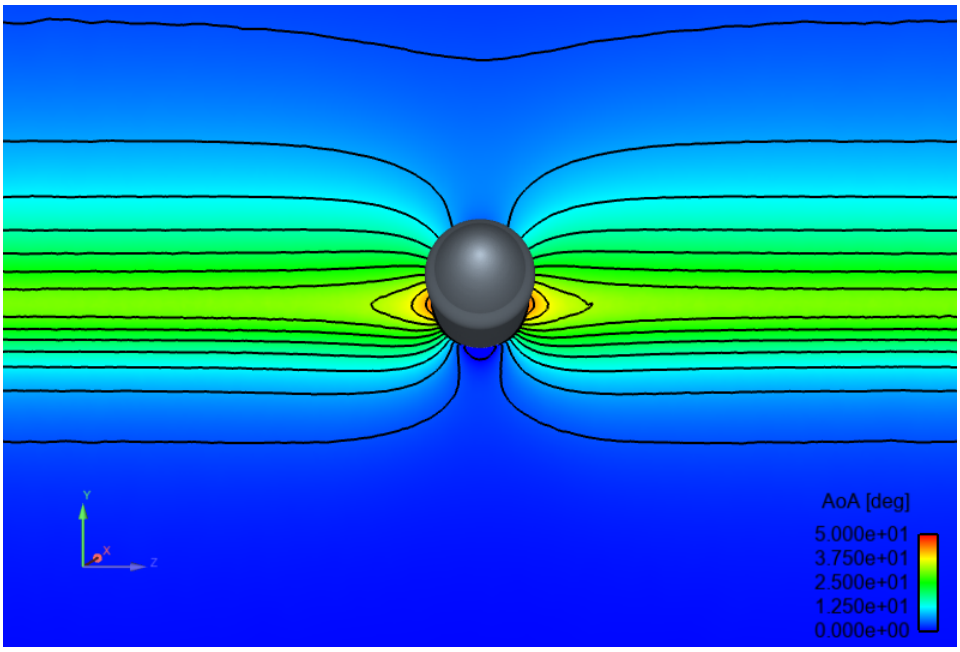

Figure 6.2: Induced flow incidence angle contour plot as a result of the wing and nacelle geometry in the region adjacent to the nacelle

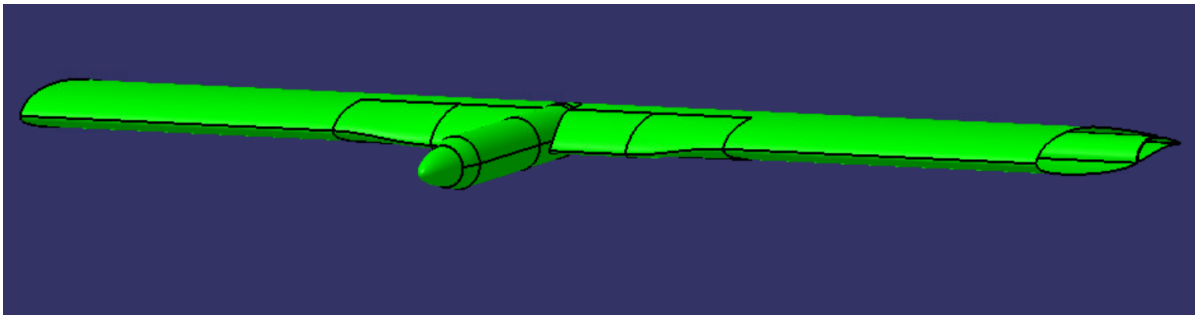

Figure 6.3: Isometric view of the drooped wing geometry

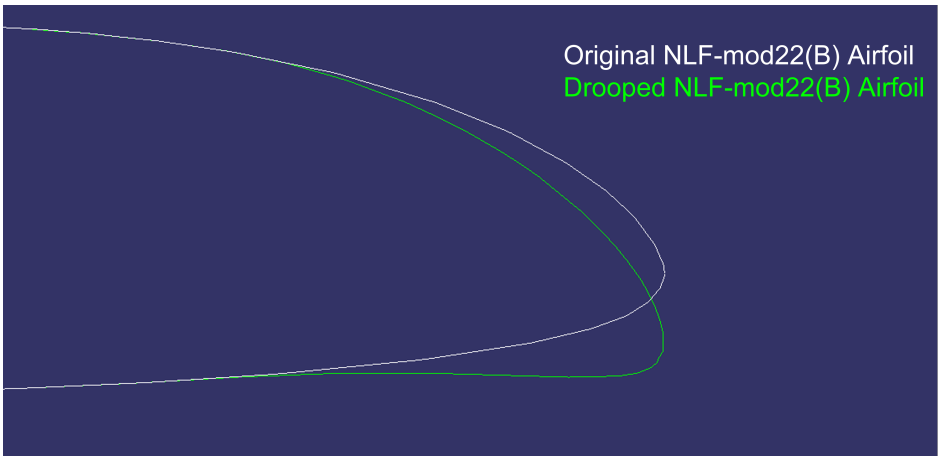

Figure 6.4: Comparison of the wing leading edge of the original and drooped NLF-mod22(B) airfoil

6.2.2. Nacelle Junction Fillet

The next modification to be tested to address the boundary layer growth is simply to fillet the junction between the nacelle and wing. This is intended to more directly address the cause of the local separation by reducing the interaction between the two bodies. As the nacelle boundary layer interacts with the developing wing boundary layer. It is theorised that the boundary layer growth on the upper surface of the wing that induces early, local separation can be reduced by improving the initial wing boundary layer. A 20mm radius fillet is used to blend the wing and nacelle in order to reduce the corner flow effect present at the nacelle-wing junction. While this modification will hopefully go some way to addressing the flow structures that originate from the nacelle in the case with and without propeller it will do little to mitigate the separation that appears either side of the propeller wake. The fillet arrangement is shown in Figure 6.5.

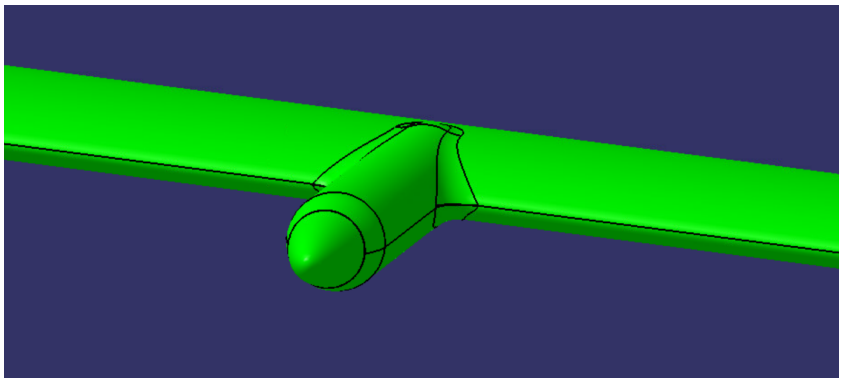

Figure 6.5: Isometric view of the wing with nacelle fillet

6.2.3. Assessment Criteria

As was outlined previously the key assessment metrics that will be used to evaluate each modification will be the global and local lift coefficient and the lift to drag ratio. The global coefficients consider the whole wing span whereas the local coefficients consider the impact on only the region that is directly influenced by the propeller in order to give a more accurate idea of how the nacelle effects and modifications might influence an aircraft. A nacelle centred span of 0.4m is considered in the nacelle only cases and a span of 0.6m for the propeller on cases. These values are based on the baseline geometry and are chosen such that the direct nacelle and propeller effects are captured. In addition to this, a qualitative assessment is performed. How the modifications alter the pressure distribution and in particular the wing stall behaviour in the presence of the nacelle is of particular interest. The performance of each option will initially be evaluated with just the nacelle and then with the propeller to assess to what extent the modifications achieve their aim when the propeller wake is considered.

This page is intentionally left blank

7

Results

This chapter presents the results of the design study that was carried out to mitigate nacelle-wing interactions. the comparison between the validation model and the simplified development model is made before the impact of the leading edge droop and fillet on improving the high angle of attack performance of the propeller-nacelle-wing system can be determined. Finally, the impact of the modifications at 0° is analysed.

7.1. Verification of the Development Model

Before the development study can be completed the impact of moving from the validation model, with the wind tunnel walls modelled to the lower fidelity development. The changes to the model primarily impact the junction between the wing and the walls however it must be determined what if any impact this has on the interactions found in the propeller-nacelle-wing system interactions.

7.1.1. Nacelle-Wing Interaction Effects

A comparison between the static pressure coefficient distribution at the wind tunnel pressure tap location is presented in Figure 7.1 shows that at this location, next to the nacelle the static pressure distribution does not differ substantially between the development and validation models. This suggests that the changes made to the wall and far-field domain did not greatly influence the nacelle-wing interactions. Similarly, Figure 7.2 shows the 3D static pressure coefficient distribution on the wing. The differences in the pressure close to the wall are apparent, the original no-slip walls caused a significant region of separated flow to form on the wing close to the junctions leading to a reduction in the local static pressure which are not present in the development model. These wall effects however seem to have virtually no impact on the pressure distribution close to the nacelle at the centre of the wing with both models displaying near-identical distributions in this region.

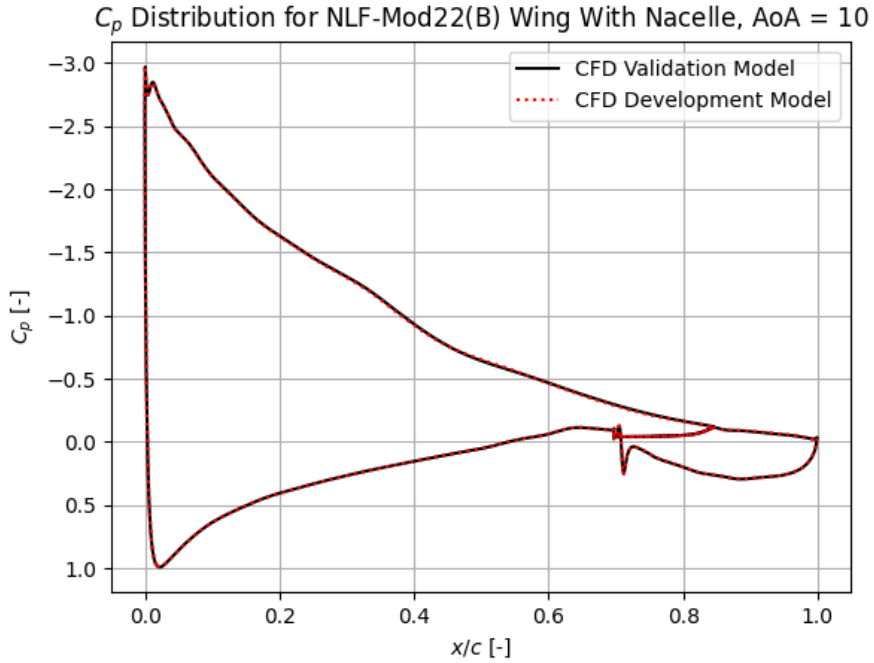

Figure 7.1: Comparison between the local static pressure coefficient at the wind tunnel pressure tap location for the CFD validation and development models at an angle of attack of 10°

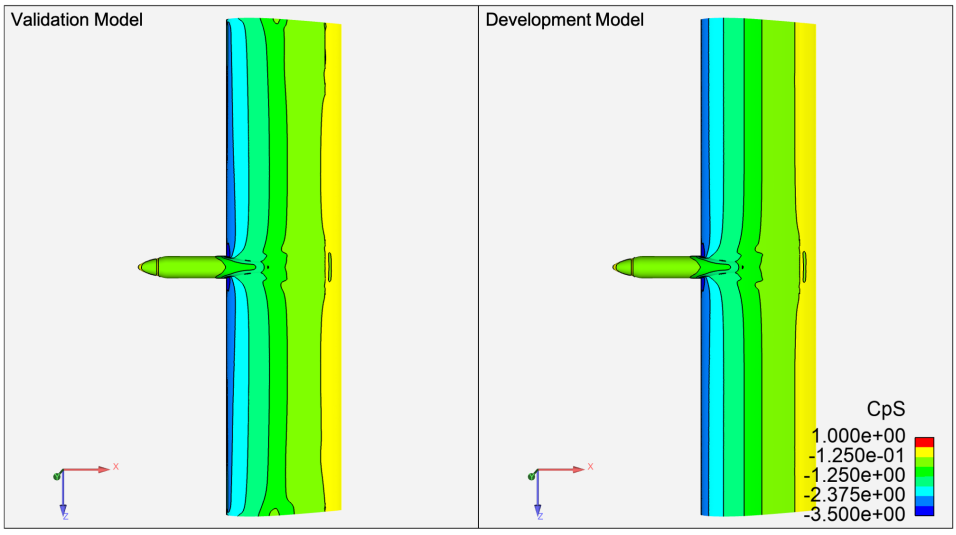

Figure 7.2: Comparison between static pressure coefficient for the CFD validation and development models at an angle of attack of 10°

Figure 7.3 shows the surface flow with regions in blue indicating negative x wall shear and therefore flow reversal. Once again the key flow structures and separation behaviour is similar for both the validation and development models. Overall this comparison shows that the development model gives a good representation of the validation model and therefore likely models real-world physics accurately enough to be able to draw conclusions about the impact of the modifications.

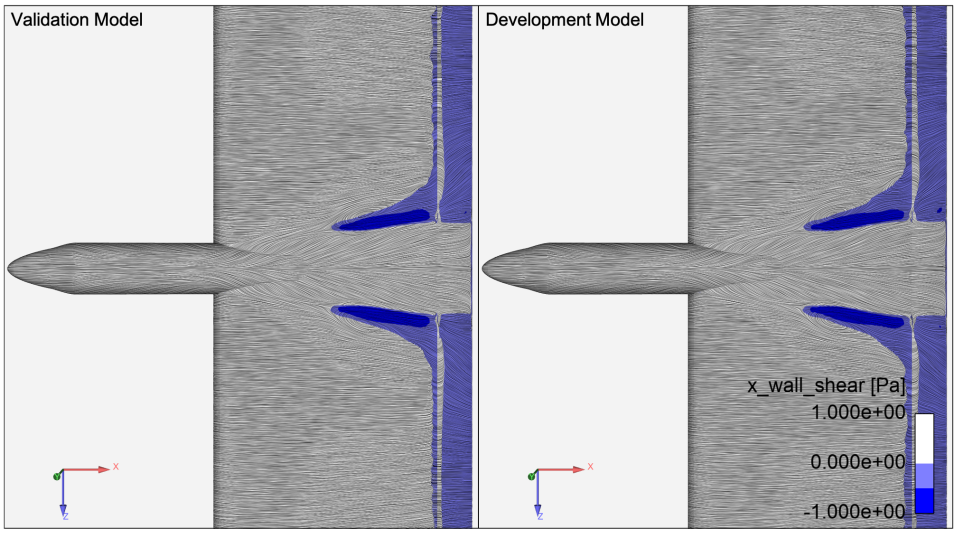

Figure 7.3: Comparison between the surface flow for the CFD validation and development models at an angle of attack of 10°

7.1.2. Propeller-Nacelle-Wing Interaction Effects

Similarly to what was observed in the case without propeller the changes in the wall boundary condition and far-field domain seem to have minimal impact on the pressure distribution in the vicinity of the propeller. Figure 7.4 shows that the pressure coefficient distributions at the wind tunnel pressure tap locations are more or less identical. Figure 7.5 similarly shows that the 3D pressure coefficient distribution close to the propeller remains largely unchanged by the domain changes. This suggests that the propeller interactions are well resolved by the development model. The changes in the domain do however alter the flow close to the wall. The influence of the propeller does seem to extend almost the entire way to the walls and seems to result in changes in the flow structures that form as a result of interactions between the wing and wall in the case of the validation model. This manifests itself in a discrepancy in the pressure distribution close to the wall in the validation model. While these asymmetries do not appear to influence the flow close to the nacelle this does imply that there is some coupling between the propeller-nacelle-wing and wing wall interactions and therefore additional care should be used when critically assessing the impact of modifications on the system.

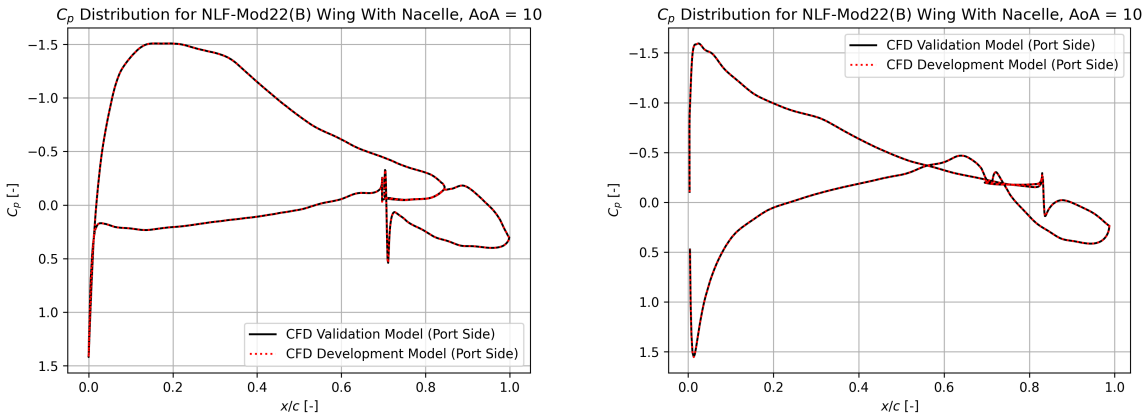

(a) Port side (up-going blade side)

(b) Starboard side (down-going blade side)

Figure 7.4: Comparison between the local static pressure coefficient at the wind tunnel pressure tap location for the CFD validation and development models at angle of attack of 10°, propeller advance ratio J = 1.0

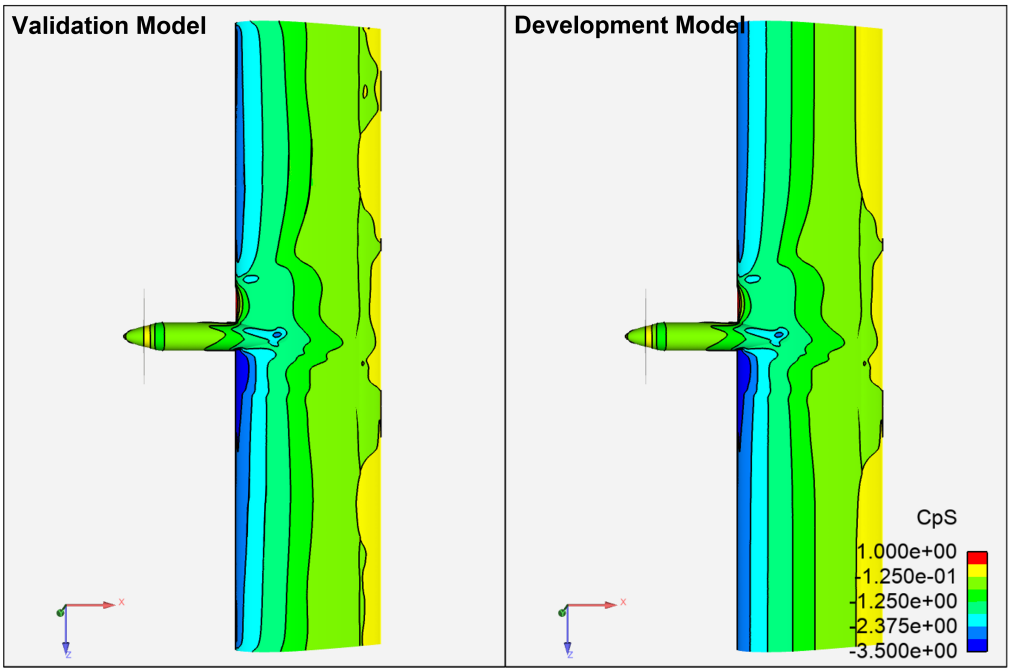

Figure 7.5: Comparison between static pressure coefficient for the CFD validation and development models with propeller at an angle of attack of 10°, advance ratio: J = 1.0

Figure 7.6 shows the stall pattern produced in the vicinity of the nacelle. The flow structures and separation behaviour seem to be relatively unaffected by the domain changes. It is therefore determined that this model adequately models the propeller-nacelle-wing interaction problem and therefore is likely usable to evaluate the effects of geometric modifications.

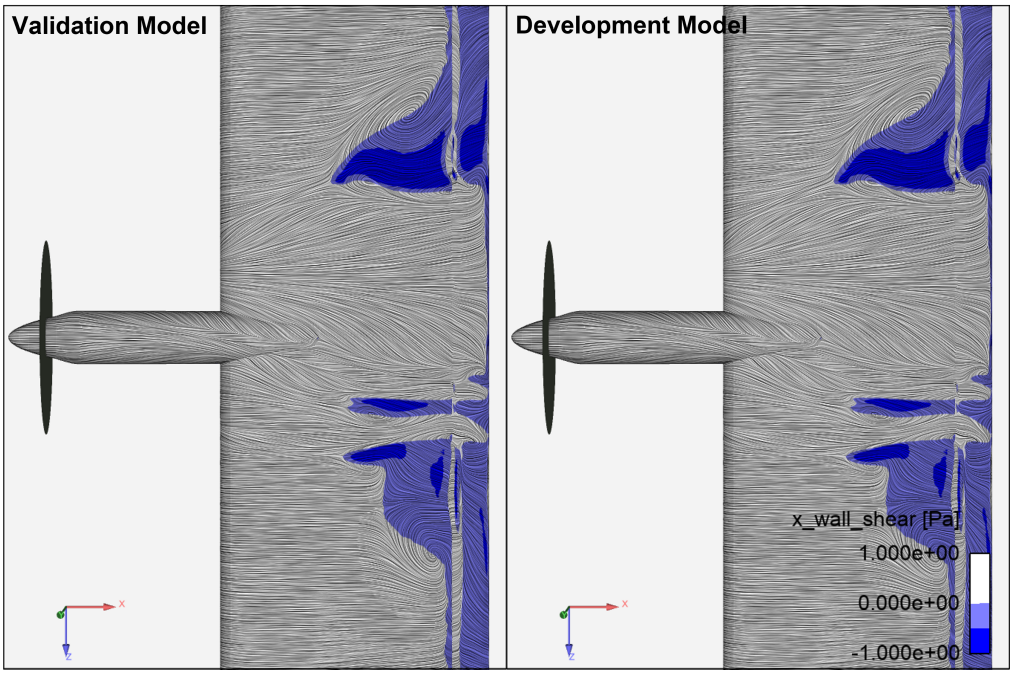

Figure 7.6: Comparison between the surface flow for the CFD validation and development models at an angle of attack of 10°, advance ratio: J = 1.0

7.2. Wing and Nacelle Modification Design Study

This section will present the results of attempts to mitigate the negative interaction effects introduced as a result of the nacelle installation. Two modifications are considered: a nacelle wing fillet and leading edge droop. Details of these modifications are shown in Chapter 6.

7.2.1. Droop

Drooping the leading aims to align the leading edge better at high angles of attack in order to reduce the leading edge pressure peak in the vicinity of the nacelle and make the wing more tolerant to the increased angles of attack induced by the nacelle.

Table 7.1 shows the wing performance coefficients at an angle of attack of 10°. This shows that the addition of droop results in a small increase in the wing lift coefficient and no change in drag. While given the magnitude of the geometric change this initially seems unlikely it is consistent with the results of Bunazzi and Radespiel [7] and Bashir et al. [4] who showed that droop has minimal impact on the overall lift coefficient below the maximum angles of attack. Additionally, the change results in an increase in moment coefficient. Table 7.2 gives the localised lift and drag coefficients in an attempt to better isolate the impact of the nacelle. These more localised variables show the same trend as was observed with the whole wing performance coefficients with a small increase in lift coefficient however these results show that the addition of droop locally increases the wing drag. Overall, the relatively minimal increase in lift and increase in drag coefficient suggests that this configuration has minimal effect on the high angle of attack performance of the nacelle-wing system. Understanding these effects requires further analysis of the flow structures.

Model	Baseline	Droop
Wing Lift Coefficient C_L [-]	1.244	1.245
Wing Drag Coefficient C_D [-]	0.035	0.035
Wing Moment Coefficient C_M [-]	0.341	0.346

Table 7.1: Wing lift, drag and moment coefficient for the baseline wing with nacelle and the modified wing with droop at angle of attack of 10°

Model	Baseline	Droop
Local Lift Coefficient C_L' [-]	1.197	1.203
Local Drag Coefficient C_D' [-]	0.041	0.037

Table 7.2: Local (0.4m span) lift and drag coefficient for the baseline wing with nacelle and the modified wing with droop at angle of attack of 10°

Figure 7.7 gives a comparison of the surface flow. Overall this image does not show a substantial change in the flow field as a result of the addition of droop with the flow expansion and separation structures still present however the separated region moves aft which is indicative of a reduction boundary layer growth adjacent to the nacelle. The changes in the size and location of the separated region close to the nacelle lead to the increase in wing lift coefficient. Despite the large differences in the leading edge pressure distribution Figure 7.8 shows a relatively small change in the pressure distribution towards the trailing edge. The use of droop achieves better local leading edge alignment as is shown in Figure 7.9 and therefore there is a reduction in the magnitude and an aft movement of the pressure peak. This redistributes the suction but overall does not change the total upper surface suction. The aft movement and spreading of the wing suction results in an aft shift of the wing centre of pressure which is responsible for the changes in moment coefficient. While overall the concept only results in a small increase in the lift performance the reduction in the size of the separated region suggests that this concept may offer additional benefits closer to the maximum lift angle of attack.

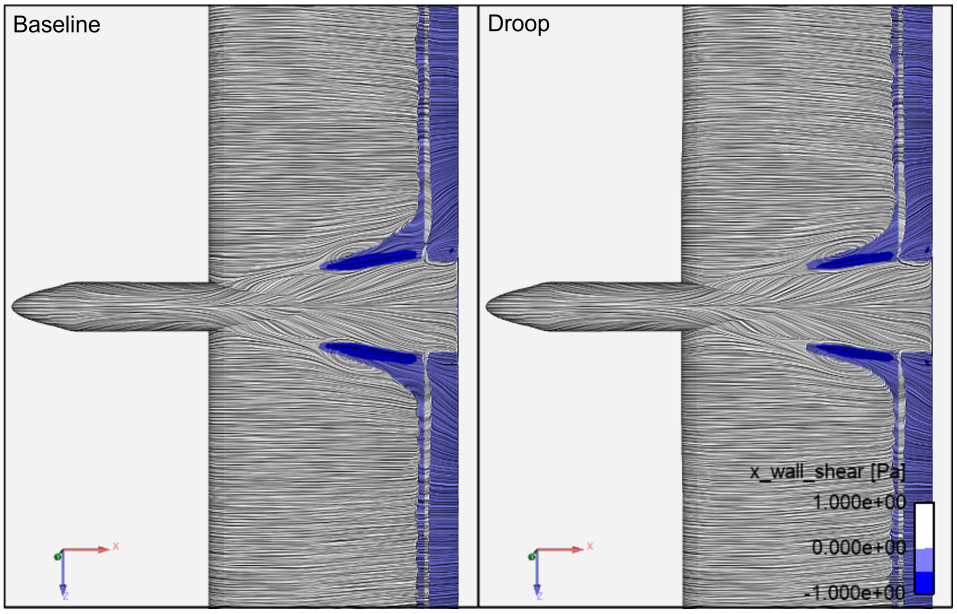

Figure 7.7: Comparison of the surface flow with regions of reverse flow highlighted in blue for the baseline and drooped wing at an angle of attack 10°

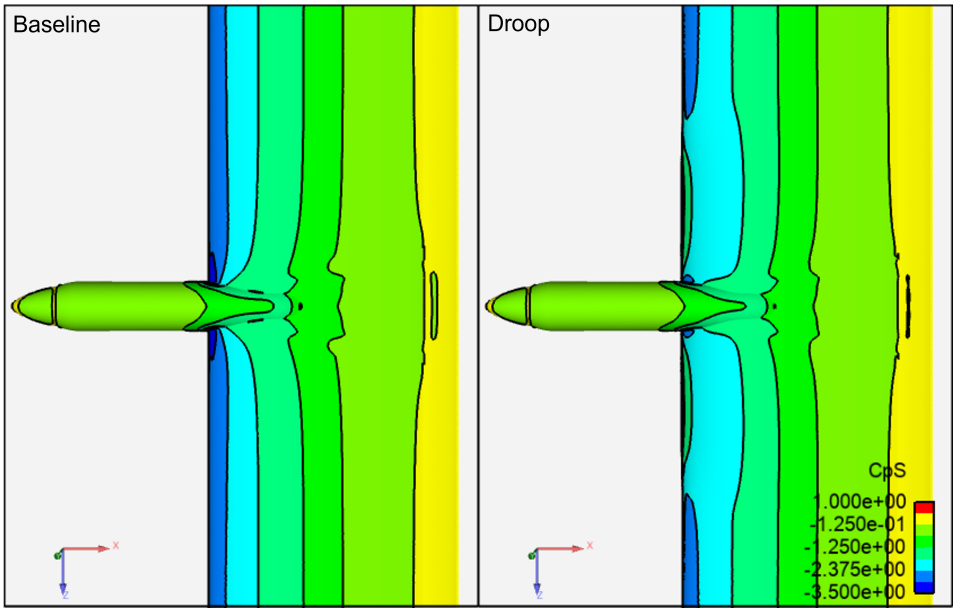

Figure 7.8: Comparison of the surface static pressure coefficient distribution for the baseline and drooped wing at an angle of attack 10°

The changes to the pressure distribution are perhaps more clear in Figure 7.10 where the leading edge pressure peak is essentially removed with a larger portion of the front of the airfoil experiencing suction. Droop not only impacts the pressure distribution in the first 20% of the chord that is modified but also results in an increase in suction over much of the forward and mid-portion of the airfoil.

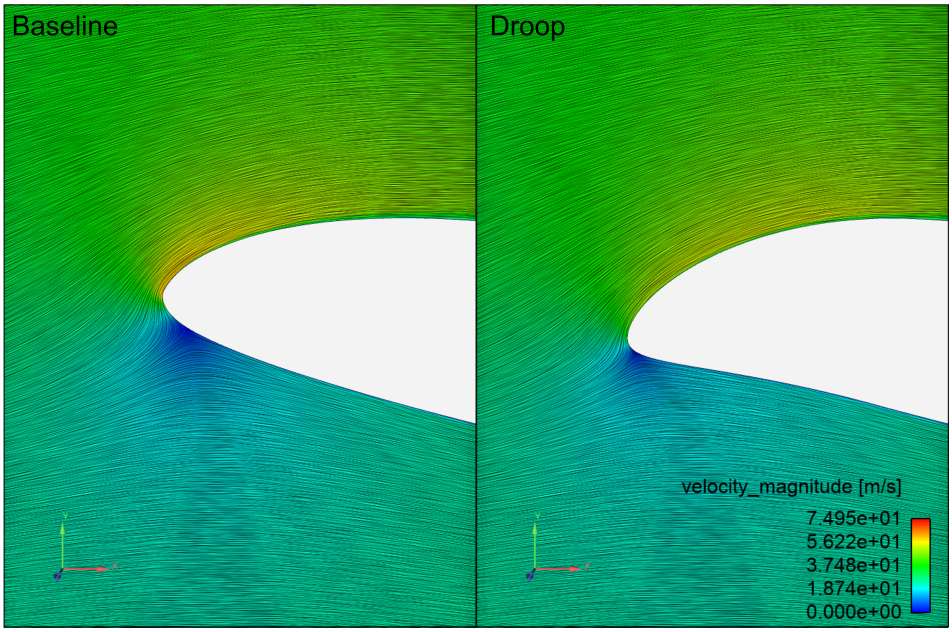

Figure 7.9: Comparison of the streamlines 0.05m away from the nacelle for the baseline and drooped wing at an angle of attack 10°

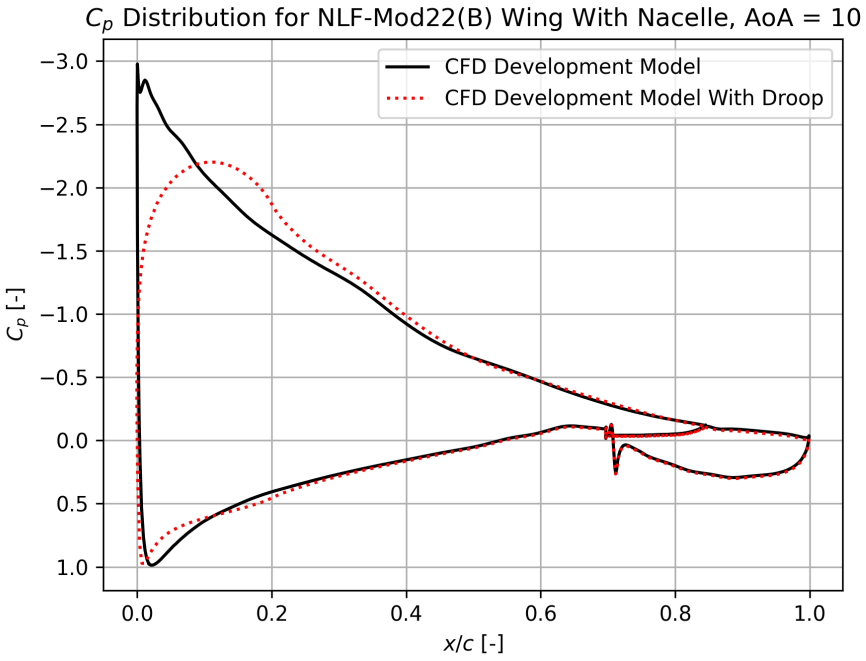

Figure 7.10: Comparison between the local static pressure coefficient at the wind tunnel pressure tap location for the CFD development and drooped model at an angle of attack of 10°

Figure 7.11 shows the wing leading edge with droop. It is clear that the addition of droop eliminates much of the additional leading edge peak induced locally by the nacelle with only a small region directly adjacent to the nacelle experiencing significant distortion and the magnitude of the pressure coefficient changes induced by the presence of the nacelle is far lower.

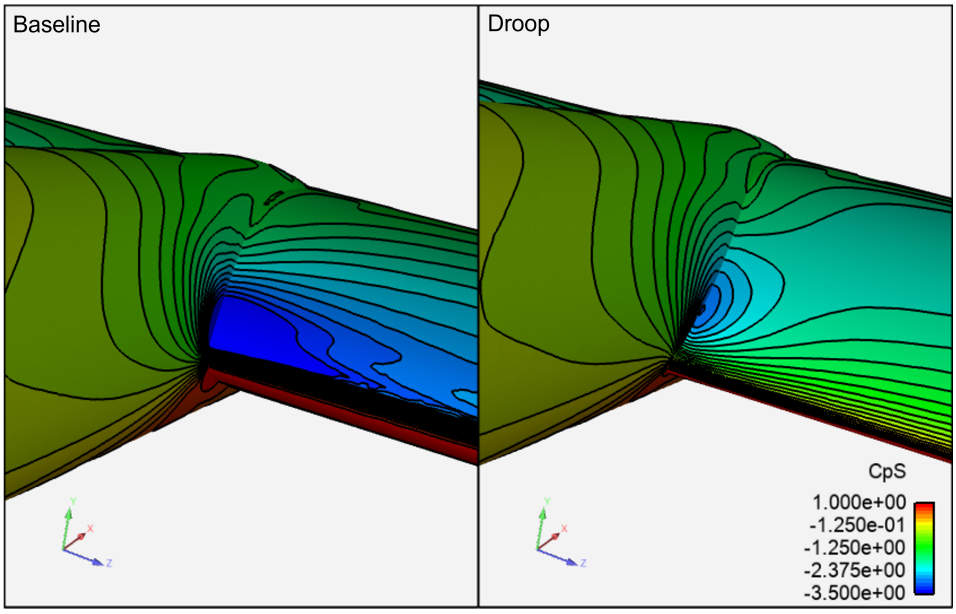

Figure 7.11: Comparison of the surface static pressure coefficient distribution at the wing leading edge close to the nacelle at an angle of attack 10°

The use of droop significantly modifies the pressure field on the forward portion of the wing and delays the formation of stall in the vicinity of the nacelle in the case without propeller however to evaluate the performance of this option it must also be analysed in the case where the wing is blown by a propeller. Table 7.3 shows that droop has a large effect on the wing lift coefficient in the presence of the propeller. The result with droop shows comparable lift to the case without propeller suggesting that the negative interaction effects between the propeller-nacelle-wing system for a drooped wing effectively mitigate any advantage produced by the propeller. In addition to this the droop results in an increase in drag. Considering the local performance coefficients presented in Table 7.4 the same trend is observed. The lift coefficient is reduced and the drag increased. The reduction in lift is perhaps not as substantial as was observed when considering the whole wing however it is important to note that the region of separated flow that forms at the edge of the propeller wake is so large when droop is used that it extends beyond the bounds of the smaller domain.

Model	**Baseline**	**Droop**
Wing Lift Coefficient C_L [-]	1.280	1.244
Wing Drag Coefficient C_D [-]	0.043	0.051
Wing Moment Coefficient C_M [-]	0.364	0.367

Table 7.3: Wing lift, drag and moment coefficient for the baseline wing with nacelle and propeller and the modified wing with droop at angle of attack of 10°, Advance ratio: J = 1.0

Model	**Baseline**	**Droop**
Local Lift Coefficient C_L' [-]	1.849	1.778
Local Drag Coefficient C_D' [-]	0.086	0.105

Table 7.4: Local (0.6m span) lift, drag and moment coefficient for the baseline wing with nacelle and propeller and the modified wing with droop at angle of attack of 10°, Advance ratio: J = 1.0

Figure 7.12 shows a comparison of the surface flow structures present on the wing. This shows that the addition of droop has led to a growth in the separated region that forms at the edge of the propeller wake. It is difficult to determine what impact the addition of droop has had on the nacelle structures as while they are less apparent in the case with droop the large growth in the separation region close to the propeller wake will undoubtedly have an effect on the other structures present on the wing and therefore it is not easy to isolate the effects. Figure 7.13 shows the pressure distribution on the wing

upper surface. Close to the leading edge the use of droop on the port (up-going blade) side results in a reduction in the leading edge pressure peak in a similar way to what was observed when considering the nacelle in isolation. On the starboard (down-going blade) side a growth in the region of high pressure close to the leading edge is apparent on the top surface with the stagnation point moving entirely onto the upper surface. The propeller downwash in this region results in the flow being poorly aligned. The use of droop aggravates this problem by lowering the leading edge making the leading edge alignment worse offloading the forward portion of the wing. The growth in the region of separated flow offloads the aft portion of the wing on both sides. Overall the modification offloads the front portion of the wing and does not yield the targeted benefits in terms of helping to keep the flow attached on the aft portion of the wing.

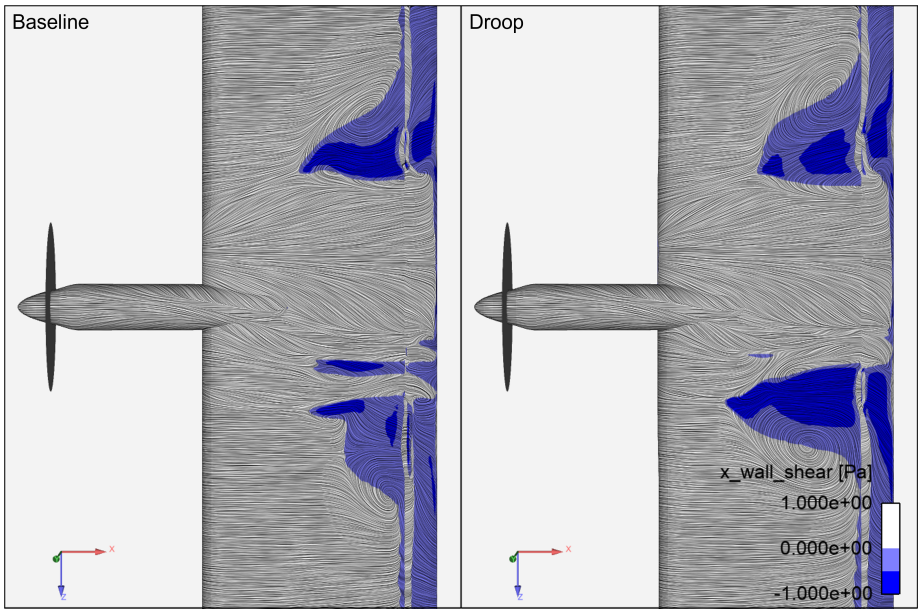

Figure 7.12: Comparison of the surface flow with regions of reverse flow highlighted in blue for the baseline wing with nacelle and propeller and the modified wing with droop at angle of attack of 10°, Advance ratio: J = 1.0

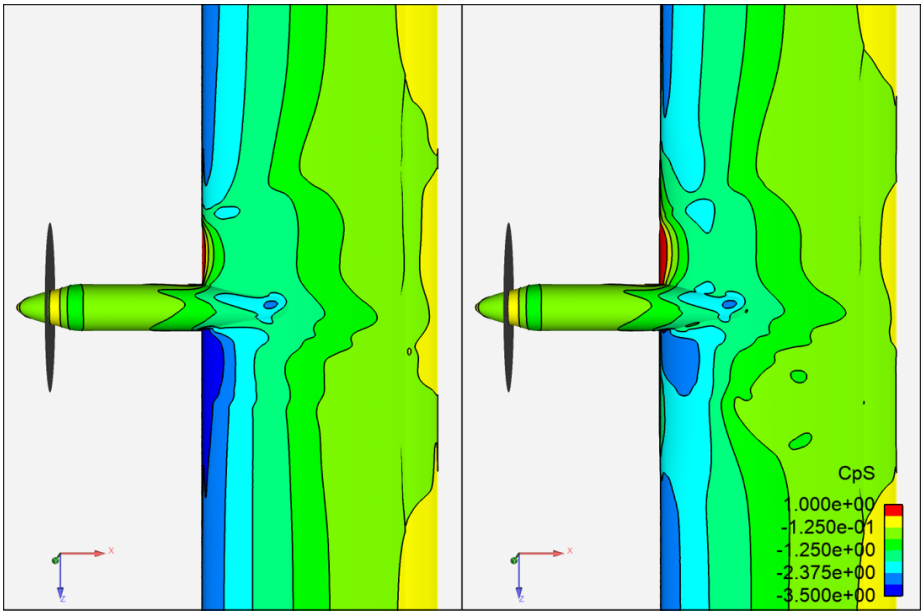

Figure 7.13: Comparison of the surface static pressure coefficient distribution for the baseline wing with nacelle and propeller and the modified wing with droop at angle of attack of 10°, Advance ratio: J = 1.0

Figures 7.14 and 7.15 shows the leading edge pressure distribution in the vicinity of the nacelle. Figure 7.14 shows a similar behaviour to what was seen in the case without propeller. The addition of leading edge droop results in a reduction in the strong leading edge pressure peak and therefore a reduction in the adverse pressure gradient close to the leading edge. Figure 7.15 shows that the impact of droop on the leading edge is more detrimental on the starboard side with the propeller swirl causing the stagnation line to lie entirely on the upper surface with some suction even being generated close to the leading edge suggesting that the flow is reversed on the very front of the wing. The wing experiences suction on the lower surface which will result in a further reduction in lift. This result illustrates why using droop particularly on the down-going blade side is undesirable, rather than helping to improve the leading edge alignment it makes it worse. Single-sided droop may therefore perform better in the condition with the propeller fitted.

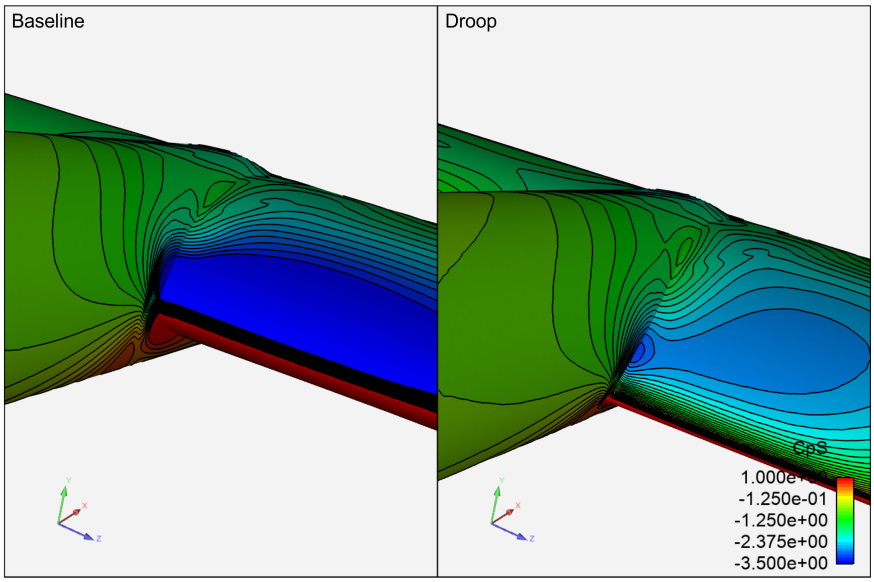

Figure 7.14: Comparison of the port side surface static pressure coefficient distribution at the wing leading edge close to the nacelle for the baseline wing with nacelle and propeller and the modified wing with droop at angle of attack of 10°, Advance ratio: J = 1.0

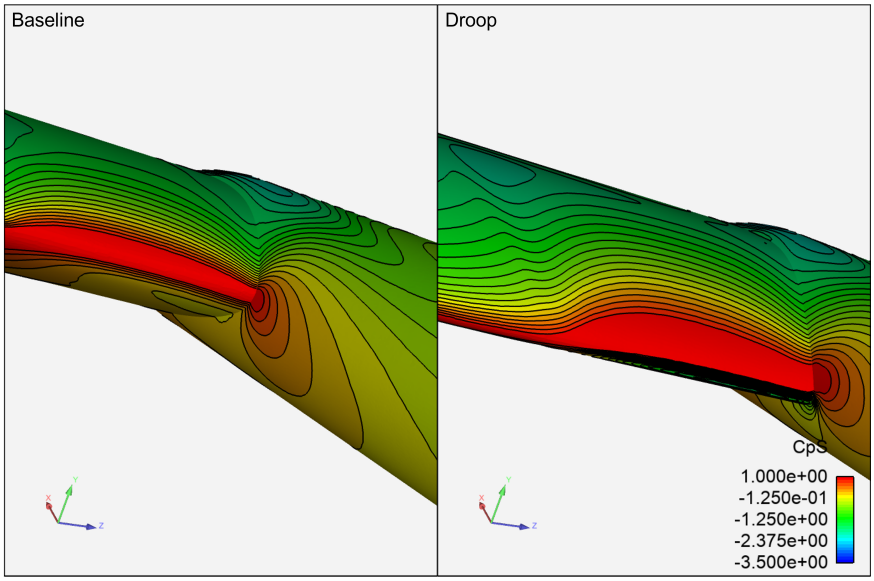

Figure 7.15: Comparison of the starboard side surface static pressure coefficient distribution at the wing leading edge close to the nacelle for the baseline wing with nacelle and propeller and the modified wing with droop at angle of attack of 10°, Advance ratio: J = 1.0

Figure 7.16 shows the boundary layer development in the region of separated flow. Determining the cause of the flow separation is not straightforward given the complex nature of the flow structures present in the propeller-nacelle-wing system. Given the approximate location of the point where the rapid boundary layer growth occurs, it is possible that the additional curvature that is introduced by the addition of droop and therefore the stronger adverse pressure gradient that is generated further aft results in flow separation. However, the separation in this region does appear to be relatively sensitive with a number of simulations showing a growth in separation on the port side of the propeller wake. The cause of this sensitivity is unclear and therefore it is possible that this effect is the result of a model deficiency or a sensitivity of this particular airfoil.

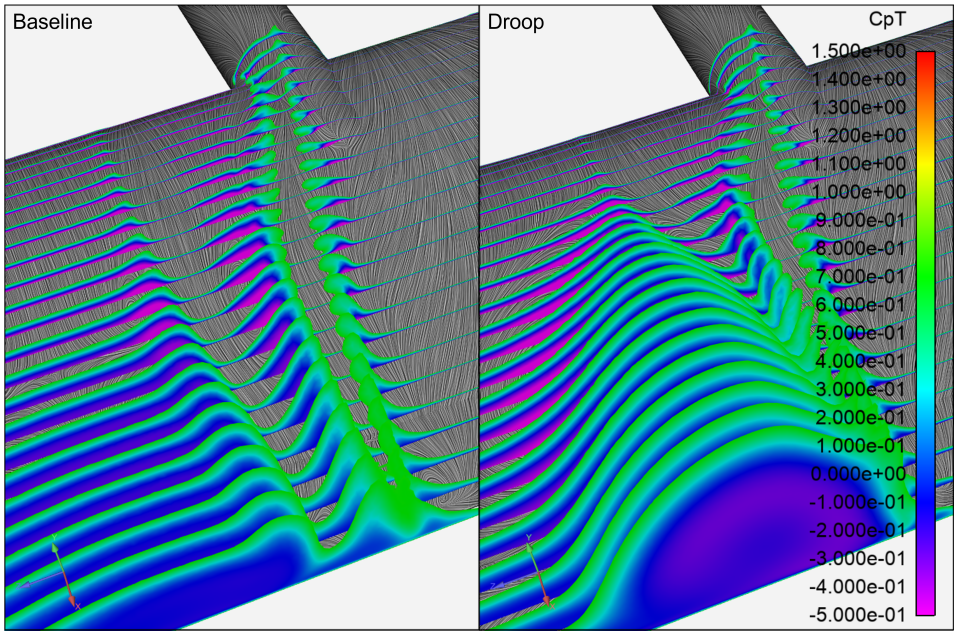

Figure 7.16: Comparison of the total pressure coefficient slices for the baseline wing with nacelle and propeller and the modified wing with droop at angle of attack of 10°, Advance ratio: J = 1.0

Finally, in order to understand the modification behaves at off-design conditions it is evaluated at an angle of attack of 0°. Table 7.5 presents the key performance figures for the baseline and drooped wing in this condition. It is clear that at this low angle of attack droop is detrimental to performance. In both the condition with and without propeller the addition of droop results in a reduction in lift and an increase in drag. The leading edge alignment at low angles of attack is worse in with droop resulting in suction forming on the lower surface. The use of droop is only really practical if it is only deployed at higher angle of attack conditions.

Model	**Baseline**		**Droop**	
	Prop off	**Prop on**	**Prop off**	**Prop on**
Wing Lift Coefficient C_L [-]	0.253	0.280	0.247	0.277
Wing Drag Coefficient C_D [-]	0.017	0.012	0.016	0.015
Wing Moment Coefficient C_M	0.104	0.115	0.107	0.121

Table 7.5: Wing lift, drag and moment coefficient for the baseline wing with nacelle and propeller and the modified wing with droop at angle of attack of 0°

Figures 7.17 and 7.18 shows that overall the addition of droop has minimal effect on the flow structures that form on the wing upper surface. It does not introduce significant structure or alter the interaction effects that are already there and therefore the reduction in performance is not the result of a specific deficiency that is introduced by the concept.

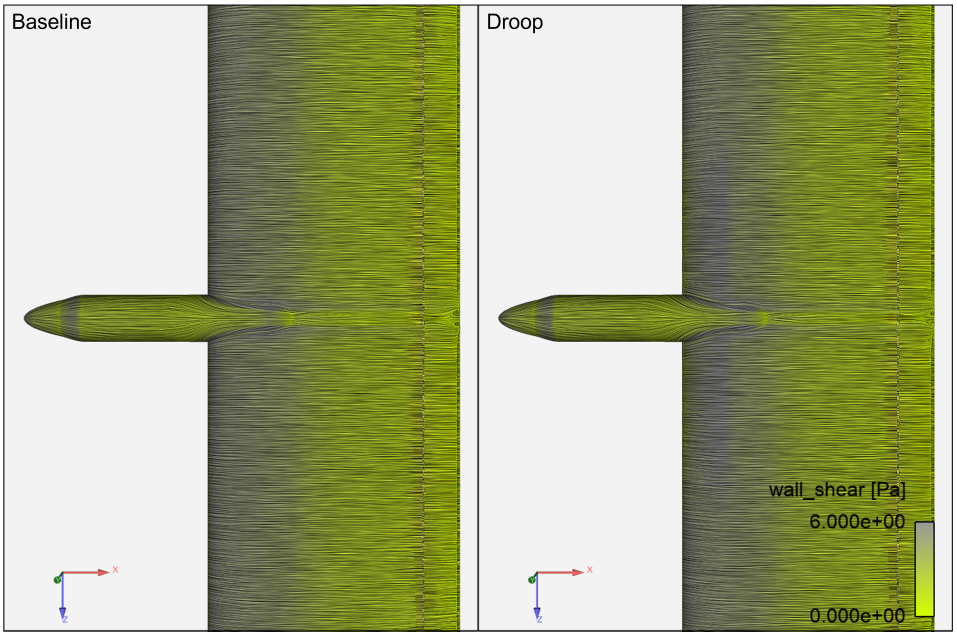

Figure 7.17: Comparison of the surface flow for the baseline wing with nacelle and the modified wing with droop at angle of attack of 0°

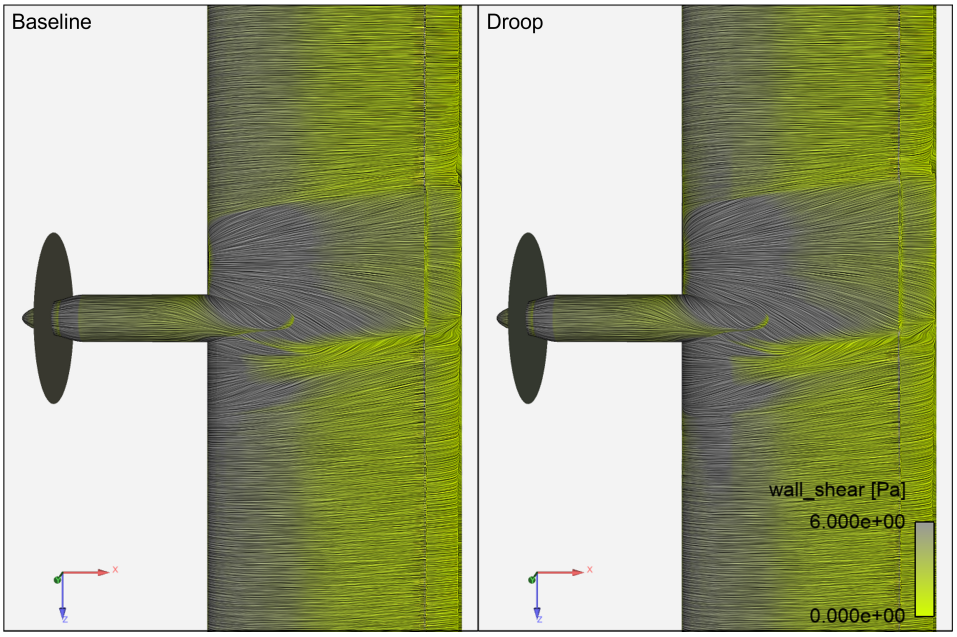

Figure 7.18: Comparison of the surface flow for the baseline wing with nacelle and propeller and the modified wing with droop at angle of attack of 0°, Advance ratio: J = 1.0

The use of droop to address the negative effects of propeller-nacelle-wing interactions overall seems unlikely to be an effective approach in this particular case. The use of droop does go some way to addressing the problems introduced by the nacelle wing interactions. The more favourable pressure distribution that is created by drooping the wing leading edge appears to delay the formation of stall on the upper surface in the vicinity of the nacelle and offers a small increase in lift at an angle of attack of 10°. It is possible that this delay in the onset of stall may result in an improvement in the maximum lift angle of attack however more research is required in this area.

The addition of the actuator disc resulted in worse performance of the drooped wing. On the starboard

(down-going blade) side the use of droop is particularly ineffective. The downwash induced by the propeller causes the droop leading edge to not be well aligned with the local flow causing a reduction in lift. It is therefore recommended to only apply droop to the up-going blade side. Additionally the leading edge droop caused a growth in the separated flow adjacent to propeller wake resulting in a substantial reduction in the upper surface suction on the up-going blade side. The cause of this increase in separation is not immediately clear with is likely caused by the changes in the pressure distribution introduced by the drooped leading edge however there is some evidence to suggest that this behaviour is a particular sensitivity of the model and therefore some caution is used when interpreting this result, particularly as leading edge droop has already been applied to aircraft like the A400M [30]. There is some hesitation to assume that this result can be generalised to all propeller wing systems.

At lower angles of attack the use of droop results in a reduction of lift and an increase in wing drag at lower angles of attack. This result is unsurprising as at lower angles of attack droop leads to worse leading edge alignment and therefore poor performance. The use of droop has the effect of producing suction on the wing lower surface and reducing the upper surface suction.

7.2.2. Fillet

The fillet aims to reduce the wing separation in the region adjacent to the nacelle by smoothing the transition between the nacelle and wing with the hope of reducing the interactions between the nacelle and wing boundary layer.

Table 7.6 shows the wing performance coefficients at an angle of attack of 10°. A comparison is made between the modified geometry with the fillet and the unmodified development model which is referred to as the baseline geometry. The addition of the fillet results in a reasonable increase in lift coefficient and is accompanied by a subtle increase in drag coefficient resulting in a net improvement in lift to drag ratio. While the performance increase is subtle it is averaged over the entire span. Analysing the local performance coefficients shown in Table 7.7 shows that the addition of the fillet increases the lift coefficient and interestingly the lift coefficient in this region is in fact higher than the total wing lift coefficient. This implies that the region near to the nacelle generates more lift that the undisturbed wing. It should be noted however that the lift in this region includes the suction generated by the nacelle and fillet however the reference area is only that of the wing and therefore in the case with the fillet the area is increased. This result does however imply that the use of the fillet eliminates much of the reduction in lift that originates from the installation of the nacelle.

Model	**Baseline**	**Fillet**
Wing Lift Coefficient C_L [-]	1.244	1.251
Wing Drag Coefficient C_D [-]	0.035	0.036
Wing Moment Coefficient C_M [-]	0.341	0.343

Table 7.6: Wing lift, drag and moment coefficient for the baseline wing with nacelle and the modified wing with fillet at angle of attack of 10°

Model	**Baseline**	**Fillet**
Local Lift Coefficient C_L' [-]	1.197	1.268
Local Drag Coefficient C_D' [-]	0.041	0.044

Table 7.7: Local (0.4m span) lift and drag coefficient for the baseline wing with nacelle and the modified wing with fillet at angle of attack of 10°

Figure 7.19 shows that the addition of the fillet leads to a growth of the separated region close to the nacelle. It results in an increase in the size of the recirculating regions. While overall this modification seems to yield additional performance this larger region of separated flow is unlikely to be a desirable characteristic. The region directly outside of the separated flow however sees an aft movement of the main element and flap separation line. This however is not a direct consequence of the modification as the flow in this region does not originate in the vicinity of the nacelle and as such is likely a consequence of the changes to recirculating flow that is directly adjacent to it. Figure 7.20 shows the impact of the

modifications on the wing pressure distribution. Overall, the modification seems to result in some reduction in the interference effects introduced in the nacelle at least close to the leading edge. This is shown by the steeper curve seen in the isobars in the vicinity of the nacelle. In addition to this the presence of the fillet seems to generate additional suction on the mid-portion of the wing in the vicinity of the nacelle. The combination of these effects is what result in the lift coefficient increase observed in Table 7.6. Although there is a net increase in top surface suction in the vicinity of the nacelle the modification does also however result in a larger spanwise pressure gradient forming on the upper surface of the wing. This manifests itself in a more significant spanwise flow close to the wind surface component shown in Figure 7.19. This is likely partly responsible for the increase in the region of separated flow.

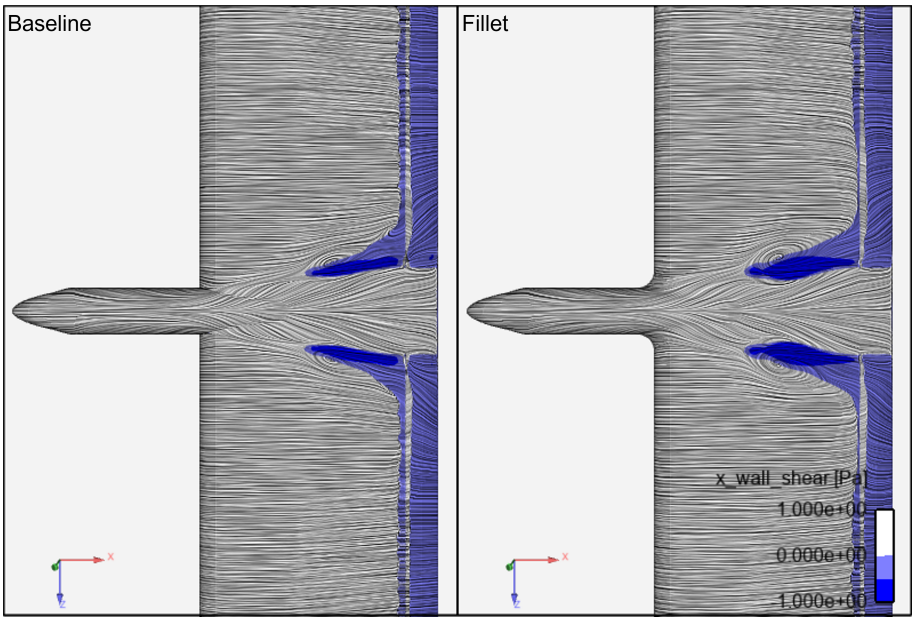

Figure 7.19: Comparison of the surface flow with regions of reverse flow highlighted in blue for the baseline and filleted wing at an angle of attack 10°

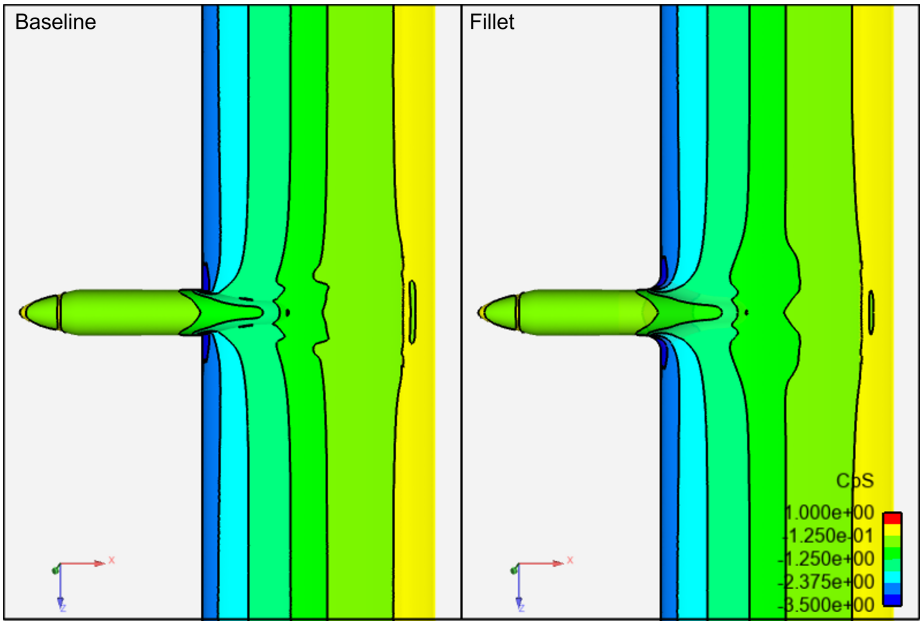

Figure 7.20: Comparison of the surface static pressure coefficient distribution for the baseline and filleted wing at an angle of attack 10°

Figure 7.21 shows the evolution of the wing boundary layer in the vicinity of the nacelle. The addition of the fillet goes a long way to cleaning up the nacelle wing junction flow which is likely responsible for the increase in suction observed on the forward and mid-portions of the wing. It is effective in spreading out the region of thickened boundary layer however this does not result in a reduction in the separated flow towards the wing trailing edge as is shown in Figure 7.22. The thickened boundary layer is still unable to overcome the adverse pressure gradient and therefore the spreading effect results in a larger region of separated flow. While the modification does show some promise as far as improving the wing performance is concerned there are still some clear deficiencies. Whether or not this type of fillet is an effective modification is likely concept specific as while in some cases the reduction in local boundary layer thickness observed on the forward portion of the wing may yield an increase in performance as was shown here but the spreading of the losses over a larger portion of the wing may not necessarily yield a performance advantage. Furthermore, while there is a subtle increase in performance at this angle of attack the result may be different closer to the maximum lift coefficient where the adverse pressure gradient that the region of thickened boundary layer must overcome is stronger.

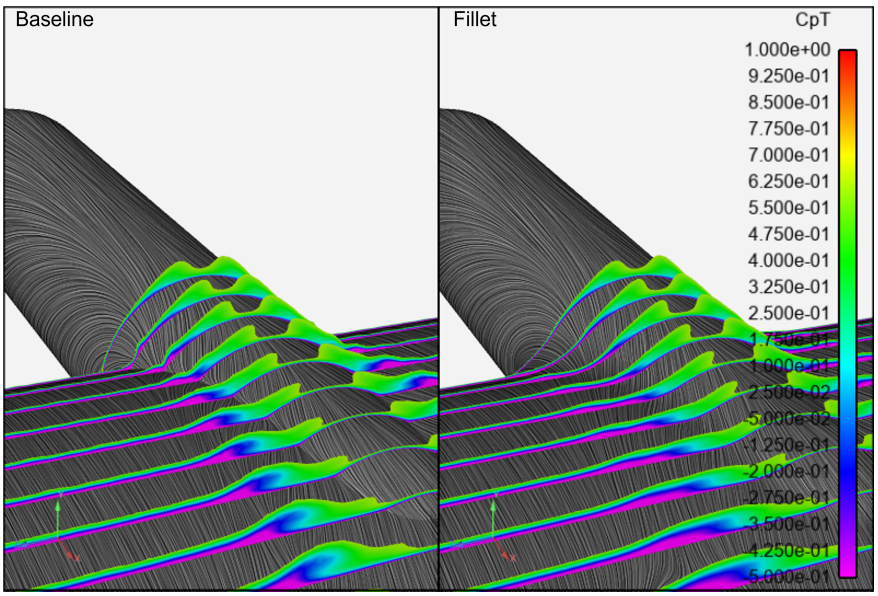

Figure 7.21: Comparison of off surface total pressure slices at the nacelle wing junction for the baseline and filleted wing at an angle of attack 10°

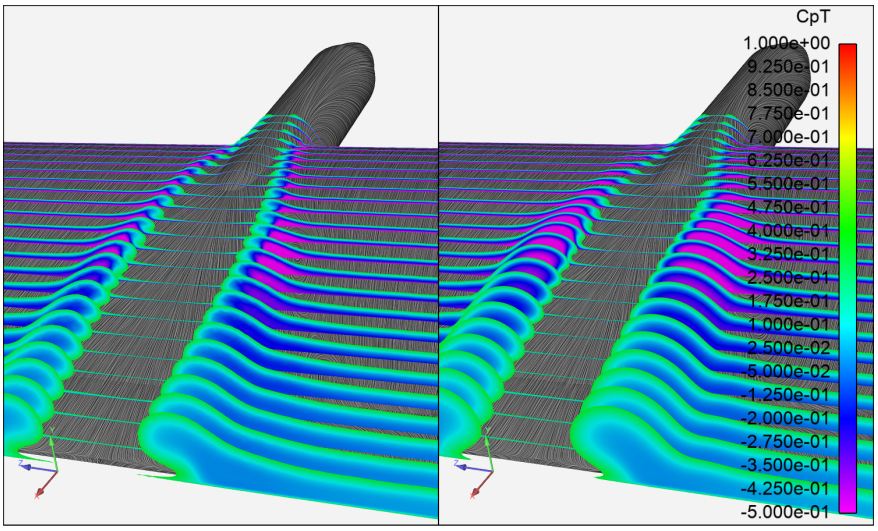

Figure 7.22: Comparison of off surface total pressure slices on the wing suction side behind the nacelle for the baseline and filleted wing at an angle of attack 10°

Analysis of the wing leading edge pressure distribution close to the nacelle shown in Figure 7.23 shows that while the fillet does blend the nacelle and wing an unintended consequence of the modification is an increase in the leading edge pressure peak over a larger region compared to the baseline geometry. The increase in this leading edge pressure peak results in a stronger adverse pressure gradient close to the leading edge which could potentially cause boundary layer growth. This effect may negate some of the flow improvements introduced by the fillet and as such may limit the modification performance. Analysis of the geometry found that an unintended consequence of the fillet was that it resulted in a local sharpening of the leading edge shown in Figure 7.24.

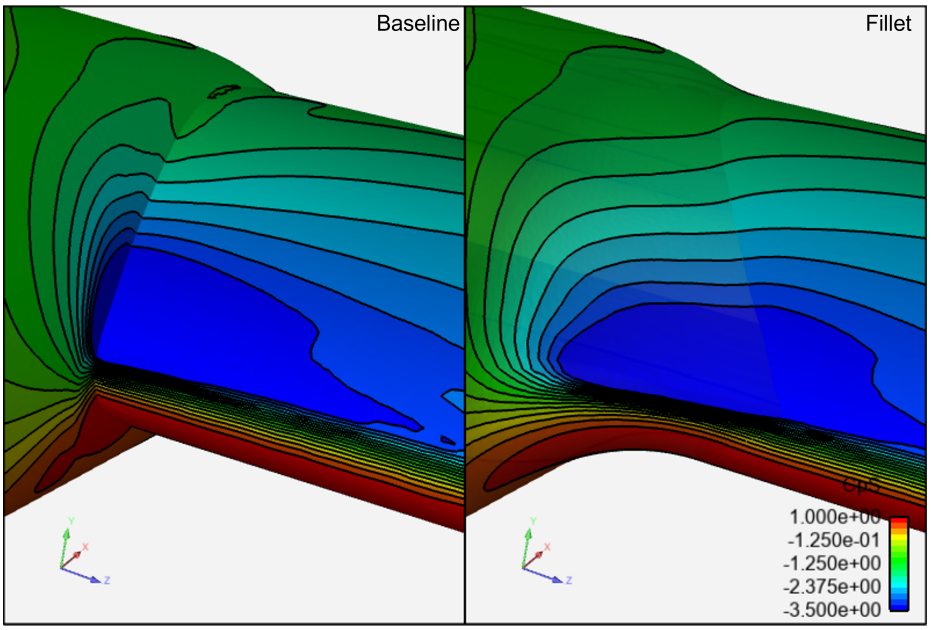

Figure 7.23: Comparison of the surface static pressure coefficient distribution at the wing leading edge close to the nacelle for the baseline and filleted wing at an angle of attack 10°

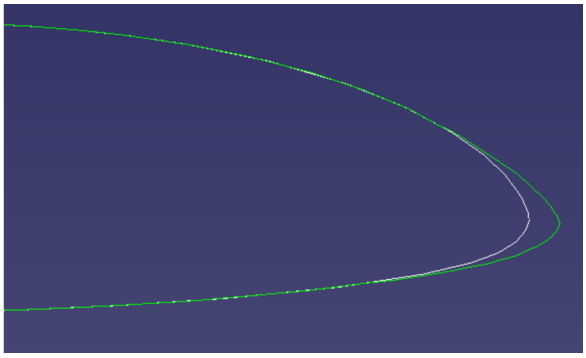

Figure 7.24: Cross section of the baseline (white) and filleted geometry (green) close to the nacelle showing the sharpening of the airfoil leading edge

In order to address this a second iteration of the fillet was created with the aim of adding volume locally in order to increase the leading edge radius. This modification aims to deliver the junction boundary layer spreading effect without introducing a less favourable wing pressure gradient with the aim of preventing the thickened boundary layer form separating. A Cross section of this modification pictured in Figure 7.25 shows that this change is able to bring the wing leading edge radius closer to closer to that of the baseline wing.

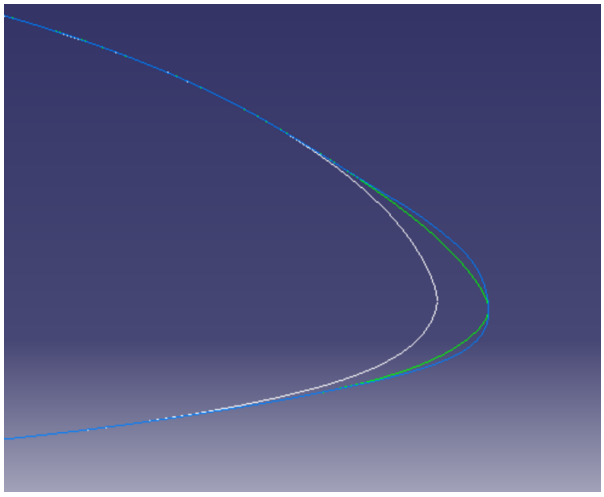

Figure 7.25: Cross section of the baseline (white), filleted geometry (green) and the modified fillet (blue) close to the nacelle showing how the addition of volume to the fillet increases the local leading edge radius

Figure 7.26 shows that the modification to the fillet geometry has gone some way to reducing the strong local leading edge pressure peak. The isobar distribution on the inboard portion of the fillet leading edge is less closely spaced than was seen in the original fillet suggesting a less aggressive pressure recovery as was hoped. This effect is however reasonably subtle.

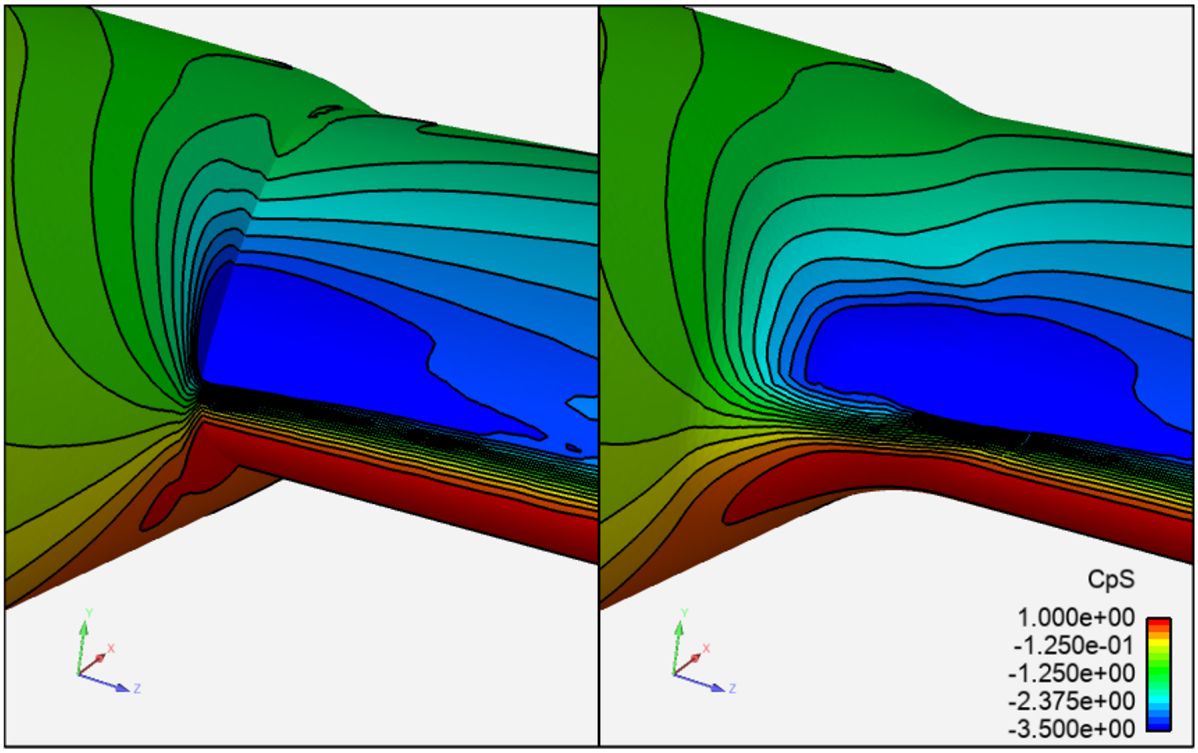

Figure 7.26: Comparison of the surface static pressure coefficient distribution at the wing leading edge close to the nacelle for the baseline and modified filleted wing at an angle of attack 10°

Table 7.8 shows the key performance coefficients of the modified fillet. The modified fillet results in a small reduction in lift coefficient for the same drag and moment coefficient as the original fillet. and is therefore not an improvement compared to the original fillet. Even when considering only the local performance coefficients the difference between the two fillets is small. The changes are very small and therefore it is important to be cautious when drawing conclusions as it is unclear whether these effects are genuine or simply just within the repeatability band of the CFD modelling tools.

Model	Baseline	Fillet	Modified Fillet
Wing Lift Coefficient C_L [-]	1.244	1.251	1.249
Wing Drag Coefficient C_D [-]	0.035	0.036	0.036
Wing Moment Coefficient C_M [-]	0.341	0.343	0.343

Table 7.8: Wing lift, drag and moment coefficient for the baseline wing with nacelle and the modified wing with fillet at angle of attack of 10°

Model	Baseline	Fillet	Modified Fillet
Wing Lift Coefficient C_L [-]	1.197	1.268	1.267
Wing Drag Coefficient C_D [-]	0.041	0.044	0.044

Table 7.9: local (0.4m span) lift, drag and moment coefficient for the baseline wing with nacelle and the modified wing with fillet at angle of attack of 10°

Figure 7.27 shows that overall the modifications to the fillet have had minimal effect of the separation behaviour. The presence of the fillet still results in a larger region of stalled flow forming adjacent to the nacelle. The stall behaviour is almost identical to what was seen in the case of the original fillet. This suggests that any reduction in the adverse pressure gradient close to the leading edge has minimal impact on the boundary layer evolution. Figure 7.28 similarly shows a very similar pressure distribution to what was observed for the original fillet with some additional suction on the front and mid-portions of the wing in the vicinity of the nacelle. Overall it seems that the impact of the modification to the fillet is small and the reduction in lift seems to be a result of subtle changes in the pressure field. This modified fillet will therefore not be considered during further analysis as it does not considerably change the behaviour of the concept or improve upon the original fillet.

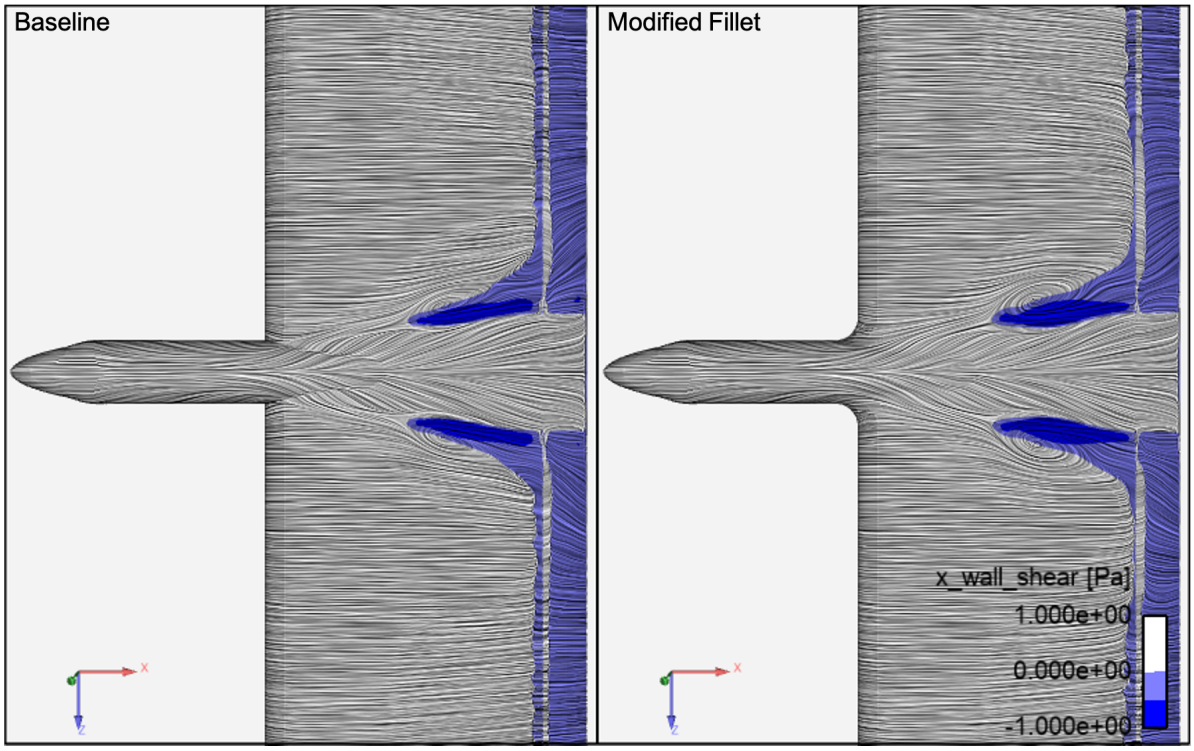

Figure 7.27: Comparison of the surface flow with regions of reverse flow highlighted in blue for the baseline and modified filleted wing at an angle of attack 10°

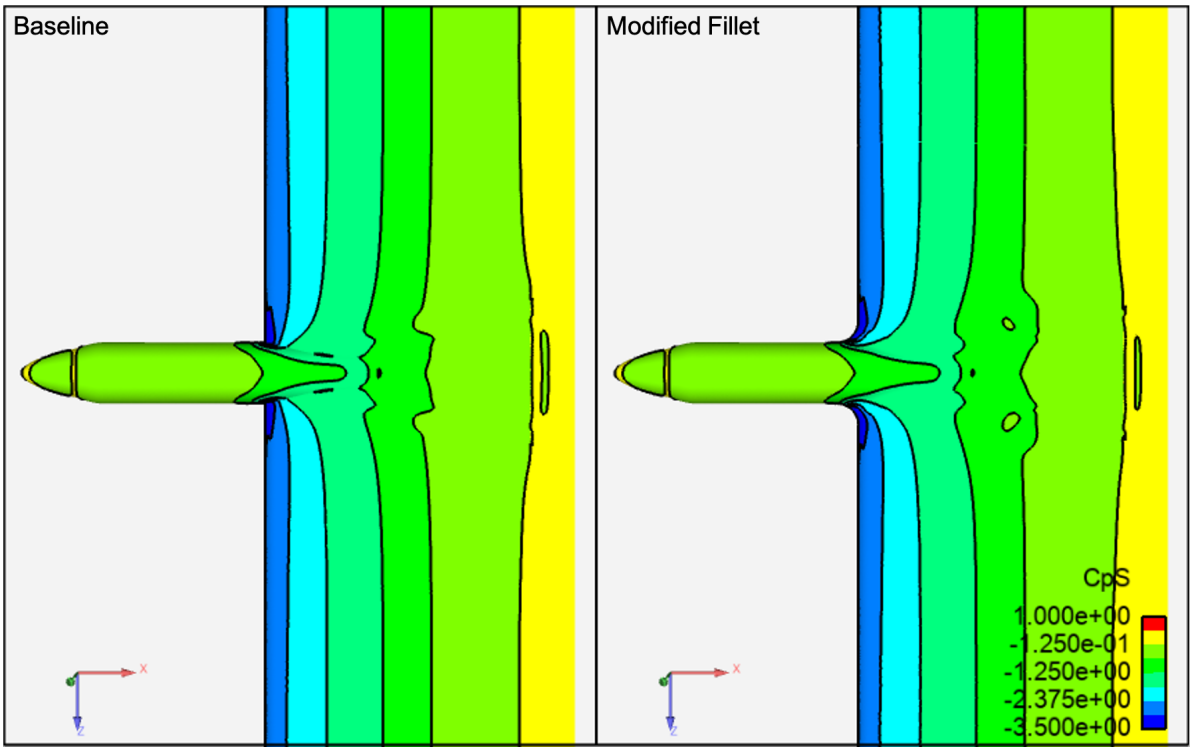

Figure 7.28: Comparison of the surface static pressure coefficient distribution for the baseline and modified filleted wing at an angle of attack 10°

Considering the performance in the presence of the propeller shown in Table 7.10 it is clear that overall the fillet has a minimal effect on the performance with the propeller. The wing lift coefficient is roughly identical with a slight increase in drag. Considering only the region that is directly influenced by the propeller-nacelle-wing interactions shown in Table 7.11 shows that locally the fillet increases the wing lift with an increase in drag coefficient however it is worth noting that this delta is relatively small in comparison to the previously observed changes.

Model	Baseline	Fillet
Wing Lift Coefficient C_L [-]	1.280	1.280
Wing Drag Coefficient C_D [-]	0.043	0.046
Wing Moment Coefficient C_M [-]	0.364	0.368

Table 7.10: Wing lift, drag and moment coefficient for the baseline wing with nacelle and propeller and the modified wing with fillet at angle of attack of 10°, Advance ratio: J = 1.0

Model	Baseline	fillet
Wing Lift Coefficient C_L [-]	1.849	1.855
Wing Drag Coefficient C_D [-]	0.086	0.096

Table 7.11: Local (0.6m span) lift, drag and moment coefficient for the baseline wing with nacelle and propeller and the modified wing with fillet at angle of attack of 10°, Advance ratio: J = 1.0

Figure 7.29 shows a comparison the surface flow field with and without the fillet. The case with fillet seems to result in a growth in the separation in the region next to the propeller wake. As was described previously there is some uncertainty regarding whether or not this behaviour is genuine or the result of the model sensitivity in this region as in this case in particular the changes in the geometry are quite far removed from the resulting changes in separation behaviour. The modifications to the nacelle junction seem to result in a reduction in the size of the separated flow region that originated at the nacelle however given the changes to the separated flow outside of the propeller wake there is likely some

influence on the other structures. Figure 7.30 shows the surface pressure distribution. Overall, the pressure distribution is similar. The influence of the larger region of separated flow is apparent on both sides of the nacelle resulting in a reduction in suction. As was seen in the case with propeller the fillet smoothing the junction does seem to provide some additional suction in the vicinity of the nacelle.

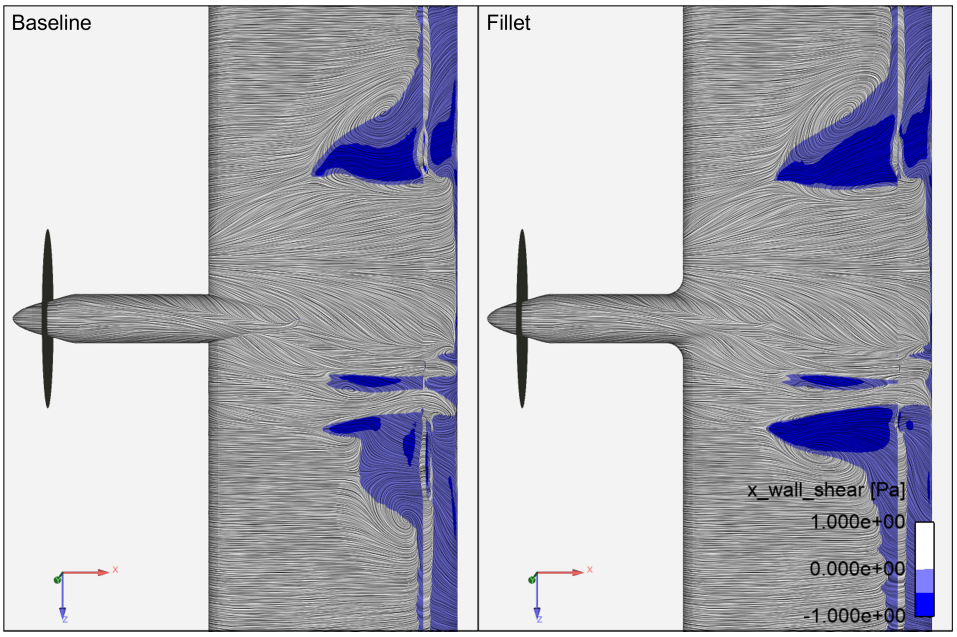

Figure 7.29: Comparison of the surface flow with regions of reverse flow highlighted in blue for the baseline wing with nacelle and propeller and the modified wing with fillet at angle of attack of 10°, Advance ratio: J = 1.0

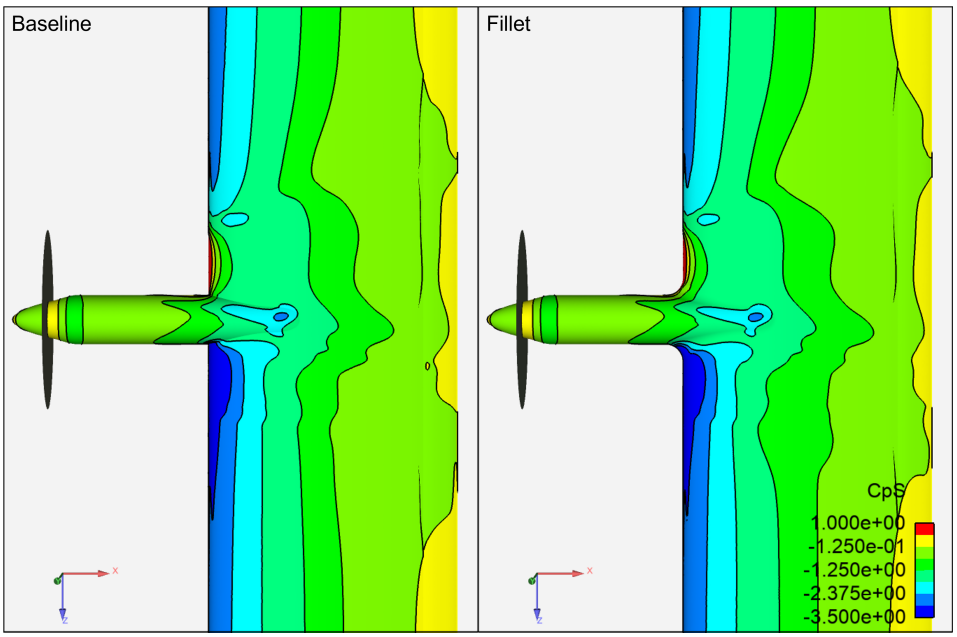

Figure 7.30: Comparison of the surface static pressure coefficient distribution for the baseline wing with nacelle and propeller and the modified wing with fillet at angle of attack of 10°, Advance ratio: J = 1.0

Figures 7.31 and 7.32 show the static pressure coefficient distribution at the nacelle wing junction. Both sides show a clear smoothing of the pressure distribution at the wing nacelle junction. Overall the pressure gradient at the junction seems to be more favourable.

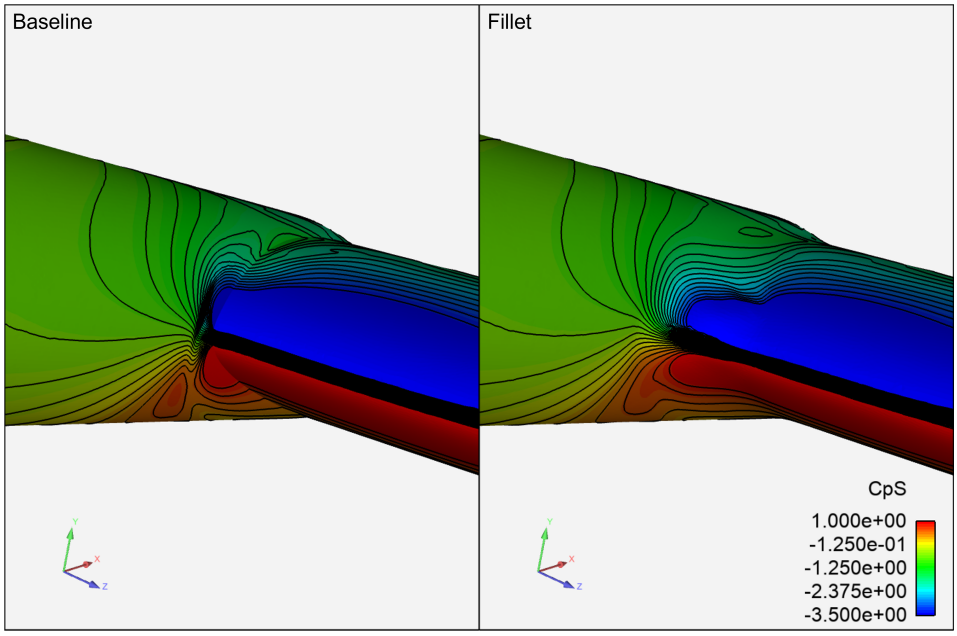

Figure 7.31: Comparison of the port side surface static pressure coefficient distribution at the wing leading edge close to the nacelle for the baseline wing with nacelle and propeller and the modified wing with fillet at angle of attack of 10°, Advance ratio: J = 1.0

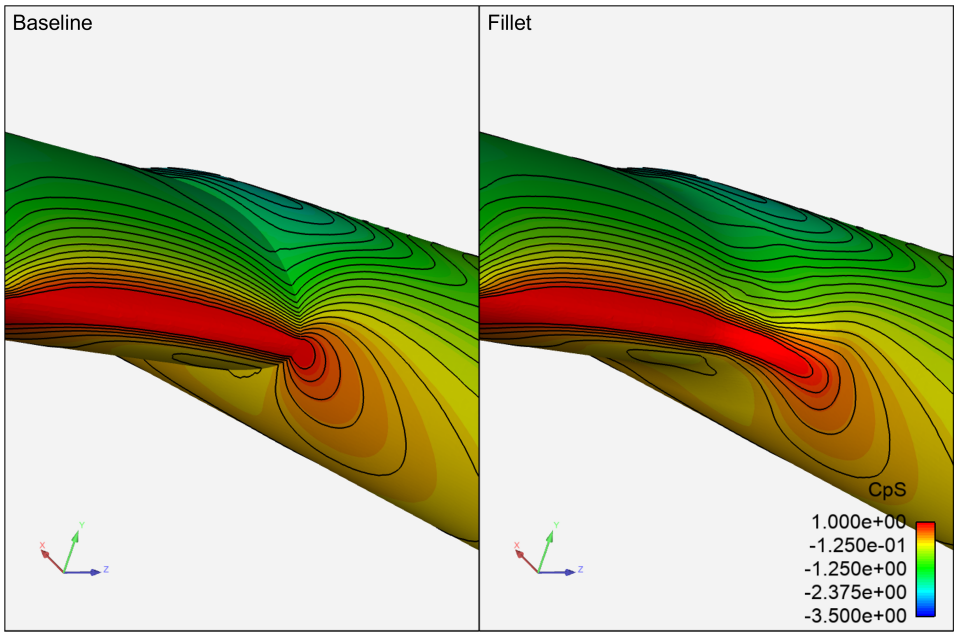

Figure 7.32: Comparison of the starboard side surface static pressure coefficient distribution at the wing leading edge close to the nacelle for the baseline wing with nacelle and propeller and the modified wing with fillet at angle of attack of 10°, Advance ratio: J = 1.0

Analysing the boundary layer development using total pressure coefficient slices as is shown as is shown in Figure 7.33 is it clear that the fillet reduces the initial formation of nacelle wing junction losses. This results in a smaller boundary layer close to the nacelle in a similar manner to in the case without propeller. This initial boundary layer clean-up perhaps results in some improvement in the separated flow associated with the nacelle wing interactions. However, as was described previously the growth in the separated region that forms close at the edge of the propeller wake likely influence the growth of the nacelle structures towards the trailing edge making it difficult to isolate the impact of the fillet.

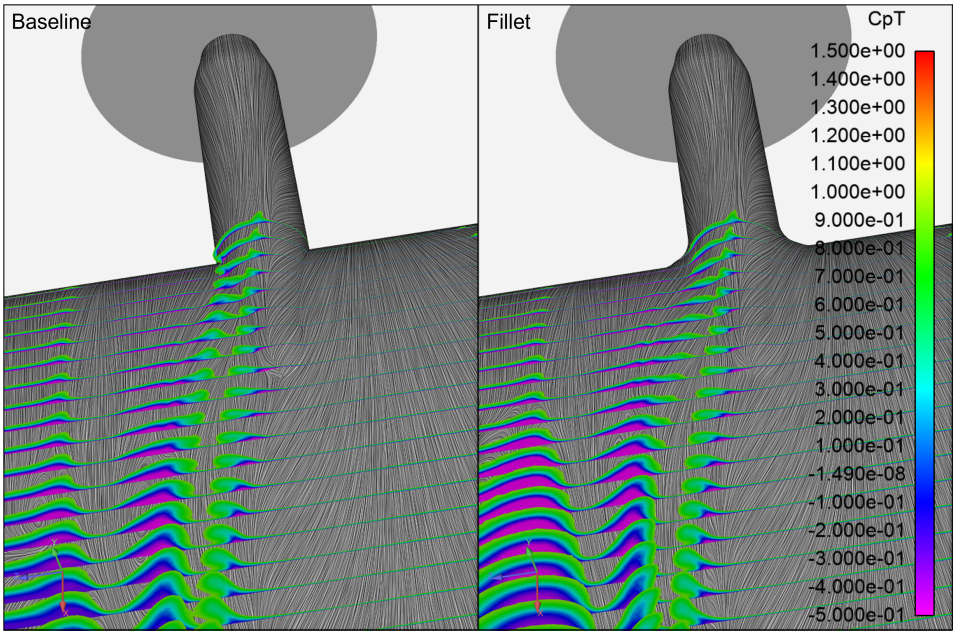

Figure 7.33: Comparison off surface total pressure slices at the nacelle wing junction for the baseline wing with nacelle and propeller and the modified wing with fillet at angle of attack of 10°, Advance ratio: J = 1.0

Table 7.12 shows that the influence of the fillet at lower angles of attack is negligible. All the key performance parameters appear to be identical to those seen in the unmodified wing suggesting that this modification does not seems to adversely influence the wing performance in off-design conditions.

Model	**Baseline**		**Fillet**	
	Prop off	**Prop on**	**Prop off**	**Prop on**
Wing Lift Coefficient C_L [-]	0.253	0.280	0.253	0.280
Wing Drag Coefficient C_D [-]	0.017	0.012	0.017	0.012
Wing Moment Coefficient C_M	0.104	0.115	0.104	0.115

Table 7.12: Wing lift, drag and moment coefficient for the baseline wing with nacelle and propeller and the modified wing with a fillet at angle of attack of 0°

Similarly Figures 7.34 and 7.35 shows that the fillet introduces minimal changes to the wing upper surface flow field in the zero angle of attack condition suggesting that it unlikely to cause a significant change in behaviour in the off design conditions

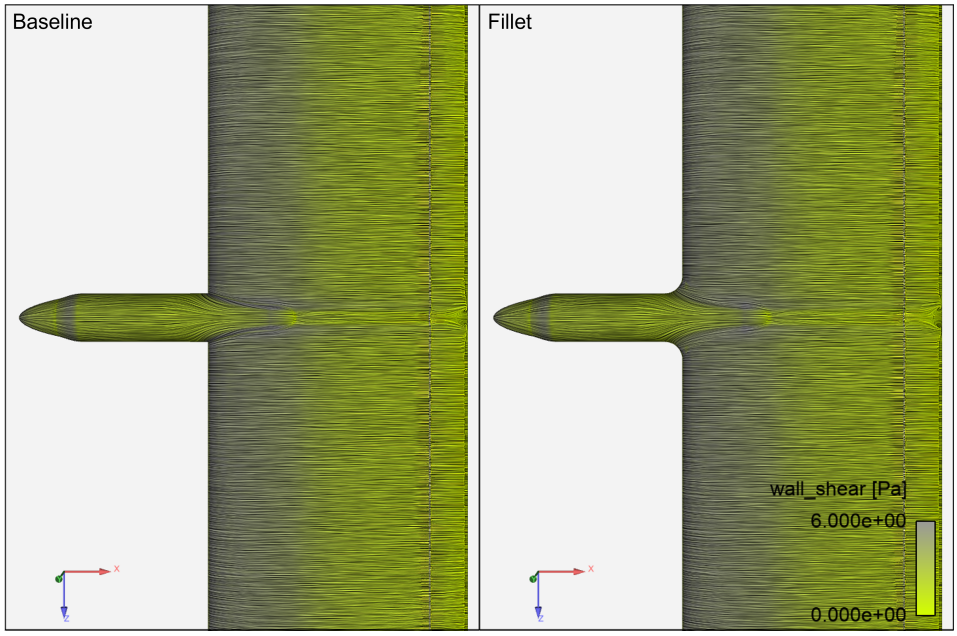

Figure 7.34: Comparison of the surface flow for the baseline wing with nacelle and the modified wing with fillet at angle of attack of 0°

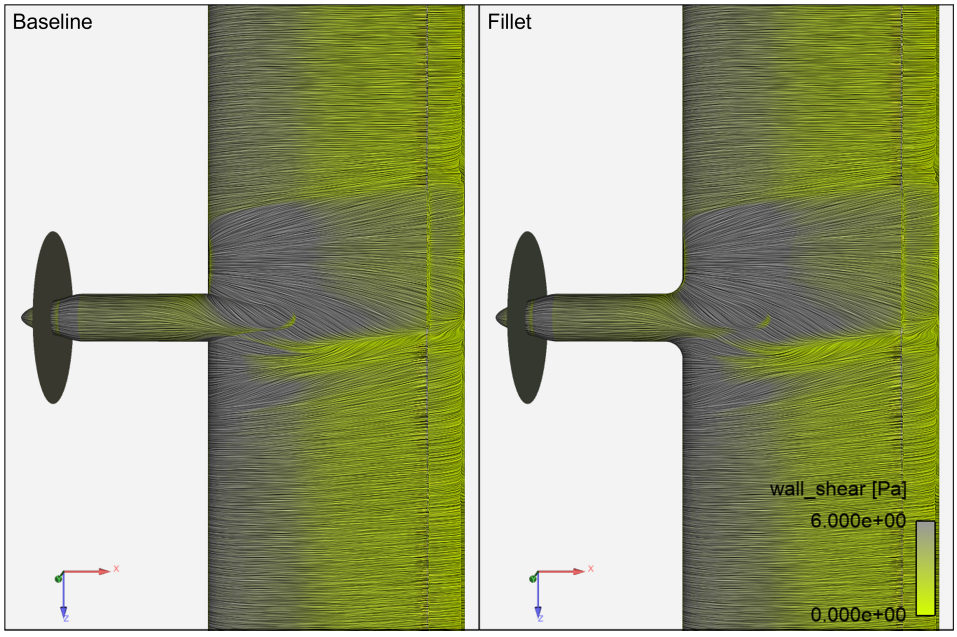

Figure 7.35: Comparison of the surface flow for the baseline wing with nacelle and propeller and the modified wing with fillet at angle of attack of 0°, Advance ratio: J = 1.0

Overall the fillet seems like a more suitable candidate to address the negative effects introduced by the propeller-nacelle-wing interactions. The smoothing of the junction reduces the boundary growth as a result of the corner flow effects introduced by the nacelle-wing junction. The fillet spreads the boundary layer losses resulting in a thinner boundary layer on the forward portion of the wing increasing the suction on this forward portion. However, the thickened boundary layer is more spread and is still unable to overcome the adverse pressure and therefore the modification increases the size of the region of separated flow.

With the actuator disc the fillet has minimal impact on the performance of the propeller-nacelle-wing

system. It is still able to clean up some of the junction flow which perhaps reduces the strength and impact of the structures shed by the nacelle however there is significant growth in the region of separated flow that forms in the vicinity of the propeller wake despite the geometry change being reasonably far from the impacted area suggesting that this may be the result of a modelling deficiency.

The fillet has virtually no effect at lower angles of attack, suggesting that the modification can be used to modify the high angle of attack performance without compromising the performance at off-design conditions.

8

Conclusions and Recommendations

This chapter presents the main conclusions that can be drawn from the research project as well as describing the recommendations for further study.

8.1. Conclusions

Literature indicates that the installation of the nacelle to the wing leading edge introduces a series of undesirable interaction effects that can lead to the early onset of stall and thus limit high angle of attack performance. The addition of a propeller while largely beneficial to performance can aggravate the deficiencies introduced by the nacelle as a result of for instance the swirl which induces a local increase in drag. Some methods have been used to try to mitigate these effects such as strakes and lowering the nacelle with some limited success. In addition, leading edge droop has been applied to improve the leading edge alignment and thus mitigate some of the increases in local angle of attack introduced by the nacelle and propeller swirl. Much of this research into this region relies heavily on numerical modelling and there is limited experimental data that focuses particularly on nacelle-wing interactions. Understanding how the nacelle effects are influenced by the propeller has also only been treated in a limited way with little consensus between these studies. additionally there a relatively few engineering studies that look to systematically understand and target mitigation techniques to address the negative interaction effects at high angles of attack for propeller-nacelle-wing interaction effects. Addressing this knowledge gap is the purpose of this research through the use of experimental work and validated CFD simulations.

The first of the key research questions to be addressed is: ”How does the presence of a nacelle influence the high angle of attack behaviour of a wing?” Based on the combination of wind tunnel and initial CFD analysis the addition of the nacelle to the wing interacts strongly with the wing at high angles of attack. Analysis of the nacelle wing system at an angle of attack of 10° the nacelle induces an increase in local angle of attack as the flow accelerates around the nacelle. In addition to this the addition of the nacelle alters the upper surface pressure distribution resulting in the development of a cross-flow component which leads to boundary layer accumulation. Finally, the nacelle boundary layer interacts with the wing boundary layer at the junction resulting in boundary layer growth. The combination of these effects induces two regions of separation either side of the nacelle. These regions of separated flow reduce the wing high angle of attack performance by reducing the lift coefficient that can be generated compared to a clean wing and increasing drag.

The addition of the propeller significantly modifies the nacelle wing interaction effects. The influence of the nacelle is still visible however the propeller swirl results in the shearing and transport of the nacelle structures. The structures shed by the nacelle even in the presence of the propeller appear to still lead to the early onset of separation and therefore addressing the nacelle wing interaction effects seems likely to offer some performance benefits in the case with the propeller mounted. In addition to the structures shed directly by the nacelle the propeller wake introduces two additional regions of separated that form either side of the wake likely as a result of a combination of the complex interactions

that occur at the boundary of the propeller slipstream. Firstly, At the boundary of the wake, a pressure and velocity gradient exists between the wake region and surrounding flow. The viscous mixing effects in this region likely interacts with the wing boundary layer and leads to growth. Additionally, the interaction between the swirling propeller wake and the wing leads to the cross-flow components developing on the surface of the wing which result in boundary layer accumulation in a similar fashion to what was described when considering the nacelle interaction effects. Addressing the structures that form at the wake boundary is difficult through the use of leading edge and nacelle modifications as the effects are not directly related to the geometry as such these effects are not directly targeted by the mitigation techniques.

In order to address the next key research question: ”What nacelle and leading edge be modifications can be used to mitigate or suppress the undesirable high angle of attack performance characteristics introduced by the nacelle?” two modifications are considered droop and the use of a nacelle wing junction fillet. Attempts to mitigate the interactions through the use of leading edge droop achieved limited success. The use of droop allowed for the creation of a more favourable pressure distribution gradient which delayed the separation in the vicinity of the nacelle. The reduction in the magnitude of the leading edge pressure peak as a result of better leading edge alignment results in a weaker adverse pressure gradient and therefore the wing boundary layer grows more slowly. This delays the onset of separated flow and reduces the size of the separated region however this modification was not able to eliminate the flow separation entirely and only results in a small improvement in wing lift and little change in drag performance.
The nacelle wing fillet similarly achieves its primary goal of reducing the interaction between the nacelle and wing boundary layer. The fillet reduces the local growth of the wing boundary layer that is formed at the junction between the nacelle and the wing. It is able to spread the junction losses over a larger area resulting in a thinner initial boundary layer in the vicinity of the nacelle and thus more suction on the forward portion of the wing. However, these improvements do not prevent the flow from separating, the spread boundary layer is still thicker than the boundary layer in the undisturbed portion of the wing and is, therefore, less able to resist the adverse pressure gradient at the trailing edge of the wing and so still separates before the flow on the surrounding airfoil. As the losses are spread over a larger portion of the wing the size of the region of separated flow increases. Overall, the modification results in an improvement in wing performance coefficients at high angles of attack, increasing the wing lift for similar drag however, it is unable to address the local regions of separated flow that originate from the installation of a nacelle and therefore cannot be considered to have met all the aims.

The addition of a propeller changes the interaction effects seen and therefore changes the result performance of the modifications. The drooped wing performed particularly poorly on the down-going blade side as a result of the poor leading edge alignment. The propeller swirl reduces the local angle of attack and therefore the droop effect is detrimental. The droop also resulted in a growth of the regions of separated flow that forms at the boundary of the propeller wake. This behaviour is somewhat more uncertain as it seems that perhaps the combination of the airfoil and modelling techniques resulting in some instability in this region and therefore further study would be required to validate this conclusion.
The fillet continues to offer some advantages in terms of reducing the interaction between the nacelle and wing boundary layers. The junction between the nacelle and propeller shows a reduction in the loss that originates from the junction. This effect seems to result in some increases in suction close to the leading edge and reduces the magnitude of the separated flow. The modification however once again increase the presence of flow separation that forms at the edges of the propeller wake and therefore it is also likely that this also impact the nacelle structures and so it is difficult to determine if this local improvement is a direct result of the fillet.

Finally considering the impact of the modifications at lower angles of attack more representative of the majority of the flight the use of droop resulted in a an increase in drag and a reduction in lift as a result of the poor leading edge alignment however did not significantly alter the flow structures seen at these lower angles of attack.
At lower angles of attack the use of a fillet has virtually no effect with similar lift and drag performance and no change in the flow structures.

Overall, it is clear that is possible to influence the high angle of attack behaviour through the use of nacelle and wing leading edge modification. The use of droop offers some potential in terms of mitigating the deficiencies of the nacelle-wing system but performs poorly at low angles of attack and in the presence of a propeller. The use of a junction fillet was overall more effective at addressing the negative interaction effects introduced by the propeller-nacelle-wing system however it was not able to improve the flow separation that occurs in the vicinity of the nacelle. It offers a small improvement to the propeller off and propeller on performance at high angles of attack and is neutral at low angles of attack and therefore seems to offer some potential as a device to maximise the high angle of attack performance. However, while the fillet does seem to offer some benefit is does not eliminate the separation that occurs as a result of the nacelle-wing interactions. The most dominant effect involved in the formation of these structures seems to be the cross-flow component introduced as a result of the changes in pressure distribution introduced by the nacelle. This phenomenon can likely be better addressed by changing the position of the nacelle to restore some of the suction lost behind the nacelle.

8.2. Recommendations

Over the course of the research, a number of further questions arose. This section aims to present these questions and suggest potential areas for further study.

Due to time and computational limitations, it was not possible to investigate the impact of high lift devices on the performance. When considering high angle of attack performance this parameter is typically most critical when considering the take-off and landing phases and as such the maximum lift performance of the wing with high lift devices deployed is more relevant. As such it is recommended to evaluate the impact of the propeller-nacelle system on multi-element airfoil systems in conditions where the flap is deployed.

In addition to this, the study did not consider the impact of multiple propellers on the propeller-nacelle-wing interaction effects. While based on literature it seems likely that the broad conclusions from the single propeller case are likely still applicable to a multi-propeller case, given the relevance of the results of this study for configurations that employ techniques like distributed propulsion it is important to verify this assumption.It is therefore recommended to investigate the impact of multiple propellers on the wing high angle performance.

It is also recommended to investigate the propeller-nacelle-wing interactions at more angles of attack and conditions. This study considered the impact of the propeller and nacelle as well as the various modifications primarily at a single angle of attack of 10° and free stream velocity of 30m/s while some additional analysis was performed at 0° angle of attack in order to verify the conclusions regarding the impact of the modifications on both the high angle of attack and cruise condition performance generation of full lift and drag polar is likely of interest. In addition analysis of the propeller-nacelle-wing interaction effects at different Reynolds numbers would yield further understanding regarding them.

This study focused on a simple propeller wing configuration however this configuration is not representative of novel (electric) propeller-driven aircraft and therefore the impact of real engine integration and the impact of parameters like leading edge sweep should be understood.

The goal of this study was largely exploratory and therefore no geometry optimisation was performed and the use of strakes and an understanding of the nacelle height was not extensively explored. Geometric optimisation will be required in order to maximise the wing high angle of attack performance of a specific configuration. Additionally, this study did not consider the impact of the combined effects of geometric modifications.

Finally, the simplified actuator disc used to investigate the impact of a propeller on the nacelle-wing interaction effects does not accurately model the disc loading distribution or the impact of blade passage on the wing boundary layer. Further understanding of the impact of the propeller through the use of either higher-fidelity numerical simulations or additional wind tunnel tests would likely be advantageous to the understanding of the high angle of attack behaviour as well as generating further understanding

of the separation phenomenon that occurs at the boundary of the propeller wake.

Bibliography

[1] S. M. Aftab, A. S. Rafie, N. A. Razak, and K. A. Ahmad. Turbulence model selection for low reynolds number flows. *PLoS ONE*, 11(4):1–15, 2016. ISSN 19326203. doi: 10.1371/journal.pone.0153755.

[2] J. Anderson. *Fundmentals of Aerodynamics*. McGraw-Hill Education, New York, sixth edition, 2017. ISBN 978125925134-4.

[3] P. Aref, M. Ghoreyshi, A. Jirasek, M. J. Satchell, and K. Bergeron. Computational study of propeller-wing aerodynamic interaction. *Aerospace*, 5(3):1–20, 2018. ISSN 22264310. doi: 10.3390/aerospace5030079.

[4] M. Bashir, S. Longtin-Martel, R. M. Botez, and T. Wong. Aerodynamic design optimization of a morphing leading edge and trailing edge airfoil–application on the uas-s45. *Applied Sciences (Switzerland)*, 11(4):1–34, 2021. ISSN 20763417. doi: 10.3390/app11041664.

[5] L. M. M. Boermans and P. B. Rutten. Two-dimensional Aerodynamic Characteristics of Airfoil NLF-MOD22 with Fowler Flap, 1995.

[6] M. E. Brenckmann. Experimental Investigation of the Aerodynamics of a Wing in a Slipstream. *Journal of the Aerospace Sciences*, 25(5):324–328, 1958. doi: 10.2514/8.7650.

[7] M. Burnazzi and R. Radespiel. Design and analysis of a droop nose for Coanda flap applications. *Journal of Aircraft*, 51(5):1567–1579, 2014. ISSN 15333868. doi: 10.2514/1.C032434.

[8] Y. Cao and T. Tamura. Aerodynamic characteristics of a rounded-corner square cylinder in shear flow at subcritical and supercritical Reynolds numbers. *Journal of Fluids and Structures*, 82 (March):473–491, 2018. ISSN 10958622. doi: 10.1016/j.jfluidstructs.2018.07.012. URL https://doi.org/10.1016/j.jfluidstructs.2018.07.012.

[9] F. Catalano. On the Effects of a Installed Propeller Slipstream on a Wing Boundary Layer. *ICAS 22nd International Congress of Aeronautical Sciences*, 2000.

[10] R. de Vries, N. van Arnhem, T. Sinnige, R. Vos, and L. L. Veldhuis. Aerodynamic interaction between propellers of a distributed-propulsion system in forward flight. *Aerospace Science and Technology*, 118:107009, 2021. ISSN 12709638. doi: 10.1016/j.ast.2021.107009. URL https://doi.org/10.1016/j.ast.2021.107009.

[11] R. Emunds. Leading edge vortex system of the A380 at high angles of attack in landing configuration. *Third Symposium Simulation of Wing and Nacelle Stall*, (June):1–4, 2012.

[12] X. Fei, B. J. German, and M. D. Patterson. Exploring the effects of installation geometry in high-lift propeller systems. *AIAA Aerospace Sciences Meeting, 2018*, (210059):1–24, 2018. doi: 10.2514/6.2018-0277.

[13] M. Felli and M. Falchi. Propeller tip and hub vortex dynamics in the interaction with a rudder. *Experiments in Fluids*, 51(5):1385–1402, 2011. ISSN 07234864. doi: 10.1007/s00348-011-1162-7.

[14] J. Fischer. Simulation and Analysis of the Aerodynamic Interactions between Distributed Propellers and Wings. *Thesis at Delft University of Technology*, page 109, 2017. URL https://repository.tudelft.nl/islandora/object/uuid:db908fbf-66ca-4b02-8688-3d5b35b8deb2.

[15] Y. Hasan. *Numerical Parameter Study of a Strake on a Turboprop Engine in Active High-Lift Configuration Studienarbeit*. PhD thesis, Deutsches Zentrum fur Luft und Raumfahrt e.V., 2017.

[16] A. Jirásek and O. Amoignon. Design of a high lift system with a leading edge droop nose. *Collection of Technical Papers - AIAA Applied Aerodynamics Conference*, (February), 2009. ISSN 10485953. doi: 10.2514/6.2009-3614.

[17] D. Keller and R. Rudnik. Numerical investigations of aerodynamic properties of a propeller blown circulation control system on a high wing aircraft. *CEAS Aeronautical Journal*, 7(3):441–454, 2016. ISSN 18695590. doi: 10.1007/s13272-016-0195-2.

[18] D. Keller, Y. J. Hasan, and R. Rudnik. Nacelle strake design for short takeoff and landing configuration with turboprop engines. *Journal of Aircraft*, 55(6):2444–2453, 2018. ISSN 15333868. doi: 10.2514/1.C035065.

[19] R. E. Kuhn and J. W. Draper. Investigation of the Aerodynamic Characteristics of a Model Wing-Propeller Combination and of the Wing and Propeller Separately At Angles of Attack Up To 90 Degree. *National Advisory Committee for Aeronautics Report 1263*, 1956.

[20] J. E. Lamar. Flow-visualization techniques used at high speed by configuration aerodynamics Wind-Tunnel-Test Team. *NASA Technical Memorandum*, (210848), 2001. ISSN 04999320.

[21] Y. Leng, M. Bronz, T. Jardin, and J. M. Moschetta. Slipstream Deformation of a Propeller-Wing Combination Applied for Convertible UAVs in Hover Condition. *Unmanned Systems*, 8(4):295–308, 2020. ISSN 23013869. doi: 10.1142/S2301385020500247.

[22] S. J. Miley, R. M. Howard, and B. J. Holmes. Wing laminar boundary layer in the presence of a propeller slipstream, 1988. ISSN 00218669.

[23] H. P. Monner, M. Kintscher, T. Lorkowski, and S. Storm. Design of a smart droop nose as leading edge high lift system for transportation aircrafts. *Collection of Technical Papers - AIAA/ASME/ASCE/AHS/ASC Structures, Structural Dynamics and Materials Conference*, (May): 1–10, 2009. ISSN 02734508. doi: 10.2514/6.2009-2128.

[24] L. Müller, W. Heinze, D. Kožulović, M. Hepperle, and R. Radespiel. Aerodynamic installation effects of an over-The-wing propeller on a high-lift configuration. *Journal of Aircraft*, 51(1):249–258, 2014. ISSN 15333868. doi: 10.2514/1.C032307.

[25] A. V. Petrov. Aerodynamics of stol airplanes with powered high-lift systems. *28th Congress of the International Council of the Aeronautical Sciences 2012, ICAS 2012*, 2:1537–1545, 2012.

[26] B. W. Pomeroy, J. M. Diebold, P. J. Ansell, and M. S. Selig. Study of burst wakes in a multi-element airfoil flowfield. *AIAA Journal*, 52(4):821–831, 2014. ISSN 00011452. doi: 10.2514/1.J052680.

[27] L. Prandtl. Mutual Influence of Wings and Propeller. Technical report, National Advisory Committee for Aeronautics Technical Report No. 74, 1921.

[28] Y. Qiu, J. Bai, and L. Qiao. Aerodynamic effects of wing-mounted engine nacelle on high-lift configuration of turboprop airliner. *Journal of Aircraft*, 55(3):1082–1089, 2018. ISSN 15333868. doi: 10.2514/1.C034529.

[29] R. Radespiel, W. Heinze, and L. Bertsch. High-Lift Research for Future Transport Aircraft. *66. Deutscher Luft- and Raumfahrtkongress (DLRK)*, pages 1–15, 2017.

[30] D. Reckzeh. Aerodynamic design of the A400M high-lift system. In *ICAS Secretariat - 26th Congress of International Council of the Aeronautical Sciences 2008, ICAS 2008*, volume 3, pages 2195–2202, 2008. ISBN 9781605607153.

[31] A. Rezaeiha, H. Montazeri, and B. Blocken. On the accuracy of turbulence models for CFD simulations of vertical axis wind turbines. *Energy*, 180:838–857, 2019. ISSN 03605442. doi: 10.1016/j.energy.2019.05.053. URL https://doi.org/10.1016/j.energy.2019.05.053.

[32] J. Roskam. *Airplane Design Part 2 - Preliminary Configuration Design and Integeration of the Propulsion System*. DARcorpoation, 1985. ISBN 10: 1884885438.

[33] R. Rudnik. Stall behaviour of the EUROLIFT high lift configurations. In *46th AIAA Aerospace Sciences Meeting and Exhibit*, number January, pages 1–30, 2008. ISBN 9781563479373. doi: 10.2514/6.2008-836.

[34] T. Sinnige. XPROP description, performance data (unpublished, internally distributed data), 2021.

[35] TU Delft. Low Turbulence Tunnel, 2015. URL https://www.tudelft.nl/lr/organisatie/afdelingen/aerodynamics-wind-energy-flight-performance-and-propulsion/facilities/low-speed-wind-tunnels/low-turbulence-tunnel.

[36] D. Usai. *Aerodynamic Interaction Between Overlapping Propellers*. PhD thesis, Delft Univeristy of Technology and Politecnico Torino, 2019.

[37] N. Van Arnhem. *Uncoventional Propeller–Airframe Integration for Transport Aircraft Configurations*. PhD thesis, Delft University of Technology, 2022.

[38] N. van Arnhem, R. de Vries, T. Sinnige, R. Vos, G. Eitelberg, and L. L. Veldhuis. Engineering method to estimate the blade loading of propellers in nonuniform flow. *AIAA Journal*, 58(12): 5332–5346, 2020. ISSN 1533385X. doi: 10.2514/1.J059485.

[39] L. Veldhuis, T. Stokkermans, T. Sinnige, and G. Eitelberg. Analysis of swirl recovery vanes for increased propulsive efficiency in tractor propeller aircraft. *30th Congress of the International Council of the Aeronautical Sciences, ICAS 2016*, 2016.

[40] L. L. M. Veldhuis. Review of Propeller-Wing Aerodynamic Interference. *24th International Congress of The Aeronautical Sciences*, 2004. URL http://icas.org/ICAS_ARCHIVE/ICAS2004/PAPERS/065.PDF.

[41] L. L. M. Veldhuis. *Propeller Wing Aerodynamic Interference*. Phd thesis, Delft University of Technology, 2005.

[42] W. Zhang, H. Chen, Y. Zhang, S. Fu, Y. Chen, Y. Li, and T. Zhou. Numerical research of the nacelle strake on a civil jet. In *28th Congress of the International Council of the Aeronautical Sciences 2012, ICAS 2012*, volume 1, pages 745–752, 2012. ISBN 9781622767540.

[43] Y. Zhang, H. Chen, and Y. Zhang. Numerical Research of a Propeller Plane Based on Actuator Disc Model. In *7th European Conference For Aeronautics and Space Sciences (EUCASS)*, Milan, 2017. doi: 10.13009.

[44] T. Zill, M. Iwanizki, P. Schmollgruber, S. Defoort, C. Döll, M. Hoogreef, R. de Vries, J. Vankan, and W. Lammen. An Overview of the Conceptual Design Studies of Hybrid Electric Propulsion Air Vehicles in the Frame of Clean Sky 2 Large Passenger Aircraft. *NLR – Royal Netherlands Aerospace Centre*, (May), 2020.

This page is intentionally left blank

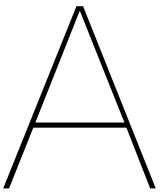

Scale Drawings of the Wing and Nacelle

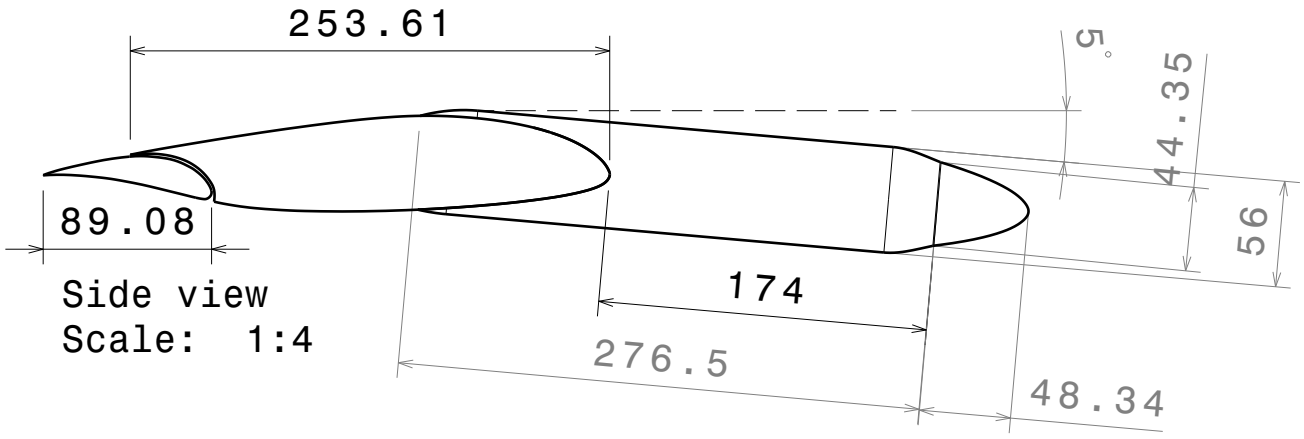

Side view
Scale: 1:4

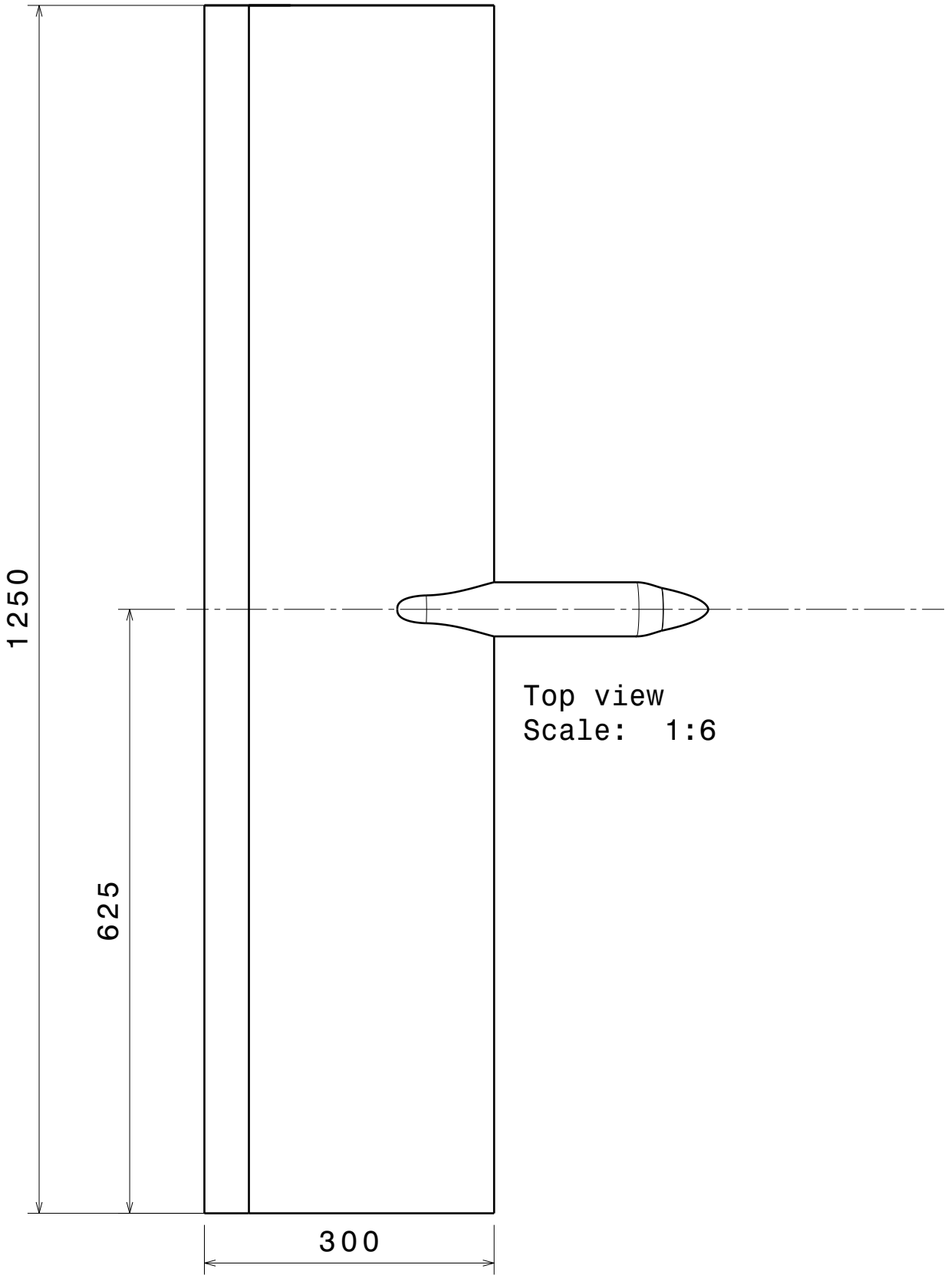

Top view
Scale: 1:6

B

Scale Drawings of the Initial Leading Edge Extensions

LEx 1

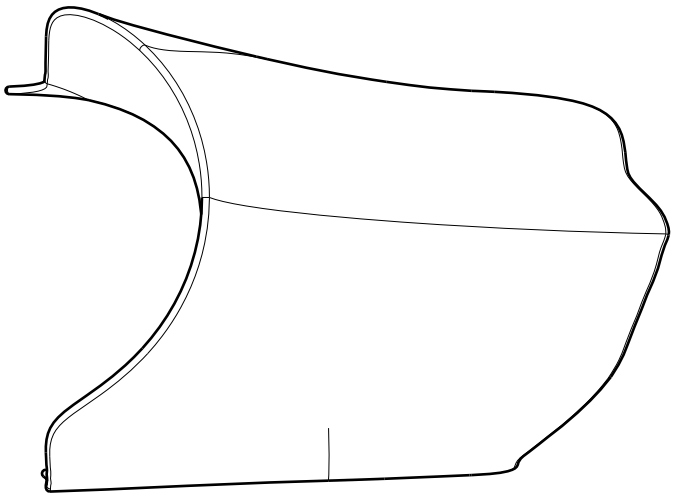

Bottom view
Scale: 1:1

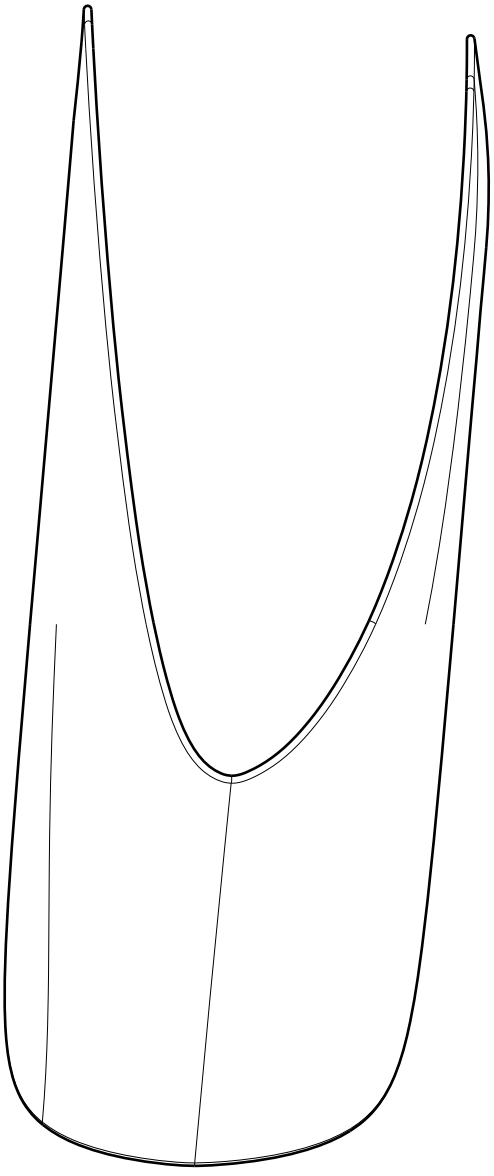

Right view
Scale: 1:1

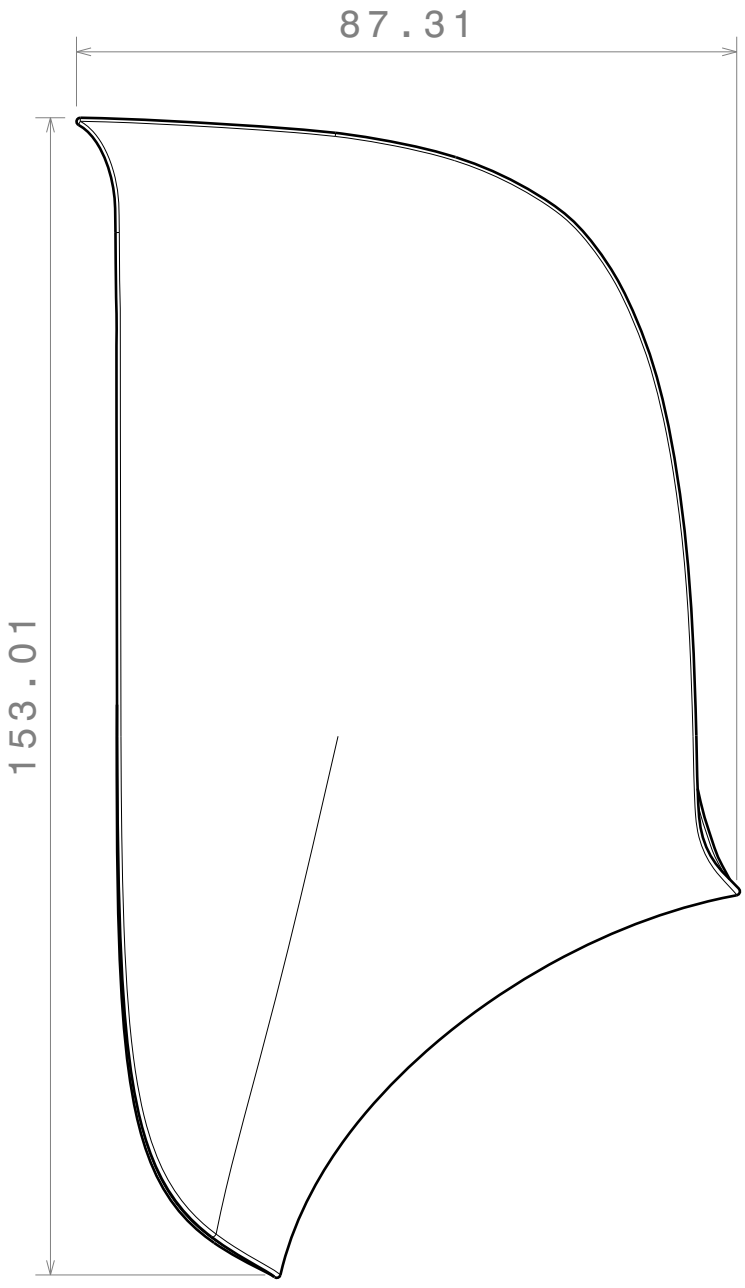

Front view
Scale: 1:1

LEx 2

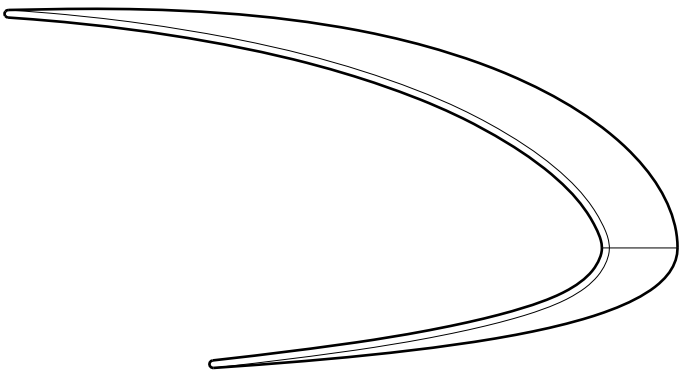

Bottom view
Scale: 1:1

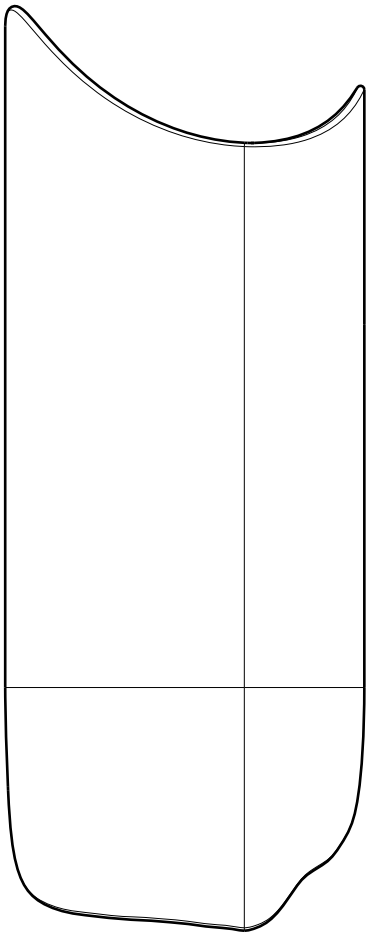

Right view
Scale: 1:1

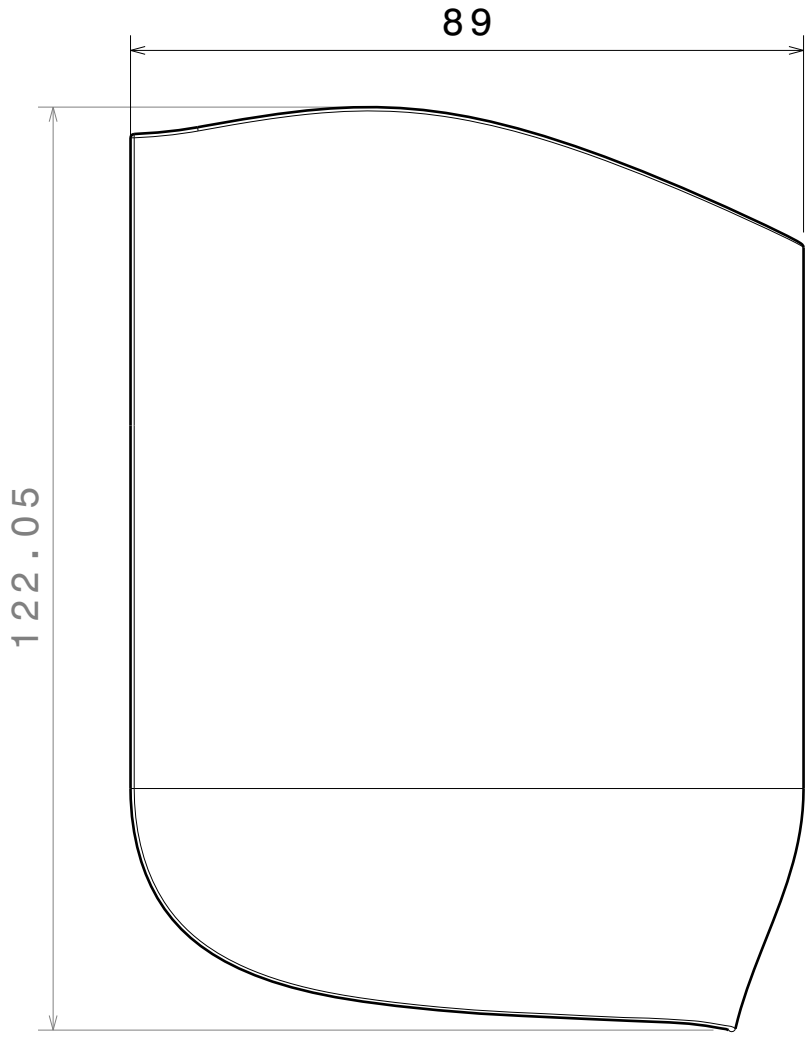

Front view
Scale: 1:1